



Title of thesis

The Correlation between Compaction Degree and Performance  
Life of Asphalt Concrete

I, INTAN KUMALASARI,

hereby allow my thesis to be placed at the Information Resource Center (IRC) of  
University Teknologi PETRONAS (UTP) with the following conditions:

- 1. The thesis becomes the property of UTP
- 2. The IRC of UTP may make copies of the thesis for academic purposes only.
- 3. This thesis is classified as

Confidential

Non-confidential

Endorsed by



Signature of Author

Signature of Supervisor

Jln. Pratista Utara 1 No.12

Antapani, Bandung, Indonesia

Date: January 21<sup>th</sup> 2008

Date: \_\_\_\_\_

## UNIVERSITI TEKNOLOGI PETRONAS

## Approval by Supervisors

The undersigned certify that have read, and recommend to The postgraduate Studies Programme for acceptance, a thesis entitled “The Correlation between Compaction Degree and Performance Life of Asphalt Concrete” submitted by Intan Kumalasari for the fulfillment of the requirements for the DEGREE OF MASTER OF SCIENCE IN CIVIL ENGINEERING



June 12<sup>th</sup>, 2007

Signature: \_\_\_\_\_

Main Supervisor : Assoc. Prof. Dr. Modzlan Napiah

Date : \_\_\_\_\_

Co- Supervisor : Assoc. Prof. Dr. Ibrahim Kamaruddin

UNIVERSITI TEKNOLOGI PETRONAS

**The Correlation between Compaction Degree  
and Performance Life of Asphalt Concrete**

By

Intan Kumalasari

A THESIS

SUBMITTED TO THE POSTGRADUATE STUDIES PROGRAMME

AS A REQUIREMENT FOR THE

DEGREE OF MASTERS OF SCIENCE IN CIVIL ENGINEERING

CIVIL ENGINEERING PROGRAMME

BANDAR SERI ISKANDAR

PERAK

JANUARY 2008

**DECLARATION**

I hereby declare that the thesis is based on my original work except for quotations and citations which have been duly acknowledged. I also declare that it has not been previously or concurrently submitted for any other degree at UTP or other institutions.

Signature : 

Name : Intan Kumalasari

Date : January 21<sup>th</sup> 2008

## ACKNOWLEDGEMENTS

I hereby acknowledge my sincere appreciation and due gratitude to my advisor and study leader, Assoc. Prof. Dr. Madzlan Napiah and Assoc. Prof. Dr. Ir. Ibrahim Kamaruddin, for the academic guidance, mentorship and technical advice rendering during the course of this study.

Furthermore I would like also to give a special word of appreciation to my beloved parents and family for pray and encouragement, Mrs. Zaherah Ismail for reading and correcting the manuscript, all the civil engineering technicians, especially Mr. Zaini, Mr. Mior and Mr. Idris, all the civil engineering lecturers, all postgraduate officers, especially Mrs. Haslina, Mrs. Norma and Mrs. Kamaliah, all the lovely friends who became my convergent thinker during my stay at Universiti Teknologi PETRONAS, my second family, "satuhati" and all those responsible in supporting me to complete this study.

Finally, I would like to acknowledge the scholarship granted by Universiti Teknologi PETRONAS.

## ABSTRACT

Inadequate compaction of wearing course of asphalt concrete is a common phenomenon in road construction. Contractors choose to apply a minimum compaction effort in order to cut costs and speed up construction process. Even though the requirement set by relevant authorities such as Jabatan Kerja Raya (JKR), most of the end product failed to achieve this requirement. Inadequate compaction results in pavement with reduced rutting and fatigue life. This study aims to establish a correlation between compaction degree and performance life of asphalt concrete. Such correlations will provide awareness to the practitioner that the void content is a crucial factor in the performance life of asphalt concrete. Three types of tests were carried out to provide quantitative information on performance life of asphalt concrete at various degrees of compaction. The tests were dynamic creep test, fatigue test and wheel tracking test. The mix type is wearing course and the mix designation is asphalt concrete wearing course or ACW20. The material includes asphalt cement, aggregate and cement as filler. Based on JKR recommendation, penetration graded asphalts were used. The sieve analysis was performed according to JKR specifications. From dynamic creep test, the correlation between compaction degree and rutting life obtained was  $Y_A = (4 \times 10^{-145}) X_A^{77.676}$  (low porosity),  $Y_A = 10^{-232} X_A^{120.7}$  (medium porosity) and  $Y_A = (3 \times 10^{-256}) X_A^{133.08}$  (high porosity), where  $Y_A$  as rutting life in msa and  $X_A$  as compaction degree in percentage. Low porosity specimen is less susceptibility to rut depth than the high porosity specimen. The correlation between porosity and rate of wheel tracking obtained in this study was  $Y_B = 0.0018 X_B^{1.8624}$  with  $R^2 = 0.7138$ , where  $Y_B$  is rate of wheel tracking in mm/min and  $X_B$  is porosity. This correlation emphasizes that low porosity specimen is more resistant to permanent deformation than high porosity specimen. For fatigue failure, the same trend can be concluded.

### Keywords

Compaction, asphalt concrete, porosity, performance life, rutting, fatigue failure

## ABSTRAK

Kekurangan kepadatan pada lapis haus di dalam konkrit asphalt adalah fenomena yang biasa dalam pembinaan jalanraya. Kontraktor-kontraktor memilih untuk menggunakan kepadatan minimum untuk mengurangkan kos dan mempercepatkan proses pembinaan. Walau pun, keperluan yang ditetapkan oleh pihak berkuasa yang berkenaan seperti Jabatan Kerja Raya (JKR), kebanyakan dari hasil terakhir gagal memenuhi keperluan ini. Kekurangan kepadatan akan menghasilkan kaki lima yang mempunyai kesan roda dan umur lesu yang berkurangan. Kajian ini bertujuan untuk menghasilkan hubungkait antara peratusan kepadatan dan jangka hayat penggunaan konkrit asphalt. Hubungkait sebegini akan memberi kesedaran kepada pengamal bahawa kandungan ruang kosong adalah faktor yang genting dalam jangka hayat penggunaan konkrit asphalt. Tiga ujian telah dijalankan untuk memberi maklumat kuantitatif tentang jangka hayat penggunaan konkrit asphalt pada pelbagai tahap kepadatan. Ujian-ujian tersebut adalah ujian creep dinamik, ujian lesu dan ujian pengesanan roda. Jenis campuran terdiri dari lapis haus dan nama campuran ialah lapis haus simen asphalt atau ACW 20. Bahan-bahannya termasuk simen asphalt, agregat dan simen sebagai pengisi. Berdasarkan cadangan dari JKR, asphalt gred penetrasi telah digunakan. Analisis saringan dilakukan mengikut spesifikasi JKR. Dari ujian creep dinamik, hubungkait antara tahap kepadatan dan jangka hayat kesan roda adalah  $Y_A = (4 \times 10^{-145}) X_A^{77.676}$  (porositi rendah),  $Y_A = 10^{-232} X_A^{120.7}$  (porosity medium) and  $Y_A = (3 \times 10^{-256}) X_A^{133.08}$  (porositi tinggi) di mana  $Y_A$  sebagai jangka hayat kesan roda dalam msa dan  $X_A$  sebagai tahap kepadatan dalam peratusan. Kecenderungan pada kedalaman jejak roda adalah lebih sedikit untuk specimen berporositi rendah berbanding specimen berporositi tinggi. Hubungkait antara keporosan dan kadar pengesanan roda yang diperolehi dari kajian ini adalah  $Y_B = 0.0018 X_B^{1.8624}$  dengan  $R^2 = 0.7138$ , di mana  $Y_B$  sebagai kadar pengesanan roda dalam mm/min dan  $X_B$  sebagai keporosan. Hubungkait ini menekankan bahawa specimen berporositi rendah lebih berupaya menentang kerosakan kekal berbanding specimen berporositi tinggi. Kecenderungan yang sama boleh dirumuskan untuk kegagalan lesu.

### Kata kunci

Kepadatan, konkrit asphalt, keporosan, jangka hayat penggunaan, kesan roda, kegagalan lesu



## TABLE OF CONTENTS

DECLARATION.....	IV
ACKNOWLEDGEMENTS.....	V
ABSTRACT .....	VI
TABLE OF CONTENTS.....	VIII
LIST OF TABLES .....	XI
LIST OF FIGURES .....	XII
LIST OF ABBREVIATIONS.....	XIV
<b>1 CHAPTER ONE: INTRODUCTION .....</b>	<b>1</b>
1.1 BACKGROUND	1
1.2 PROBLEM STATEMENT	2
1.3 OBJECTIVE OF RESEARCH	2
1.4 SCOPE OF RESEARCH	3
<b>2 CHAPTER TWO: DISTRESSES IN ASPHALT CONCRETE.....</b>	<b>4</b>
2.1 INTRODUCTION	4
2.2 SURFACE DEFORMATION	6
2.2.1 Rutting	7
2.2.2 Primary Rutting	9
2.2.3 Causes of Rutting	10
2.3 PAVEMENT CRACKS	11
2.3.1 Fatigue Cracking	11
2.3.2 Causes of Fatigue Cracking	14
2.3.3 Critical Tensile Strain	14
2.4 TRAFFIC LOADING AND VOLUME	15
2.5 SUMMARY	16
<b>3 CHAPTER THREE: COMPACTION OF ASPHALT CONCRETE.....</b>	<b>17</b>
3.1 INTRODUCTION	17
3.1.1 Compactive Effort	20
3.1.2 Insufficient Pressure for Compaction	21
3.1.3 Vertical Pressure and Angle of Gyration	21
3.1.4 Laboratory Compaction Method	21
3.1.5 Mixing and Compaction Temperature	22
3.1.6 Size of Gyrotory Mould	23
3.1.7 Number of Gyration	25
3.2 AIR VOID/ POROSITY	26
3.2.1 Initial and Final Air Void	31
3.2.2 Air Void vs. Permanent Deformation	32

3.2.3	Air Void vs. Fatigue Life	34
3.3	SUMMARY	39
<b>4</b>	<b>CHAPTER FOUR: PERFORMANCE TEST</b> .....	<b>40</b>
4.1	INTRODUCTION	40
4.2	STIFFNESS MODULUS	40
4.2.1	The Resilient Modulus	41
4.2.2	The Dynamic Complex Modulus (Dynamic Modulus)	42
4.2.3	The Dynamic Stiffness Modulus	43
4.3	PERMANENT DEFORMATION TEST	44
4.3.1	Creep Test	45
4.3.2	Rutting Test	48
4.3.3	Comparison between Creep Test and Rutting Test	48
4.3.4	Correlation $S_{mix}$ and $S_{bit}$	49
4.4	FATIGUE TEST	54
4.4.1	Four-Point Bending Test	57
4.4.2	Fatigue Failure	57
4.4.3	Output of Fatigue Test/ Fatigue Characteristics	58
4.5	SUMMARY	60
<b>5</b>	<b>CHAPTER FIVE: EXPERIMENTAL WORK</b> .....	<b>61</b>
5.1	MATERIALS	61
5.2	TEST ON AGGREGATE	63
5.2.1	Particle Size Analysis	63
5.2.2	Specific Gravity	63
5.3	BITUMEN TESTS	63
5.4	MIX DESIGN	64
5.4.1	Preparation	65
5.4.2	Mixing	65
5.4.3	Compaction	66
5.4.4	Density Determination	68
5.5	DYNAMIC CREEP TEST	69
5.6	FATIGUE TEST	71
5.7	WHEEL TRACKING TEST, SIMULATIVE TEST	72
<b>6</b>	<b>CHAPTER SIX: RESULTS AND DISCUSSION</b> .....	<b>74</b>
6.1	INTRODUCTION	74
6.2	PARTICLE SIZE OF AGGREGATE	74
6.3	CREEP TEST RESULTS	76
6.3.1	Correlation between Bitumen Stiffness vs. Mixture Stiffness	77
6.3.2	Calculation of Viscous Bitumen Stiffness ( $S_{bit\ viscous}$ ) and Mixture Stiffness	79
6.3.3	Calculation of Rut Depth	80
6.3.4	Rut Depth vs. Number of Wheel Passes	81
6.3.5	Rut Depth vs. Porosity	83
6.3.6	Number of Wheel Passes vs. Porosity	86
6.3.7	Compaction Degree vs. Number of Wheel Passes (N)	86
6.4	WHEEL TRACKING TEST RESULTS	88
6.5	FATIGUE TEST RESULTS	89
6.6	THE PRACTICAL IMPLICATION OF THE STUDY	91

<b>7</b>	<b>CHAPTER SEVEN: CONCLUSIONS AND RECOMMENDATION.....</b>	<b>92</b>
7.1	CONCLUSION	92
7.2	RECOMMENDATION	93
	<b>REFERENCES.....</b>	<b>94</b>
	<b>APPENDIX A JKR STANDARD SPECIFICATION .....</b>	<b>98</b>
	<b>APPENDIX B CALCULATION OF POROSITY .....</b>	<b>99</b>

## LIST OF TABLES

Table 2.1	Distress Types of Asphalt Concrete Surface Pavement	5
Table 2.2	Distress Types of Asphalt Concrete Surface Pavement	6
Table 2.3	Rut depth of Rutting	7
Table 2.4	Quantifiable Area of Fatigue Cracking	12
Table 3.1	Compaction Issue	20
Table 3.2	Effect of Compaction on Hot Mix Asphalt Pavement	27
Table 3.3	In-place Air Voids and Density Ratio	31
Table 4.1	Some Parameters of Creep Test Used by Other Researchers	47
Table 4.2	Correction Factors for Dynamic Effects	48
Table 4.3	Some Fatigue Test Parameters Used by Other Researchers	58
Table 6.1	Particle Size Distribution of the Aggregates used in the Investigation	74
Table 6.2	Result of Sieve Analysis	75
Table 6.3	Creep Test Results	79
Table 6.4	Creep Test Results Presented as $S_{mix}$ vs. $S_{bit(v)}$	80
Table 6.5	Rut Depth for Specimen with 3% Porosity	81
Table 6.6	Rate of Rut Depth	85
Table 6.7	Compaction Degree vs. N (standard axle)	87
Table 6.8	Fatigue Curve Regression Parameter	90

## LIST OF FIGURES

Figure 2.1	Types of Cracking	4
Figure 2.2	Types of Surface Deformation	4
Figure 2.3	Rutting	7
Figure 2.4	Cross Section of Rutting	8
Figure 2.5	Primary Rutting	9
Figure 2.6	Secondary Rutting	9
Figure 2.7	Low Severity	12
Figure 2.8	Moderate Severity	13
Figure 2.9	High Severity	13
Figure 3.1	Variation in the Compactability of Bituminous Mixtures Due to Change in Composition	18
Figure 3.2	Compaction Phases	18
Figure 3.3	Percent Voids vs. Average Asphalt Viscosity	23
Figure 3.4	100 mm and 150 mm Diameter Cylinder Molds	24
Figure 3.5	Typical %Gmm vs. Gyration Curve	25
Figure 3.6	Air Void in Mixture	26
Figure 3.7	Design Life vs. % Air Void	28
Figure 3.8	Relative Rutting vs Air Void	32
Figure 3.9	Effect of Mix Variables on Estimated ESALs to 15 mm (0.6 in) Rut depth for Various Range in Air-Void Contents	33
Figure 3.10	Relationship between Permanent Shear Strain and Air Void Content	34
Figure 3.11	Influence of Air Void Content on Fatigue Performance	35
Figure 3.12	Effect of Asphalt and Air Void Contents on Simulated, Fatigue-Life Ratio for 270 Mix-Pavement Combinations	36
Figure 3.13	Relative Fatigue Life vs. Air Voids	36
Figure 3.14	Relationship between Cycle to Failure, Air Void Content, and Strain Level	38
Figure 4.1	Strain Under Repeated Loads	42
Figure 4.2	Relation between Dynamic Stiffness and Porosity	43
Figure 4.3	Effect of Compaction on Dynamic Stiffness	44
Figure 4.4	Nomograph for Viscosity of Bitumen	52
Figure 4.6	Two Types of Controlled Loading for Fatigue Testing	55
Figure 4.7	Typical Fatigue Paths for Asphalt Concrete	56
Figure 5.1	Flowchart of Research	62
Figure 5.2	Penetration Test [63]	64
Figure 5.3	Gyratory Compactor	66
Figure 5.4	Hand Compactor	66
Figure 5.5	Universal Testing Machine 4-19	70
Figure 5.6	Universal Testing Machine 4-21	72
Figure 5.7	Wheel Tracking	73
Figure 6.1	Particle Size Distribution of the Aggregates	75
Figure 6.2	Sieve Analysis	76
Figure 6.3	Porosity vs. Weight of Specimens	77
Figure 6.4	Porosity vs. Pressure	77
Figure 6.5	$S_{Mix}$ vs. $S_{Bit}$	78
Figure 6.6	Rut Depth vs. N for High Porosity	82
Figure 6.7	Rut Depth vs. N for Moderate Porosity	83

Figure 6.8 Rut Depth vs. N for Low Porosity	83
Figure 6.9 Rut Depth vs. Porosity	84
Figure 6.10 Rut Depth vs. Porosity	84
Figure 6.11 Number of Wheel Passes vs. Porosity in Limit of Severity Level	86
Figure 6.12 Compaction Degree vs. N	88
Figure 6.13 Wheel Tracking Test Results	88
Figure 6.14 Deterioration Path of Fatigue Test Result	89
Figure 6.15 Load Cycles vs. Test Tensile microstrain at 20°C	90
Figure 6.16 Cycle to Failure vs. Porosity	91

## LIST OF ABBREVIATIONS

ASG	Apparent Specific Gravity
AAPA	Australian Asphalt Pavement Association
BSG	Bulk Specific Gravity
EALF	Equivalent Axle Load Factor
ESAL	Equivalent Single-Axle Load
ESG	Effective Specific Gravity
GTM	Gyratory Testing Machine
HMA	Hot Mix Asphalt
HMAC	Hot Mix Asphalt Concrete
JKR	Jabatan Kerja Raya
FHWA	Federal Highway Administration
MATTA	Material Testing Apparatus
ME	Mechanistic Empirical
MSG	Maximum Specific Gravity
SHRP	Strategic Highway Research Program
TMD	Theoretical Maximum Density
VFA	Voids Filled with Asphalt
VTM	Voids in the Total Mix
VMA	Void in the Mineral Aggregate
LVDT	Linear Variable Displacement Transducer

## CHAPTER ONE: INTRODUCTION

### 1.1 Background

Compaction is an important aspect that influences the performance of asphalt concrete pavement. Compaction as a process by which the volume of air in an Hot Mixed Asphalt (HMA) mixture is reduced by using external forces to reorient the constituent aggregate particles into a more closely spaced arrangement [1]. This reduction of air volume produces a corresponding increase in HMA density. Others define compaction of an asphalt concrete mixture as a stage of construction which transforms the mix from its very loose state into a more coherent mass, thereby permitting it to carry traffic loads [2, 3]. All of them have the same purpose that is to increase the density in asphalt mixture, followed by a decrease in air volume.

Compaction is related to volumetric properties. The volumetric properties of asphalt mixtures include Voids in the Total Mix (VTM), Voids in the Mineral Aggregate (VMA) and Voids Filled with Asphalt (VFA). The most important property in construction is VTM or air void. The VTM is directly related to density of mixture. This property is similar to the degree of compaction defined by [3][4].

Improper compaction can cause serious problems such as rutting, fatigue cracks, longitudinal joint crack, tire marks, asphalt sticking, impact mark, and crushing/fracturing aggregate [5]. Rutting and fatigue crack can be evaluated by laboratory experiments. Both permanent deformation and fatigue crack are related to compaction degree or void content and are used as a measure of performance life of roads. Pavement performance studies have shown that an air void range of 3%-5 % in an asphalt concrete mix is desirable for its satisfactory performance in most environments [1]. Satisfactory performance cannot be achieved if proper compaction that gets good air void is not practiced.

It was also reported that for every 1% increase in air void, more than 7% of the road life is reduced by 10% of its design life [6]. Another study shows that a 1% (from 8% to 9%) increase in air void content would result in a decrease in fatigue life by roughly 41% and



a 2% air void content (8% to 10%) increasing would increase permanent shear strain by nearly 42% with majority of the permanent shear strain occurring between 9% and 10% air void content [7]

## **1.2 Problem Statement**

Inadequate compaction of wearing course of asphaltic concrete is a common phenomenon in road construction. It can cause reductions in rutting and fatigue life of pavement. Contractors choose to apply a minimum compaction effort in order to cut costs and speed up construction process. Even though, the requirement has been set by relevant authorities such as Jabatan Kerja Raya (JKR) is between 95% and 97% of Theoretical Maximum Density (TMD), most of the end product failed to achieve this requirement. Normally, JKR will inspect the thickness of layer in order to determine the quality and quantity of road built by contractor. JKR also takes the air void sample of the pavement. It is measured directly by comparing the theoretical maximum specific gravity of the material to the bulk specific gravity of the saturated surface dry sample. Void in wearing course mix that allowed in JKR specifications for asphaltic concrete is 3% to 5%. However, this specification could not be fulfilled if poor compaction is applied.

Contractors should have an awareness of the important of proper compaction in order to obtain good performance of pavement. They need to know the importance of proper compaction. A correlation between compaction degree of asphalt concrete and performance life would be useful to contractors for such purpose.

## **1.3 Objective of Research**

The aim of this research is to establish a correlation between compaction degree and performance life of asphalt concrete pavement. Two aspects of performance life that will be correlated to compaction degree are rutting life and fatigue life. For this purpose, tests including creep test, fatigue test and wheel tracking test were carried out. The intention of this study is to highlight the importance of proper compaction.

## 1.4 Scope of Research

This research was based on laboratory testing. The study concentrated on asphalt mix itself and the asphalt paving material used was asphalt concrete. Mix design follows JKR standard, accordingly Marshall Method (traditional mix design). The evaluation in this study involves asphalt concrete wearing course mixes only. To fulfill this scope, the pavement section underneath the surface layer is homogeneous. For the analysis, the percentage of asphalt compaction (air void) in this study are divided into 3%-5%, 6%-8%, 9%-11% for creep test and 5%-7%, 8%-10%, 11%-13% for fatigue test. These values were obtained from the asphalt mixes that were compacted using gyratory compactor and hand compactor.

## CHAPTER TWO: DISTRESSES IN ASPHALT CONCRETE

### 2.1 Introduction

There are five major types of distress in asphalt concrete surface. They are cracking, potholes, surface deformation, surface defects and miscellaneous distresses. The definition for each of them is presented in Table 2.1. For cracking alone, based on their name, there are six types of cracking, as shown in Figure 2.1, which is identified as fatigue, block, edge, longitudinal, reflection and transverse cracking. These are categorized based on the position and form of cracks. Patching deterioration and potholes are distresses that occur when portions of the pavement has been removed. Surface deformations are rutting, shoving, corrugation and depression as shown in Figure 2.2. Meanwhile surface defects include bleeding, polished aggregate and raveling. These distresses are caused by improper amount of aggregate or binder. Lastly, Lane-to-Shoulder Drop-off and Water bleeding and pumping are categorized as miscellaneous distresses.

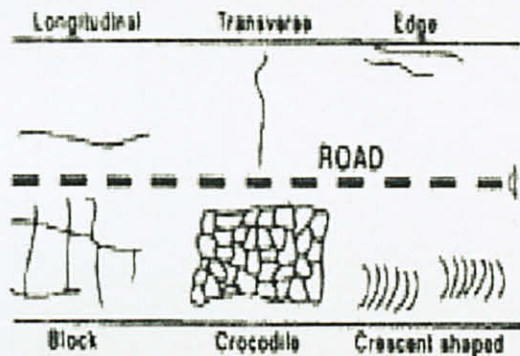


Figure 2.1 Types of Cracking  
(Source: JKR, 1992)

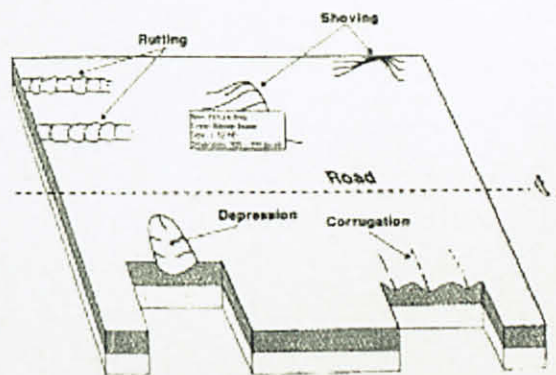


Figure 2.2 Types of Surface Deformation  
(Source: JKR, 1992)

Some difference in the classification of distress types between Jabatan Kerja Raya (JKR) and Federal Highway Administration (FHWA) are observed. JKR does not include reflection cracking as a type of cracking but JKR adds two types of surface deformation, namely corrugation and depression, to rutting and shoving, which are categorized by FHWA.

Table 2.1 Distress Types of Asphalt Concrete Surface Pavement

Definitions
Fatigue Cracking is occurs in areas subjected to repeated traffic loadings (wheel paths). Can be a series of interconnected or interlaced cracks in early stages of development. Develops into many-sided, sharp-angled pieces, usually less than 0.3 meters (m) on the longest side, characteristically with a chicken wire/alligator pattern, in later stages.
Block Cracking is a pattern of cracks that divides the pavement into approximately rectangular pieces. Rectangular blocks range in size from approximately 0.1 m <sup>2</sup> to 10 m <sup>2</sup> .
Edge Cracking is applies only to pavements with unpaved shoulders. Crescent-shaped cracks or fairly continuous cracks which intersect the pavement edge and are located within 0.6 m of the pavement edge, adjacent to the shoulder. Includes longitudinal cracks outside of the wheel path and within 0.6 m of the pavement edge.
Longitudinal Cracking is cracks predominantly parallel to pavement centerline. Location within the lane (wheel path versus non-wheel path) is significant.
Reflection Cracking is cracks in asphalt concrete overlay surfaces that occur over joints in concrete pavements.
Potholes are bowl-shaped holes of various sizes in the pavement surface. Minimum plan dimension is 150 mm.
Depression (Distortion) is localized areas within a pavement with elevations lower than surrounding area. They may not be confined to wheel paths only but may extend across several wheel paths. Generally, it results from settlement, slope failure, or volume changes due to moisture changes.
Rutting is a longitudinal surface depression in the wheel path. It may have associated transverse displacement.
Shoving is a longitudinal displacement of a localized area of the pavement surface. It is generally caused by braking or accelerating vehicles, and is usually located on hills or curves, or at intersections. It also may have associated vertical displacement.
Corrugation (Rippling) is regular transverse undulations closely spaced alternate valleys and crests with wavelengths of less than 2 m. Generally, it will result in a rough ride and will become worse with time.
Bleeding is excess bituminous binder occurring on the pavement surface, usually found in the wheel paths. May range from a surface discolored relative to the remainder of the pavement, to a surface that is losing surface texture because of excess asphalt, to a condition where the aggregate may be obscured by excess asphalt possibly with a shiny, glass-like, reflective surface that may be tacky to the touch.
Polished Aggregate is surface binder worn away to expose coarse aggregate.

Table 2.2 Distress Types of Asphalt Concrete Surface Pavement

Definitions
Raveling is wearing away of the pavement surface caused by the dislodging of aggregate particles and loss of asphalt binder. Raveling ranges from loss of fines to loss of some coarse aggregate and ultimately to a very rough and pitted surface with obvious loss of aggregate.
Lane-to-Shoulder Drop-off is difference in elevation between the traveled surface and the outside shoulder. Typically occurs when the outside shoulder settles as a result of pavement layer material differences.
Water Bleeding is seeping or ejection of water from beneath the pavement through cracks. In some cases, detectable by deposits of fine material left on the pavement surface, which were eroded from the support layers and have stained the surface.

From all types of distress presented in Table 2.1, two most common structural distresses that occur in flexible pavements as a result of vehicle loading are cracking in bituminous material and longitudinal depressions, or ruts, which is apparent at the surface in the paths repeatedly tracked by vehicle wheels. These two major distress conditions affect the performance of asphalt pavements [8-10].

Rutting could be the subsequent failure of pavement after fatigue cracking [9]. Excessive deformation can take place because there is a progressive weakening of bound layer, which increases the level of stress transmitted to the lower layers and subgrade. This weakening occurs as a result from fatigue cracking, which originates at the bottom of bituminous pavement layer and propagates upward through the bound layers to the pavement surface. The onset of fatigue cracking is controlled by the horizontal strains repeatedly generated by traffic loading.

## 2.2 Surface Deformation

Surface deformation takes place when a road surface undergoes changes from its original constructed profile. It may occur after construction due to trafficking or environmental influences. In some cases, deformation may be built into a new pavement owing to inadequate control during construction. It influences the riding quality of a pavement and may reflect structural inadequacies. It may lead to cracking of the surface layer.

### 2.2.1 Rutting

One of the most important properties of an asphalt paving mix is its ability to resist permanent deformation (rutting) under moving or stationary wheels of vehicles. An element of the deformation that is induced under the application of a vehicle load is, therefore, irrecoverable and with repeated load applications, this permanent deformation accumulates leading to the formation of ruts [11].

A rutting form on an asphalt surface layer can be seen as shown in Figure 2.3. Rutting can occur at various severity levels. A classification of the severity level by JKR Malaysia is given in Table 2.3. A measurement is needed for categorizing. A 1.2 m straight edge at 15.25 m interval for each wheel path is used.

Rutting can occur in all bituminous layers. Since the distinction is not obvious, it was suggested that the engineer should cut some trench section across the pavement lane and examine the boundary lines of the various layers to determine the source of rutting [8]. The example of cross section form looks like Figure 2.4. But this figure is only for asphalt layer. Rutting is practically independent of asphalt layer thickness for thick pavement structure of more than 15 cm [12]. Small rut is defined as 5% of layer thickness, for instance 2.54 mm for 50 mm layer [13].

Table 2.3 Rut depth of Rutting

Severity Level	Low	Moderate	High
Rut Depths	<12 mm	12 mm – 25 mm	>25 mm



Figure 2.3 Rutting  
(Source: FHWA, 2003)

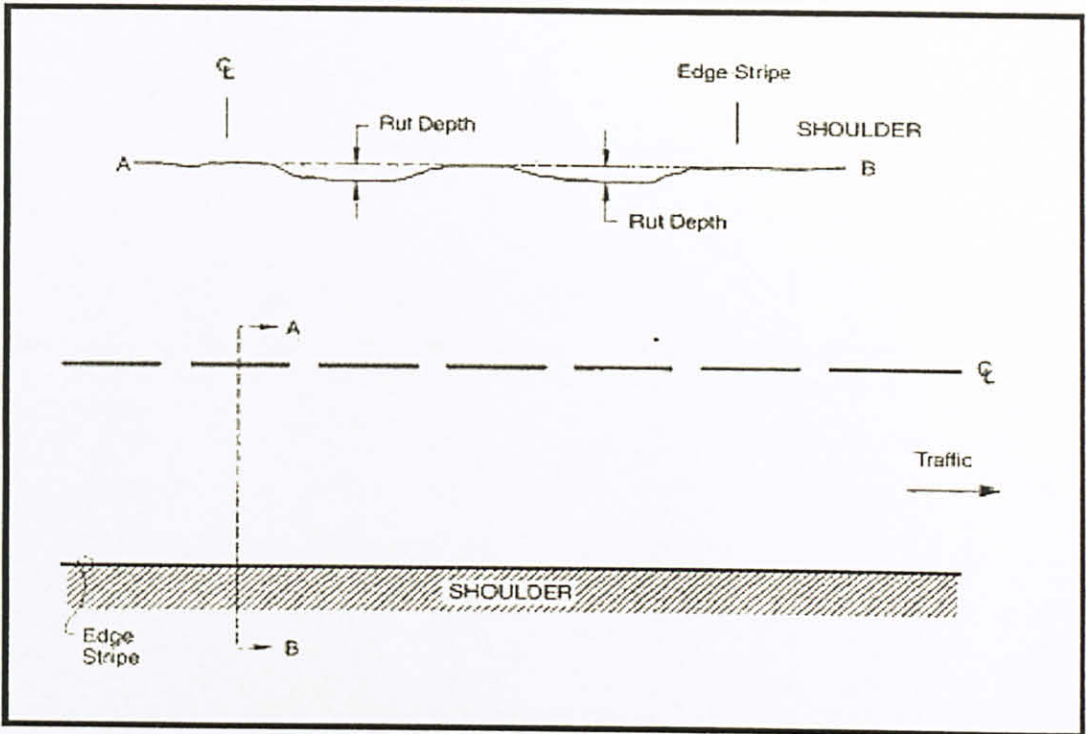


Figure 2.4 Cross Section of Rutting  
(Source: FHWA, 2003)

There are two types of rutting namely primary rutting and secondary rutting [14]. Primary rutting, as shown in Figure 2.5; defined as the total permanent deformation of the bituminous bound layers in the wheel track. Primary rutting occurs in the asphalt layer. The underlying layers perform fine and their boundary lines are unaffected by the distress occurring near the surface of the asphalt pavement [8]. Secondary rutting, as shown in Figure 2.6, which is often accompanied by cracking, has its origins in the non-bituminous components of pavement; in practice this means the unbound road base and/ or the sub grade.

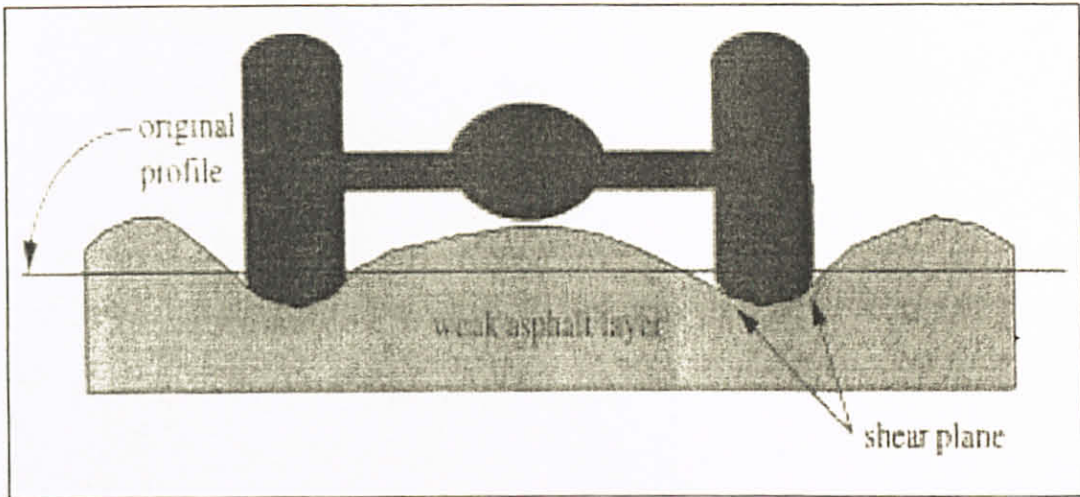


Figure 2.5 Primary Rutting  
(Source: Santucci, 2001)

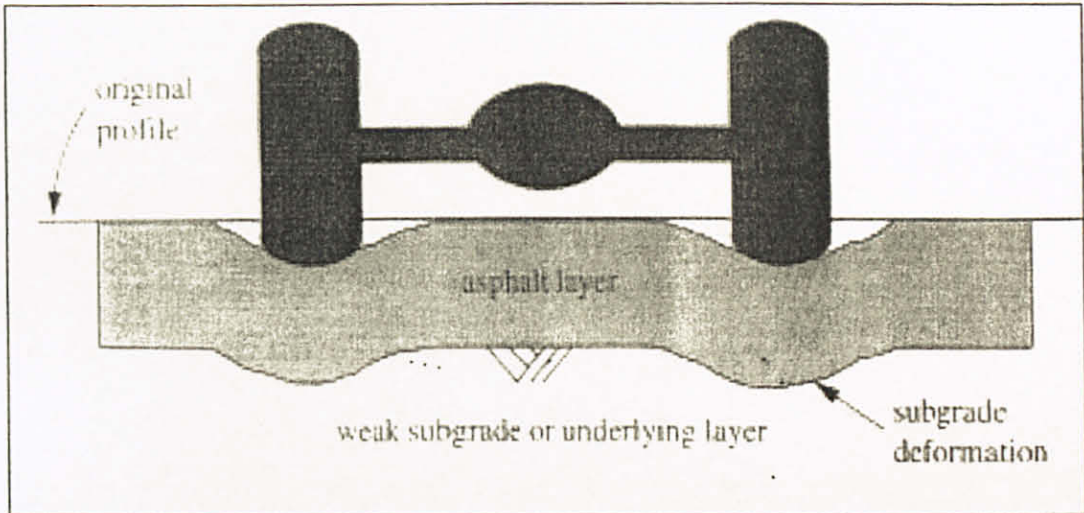


Figure 2.6 Secondary Rutting  
(Source: Santucci, 2001)

### 2.2.2 Primary Rutting

Important factors that influence primary rutting are asphalt temperature, traffic load and stress condition [14]. For rutting calculations, the traffic data must be expressed in terms of number of wheel passages per rut. An important influencing factor of traffic load on primary rutting is the loading time.

Other than the external factor as stated above, the permanent deformation resistance of a bituminous mixture is also dependent upon its composition [11]. The compositions at the



mix consist of the properties of the components and their relative proportions. The properties of the components such as binder stiffness and texture, grading, size, shape of the aggregate. Meanwhile the relative proportions are volumes of the mineral, bitumen and air voids.

The apparent mode of rutting in the asphalt concrete layer (primary rutting) are structural rutting (densification) and non-structural rutting (shear deformation ) [1, 8, 11, 15-17]. The densification (compaction) of pavement can be seen as collapsing of the voids in the asphalt concrete layer as the wheel apply a compressive force on it. In this mode, a rut is a longitudinal surface depression in the wheel path and no significant lateral material movement from under the wheel. Shear deformation is associated with transverse displacement. Deformation causes the material to move laterally from under the wheels and accumulate in between and to the side of the wheel paths. In well-compacted pavements, shear deformation becomes the rutting mechanism because the densification under the wheel path is not significant [17].

### 2.2.3 Causes of Rutting

Bitumen stiffness has a strong influence on pavement performance [11, 18] because stiffness of the asphalt layers affects the response of pavements to traffic loads materially. At low binder stiffness, associated with high temperature and/or long load duration due to the visco-elastic nature of the material, the aggregate fraction of the mixture has a more significant effect on response and also influences deformation resistance [8, 11]. Low stiffness, refers to stiffness at temperature at which rutting propensity is being determined, will lead to a lower rutting resistance of mixture.

Repetitive loading can cause the flow and subsequent rutting of the material under the wheel load [8, 12, 16]. This phenomenon occurs because repeated wheel load applications create a shear stress that exceeds the shear strength of the mix [8].

Rutting throughout the entire asphalt pavement structure is caused by over stressing the underlying base or subgrade layers (excessive the compressive strain in the subgrade). This overstressed condition can be the result of inadequate thickness design for the

applied traffic or for the strength properties of the underlying materials [8]. The rutted condition in the underlying layers is then reflected to the pavement surface.

The other cause of rutting is densification. Densification is caused by "post-compaction". If properly designed material is insufficiently compacted, the void content of the asphalt mix will decrease under the action of traffic [12]. The decreasing air void will cause overfilling the void between the mineral aggregate [19]. The changes of this void content give effect to pavement tendency to rutting.

### **2.3 Pavement Cracks**

Cracks are fissures resulting from partial or complete fractures of the pavement surface. Cracking of road pavement surfaces can happen in a wide variety of patterns, ranging from isolated single crack to an interconnected pattern extending over the entire pavement surface. The detrimental effects associated with the presence of cracks are loss of water-proofing of the pavement layers, loss of load spreading ability of the cracked material, pumping and loss of fines from the base course, loss of riding quality through loss of surfacing and loss of appearance.

The loss of load spreading ability and water-proofing will usually lead to accelerated deterioration of the pavement condition. The possible causes of cracks include depression, fatigue life of the surface being exceeded, brittle surfaces, reflection of cracks in underlying layers, shrinkage, and poor construction joints.

#### **2.3.1 Fatigue Cracking**

Fatigue cracking (alligator/ chicken wire/ fish net/ polygonal cracking) was identified in the Strategic Highway Research Program (SHRP) as the major distress condition, beside rutting, affecting the long term performance of asphalt pavement. This complex phenomenon is associated with stresses induced in the asphalt layers by wheel loads, temperature changes or a combination of the two. Two phases of fatigue cracking are crack initiation and crack propagation. Fatigue cracking generally starts as a series of

short longitudinal cracks in areas subjected to repeated wheel loadings. With additional traffic, the number of cracks increases and interconnects into a typical pattern, as presented in Table 2.4. The severity levels are divided into three types namely, low, moderate and high, depending on the crack formation.

Table 2.4 Quantifiable Area of Fatigue Cracking

Severity Levels	Low	Moderate	High
Description	An area of cracks with no or only a few connecting cracks; cracks are not spalled or sealed; pumping is not evident as shown in Figure 2.7	An area of interconnected cracks forming a complete pattern; cracks slightly spalled; cracks sealed; pumping is not evident as shown in Figure 2.8	An area of moderately or severely spalled interconnected cracks forming a complete pattern; pieces move when subjected to traffic; cracks sealed; pumping evident as shown in Figure 2.9
How to Measure	Record square meters of affected area at each severity level. If different severity levels existing within an area cannot be distinguished, rate the entire area at the highest severity present.		



Figure 2.7 Low Severity  
(Source: FHWA, 2003)

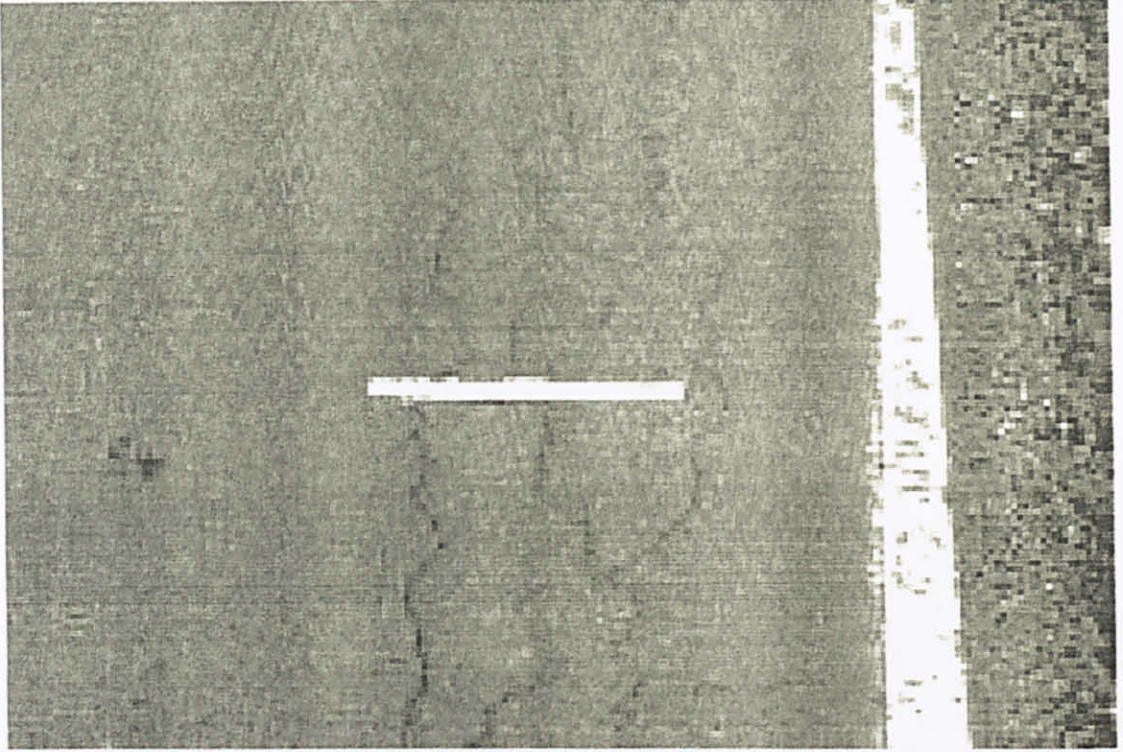


Figure 2.8 Moderate Severity  
(Source: FHWA, 2003)

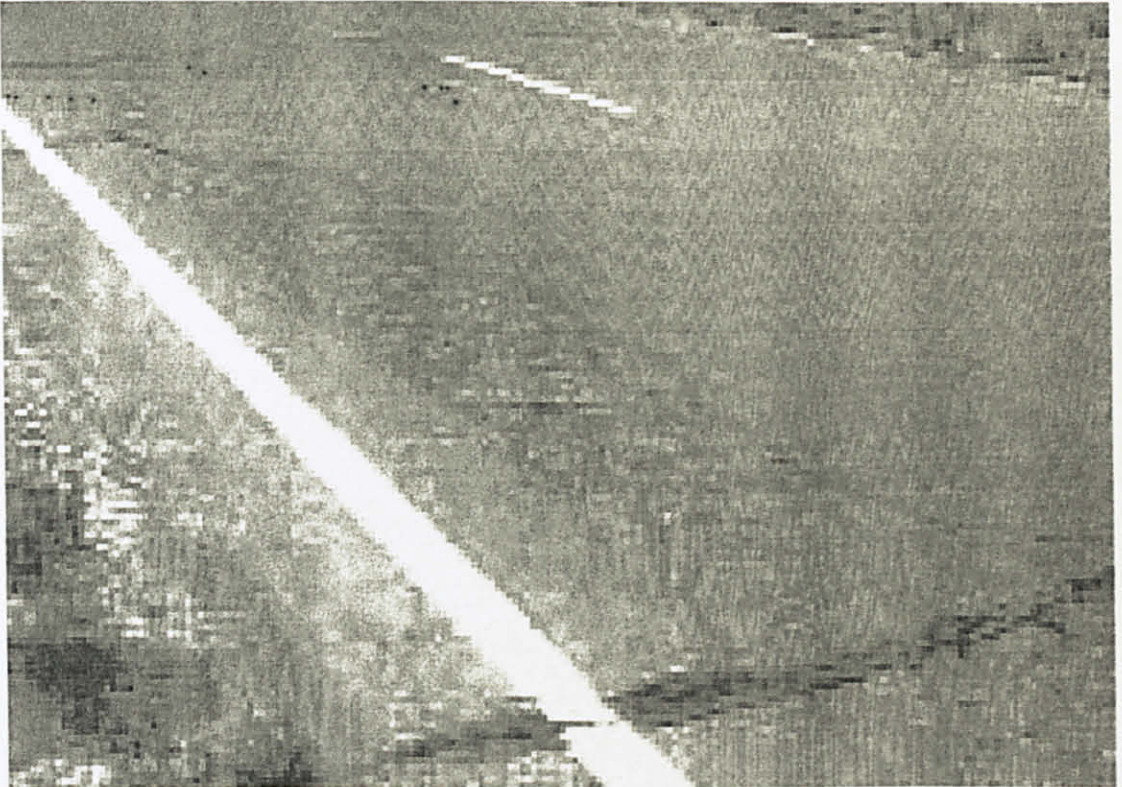


Figure 2.9 High Severity  
(Source: FHWA, 2003)

### 2.3.2 Causes of Fatigue Cracking

The stiffness of an asphalt mix plays a major role in the fatigue resistance of asphalt pavement. Higher mix stiffness can result from the use of harder asphalt, a lower pavement temperature, or a denser (better compacted) mix. Just as with increasing pavement thickness (greater than 10 cm), higher mix stiffness reduces the tensile stresses at the bottom of the asphalt layer and the likelihood of crack initiation. However, for thin asphalt pavements (less than 10 cm) or pavements subjected to high deflection (weak subgrade), a less stiff or more flexible mix will produce a more fatigue resistant pavement [16, 20]. The stiffness determines magnitude of the stress of load repetitions. Tensile stress is 50-200 microstrains for standard wheel load. It is possible for fatigue cracking to exist when bituminous material is subjected to a stress smaller than breaking strength fractures.

Fatigue cracking could also be the consequence of the inability of the structure to support the repeated loads due to "softening" of the material normally associated with increase in moisture content [21]. Increasing moisture content is related to compaction process to obtain a certain air void. Improper compaction can cause fatigue in wearing course [22] because the air void in an asphalt mix act as stress concentration points and are likely the place where the crack begins [20].

Not only the condition of asphalt layer, the conditions of base course also influence the fatigue resistance. Brittle base and poor base drainage tend to fatigue failure [22].

### 2.3.3 Critical Tensile Strain

The tensile strains at the bottom of asphalt layer have been used as a design criterion to prevent fatigue cracking. Two types of principal strains could be considered. One is the overall principal strain based on all six components of normal and shear stresses only. The overall principal strain is slightly greater than the horizontal principal strain, so the use of overall principal strain on the safe side [23].

The critical tensile strain is the overall strain and can be determined from

$$e = \frac{q}{E_1} F_e \quad \text{Equation 2-1}$$

In which  $e$  is the critical tensile strain and  $F_e$  is the strain factor. In most cases, the critical tensile strain occurs under the center of the loaded area, where the shear stress is zero. The tensile stress and strain at the base of the asphalt layer are assumed to be the parameters controlling the crack development and are used to estimate pavement fatigue life [24, 25].

## 2.4 Traffic Loading and Volume

Traffic influences failure of pavement. There are three different procedures for considering vehicular and traffic effects in pavement design: fixed traffic, fixed vehicle, and variable traffic and vehicle. Most of the design methods in use today are based on the fixed-vehicle concept [23].

In the fixed vehicle procedure, the thickness of pavement is governed by the number of repetitions of a standard vehicle or axle load, usually the 18-kip (80-kN) single-axle load. If the axle load is not 18-kip, it must be converted to an 18-kip single axle load by an Equivalent Axle Load Factor (EALF). EALF defines the damage per pass to a pavement by the axle in question relative to the damage per pass of a standard axle load. The design is based on the total number of passes of standard axle load during the design period, defined as the Equivalent Single-Axle Load (ESAL) and can be computed by

$$ESAL = \sum_{i=1}^m F_i n_i \quad \text{Equation 2-2}$$

In which  $m$  is the number of axle load group,  $F_i$  is the EALF for the  $i$ th-axle load group, and  $n_i$  is the number of passes of the  $i$ th-axle load group during the design period.

## 2.5 Summary

Two types of distress have particular reason to take place and these distresses can occur in the asphalt layer. However unlike fatigue cracking, permanent deformation can occur in all layers of the pavement.

## CHAPTER THREE: COMPACTION OF ASPHALT CONCRETE

### 3.1 Introduction

Compaction is defined as “the act or process of compacting; the state of being compacted; to closely unite or pack, to concentrate in a limited area or small space; the densification of material by the application of pressure”. Compaction is thus a process whereby particles are forced together to contact one another at as many “points” as is physically possible with the material, equipment, and procedure being utilized. By this process, inter-particle friction is maximized.

The term degree of compaction is similar to air void [3, 4], while others defined degree of compaction as the ratio of Bulk Specific Gravity (BSG) to Maximum Specific Gravity (MSG) [2, 26]. The degree of compaction of an asphalt pavement depends on the thickness of the pavement layer, the compatibility of the mix, the compaction equipment, the rolling and ambient temperatures and the rolling sequence [27]. Compactability is a concept related to the ease with which a material can be compacted. It is usually expressed in relative terms. All material with a high compactability requires less compaction to achieve the desired void content.

A number of factors affect the compactability of a mixture and these are illustrated in Figure 3.1. These entire factors are part of compaction process as illustrated in Figure 3.2. One important point in the compaction process is the point where the supporting power becomes equal to the applied energy. This defines the point at which no further internal movement of material occur, and the compaction process is terminated [28].

The major variables in the process of compaction into two general categories namely properties of the mix and properties of the roller [1]. The properties of the mix include angle of internal friction and viscosity of the bituminous mix. The properties of the roller include the weight, the length, and the diameter of the roller, the speed of rolling and the number of coverage.



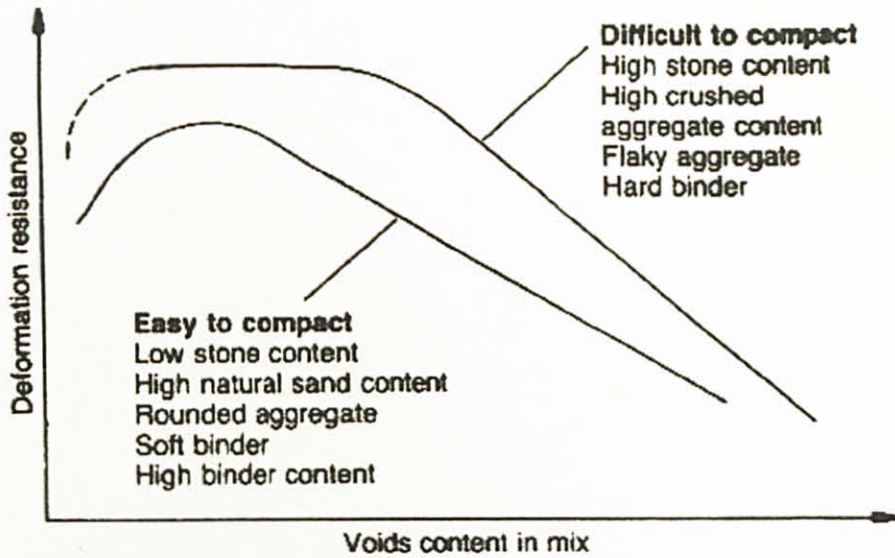


Figure 3.1 Variation in the Compactability of Bituminous Mixtures Due to Change in Composition  
(Source: Hills, 1973)

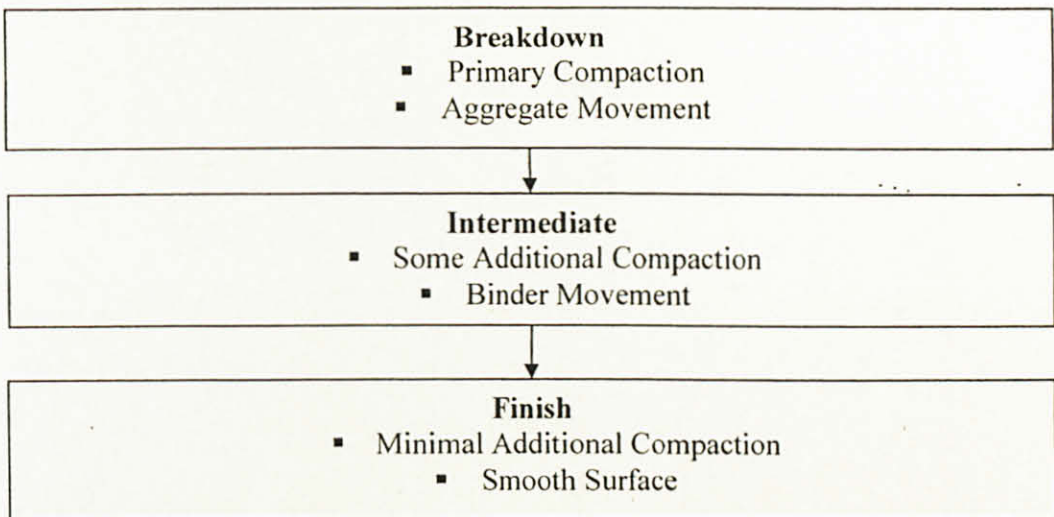


Figure 3.2 Compaction Phases

Factors contributing to harsh mixtures are : low compaction energy, low air temperature, low mix temperature, crushed aggregate, low binder content, Void in the Mineral Aggregate (VMA), modifiers/additives and low base temperature/unstable. Whereas tender mixtures are the result of excessive compaction energy, high air temperature, high mix temperature, moisture in aggregate, thick film, high binder content and low binder stiffness.

Compaction control is more important in dealing with asphalt concretes than with Hot Rolled Asphalt (HRA) [29]. Compaction of asphalt concrete in flexible pavement influences the performance of these pavements, such as resistance of permanent deformation and fatigue cracking [8, 27, 29, 30]. Some compaction issues are caused by the process of compaction itself. Rutting and fatigue cracking have contrary possible causes. If poor compaction is practiced, rutting will be resulted. On the other hand the excessive compaction will generate fatigue cracks. Others issues listed in Table 3.1 are caused by improper compactor set up such as tire pressure too high, amplitude of vibrator too high etc.

Increasing the compaction of asphalt concrete results relative increase the volume of mineral aggregates, which improves the strength of the asphalt mix by increasing the component of its frictional resistance. This appears to be valid only as long as the air voids in the mix do not reach a critical end value (less than 3%). As soon as the percentage of air voids in the mix drops below this critical value, due to further traffic densification, significant losses in the component of frictional resistance start to occur. This condition results in low stiffness value and excessive permanent deformation [31].

Table 3.1 Compaction Issue

No.	Compaction Issues	Possible causes
1	Rutting	<ul style="list-style-type: none"> <li>• Inadequate subgrade or aggregate base compaction</li> <li>• Inadequate asphalt compaction (density too low, air voids too high)</li> </ul>
2	Fatigue Cracks	<ul style="list-style-type: none"> <li>• Improper design or compaction of base aggregate</li> <li>• Excessive compaction of thin asphalt layer (density too high, air voids too low)</li> </ul>
3	Longitudinal Joint Crack	<ul style="list-style-type: none"> <li>• Insufficient material at joint during paving</li> <li>• Improper joint compaction</li> </ul>
4	Tire Marks	<ul style="list-style-type: none"> <li>• Ballast or tire pressure too high</li> <li>• Rolling too hot</li> <li>• Finish rolling too cool</li> <li>• Thick lift, tender mat</li> <li>• Tire too narrow</li> </ul>
5	Asphalt Sticking	<ul style="list-style-type: none"> <li>• Tires too cool</li> <li>• Modifiers in cement</li> <li>• Nonstick emulsion ineffective</li> </ul>
6	Impact Mark	<ul style="list-style-type: none"> <li>• Vibrating too cool</li> <li>• Vibrating on too high an amplitude</li> <li>• Finish rolling too cool</li> <li>• Finish roller too light</li> <li>• Traveling too fast</li> </ul>
7	Crushing/Fracturing Aggregate	<ul style="list-style-type: none"> <li>• Vibrating with too high an amplitude or frequency</li> <li>• Roller too heavy</li> <li>• Vibrating too cool</li> </ul>

### 3.1.1 Compactive Effort

Compactive effort is divided into several compaction variables namely angle of gyration, vertical pressure, and number of revolutions [32]. While, other researcher defined that compactive effort as air void content [18, 20]. These definitions essentially have the same meaning since air void content of mixture is determined by compaction variable.

The efficiency of the compactive effort is a function of the internal resistance of the asphalt concrete. Previous works have shown that this resistance constitutes of aggregate interlock, friction resistance, and viscous resistance [28]. Furthermore, aggregate interlock and friction resistance are the primary functions of the geometry and surface

gyratory compaction [2]. The compaction method used for a mix has a strong influence on its creep behaviors [35]. For this reason, other researchers have compared some laboratory compaction methods. These researches proved that gyratory compactor offered best simulation of field compaction, when compared to other compactors [30, 32, 36]. A good correlation between pavement voids and voids can be obtained in laboratory compacted specimen [32]. In another study, a comparison was made between four laboratory compaction methods, which were Exxon rolling wheel, Texas gyratory, rotating base Marshal hammer and Elf linear kneading compactor [36]. The results obtained further supported that Texas gyratory was able to closely replicate field cores compared to other compactors. Adjustments to certain parameters of the gyratory can produce specimens that better simulate the mechanical properties of pavement cores [37].

### **3.1.5 Mixing and Compaction Temperature**

Temperature of 275°F (135°C) is recommended as the mixing and compaction temperatures for gyratory compactor [2, 36, 38]. This recommendation was supported by other researcher who suggested a mix temperature between 160°F (71°C) and 300°F (149°C) [33]. This is acceptable since this value range give small effects of asphalt viscosity on the relative density and void changes during compaction. The compaction temperature of 135°C can also be applied on specimen that is manually compacted [39]. The percentage void altered is logarithmically proportional to the average asphalt viscosity (temperature) during compaction (shown in Figure 3.3). Other previous studies on the effect of compaction temperature on volumetric properties of asphalt mixtures show that specimens could have the same volumetric properties over a very wide range of compaction temperature [40, 41]. Temperature range between 116°C to 173°C is shown as the suitable range of compaction temperature [41].

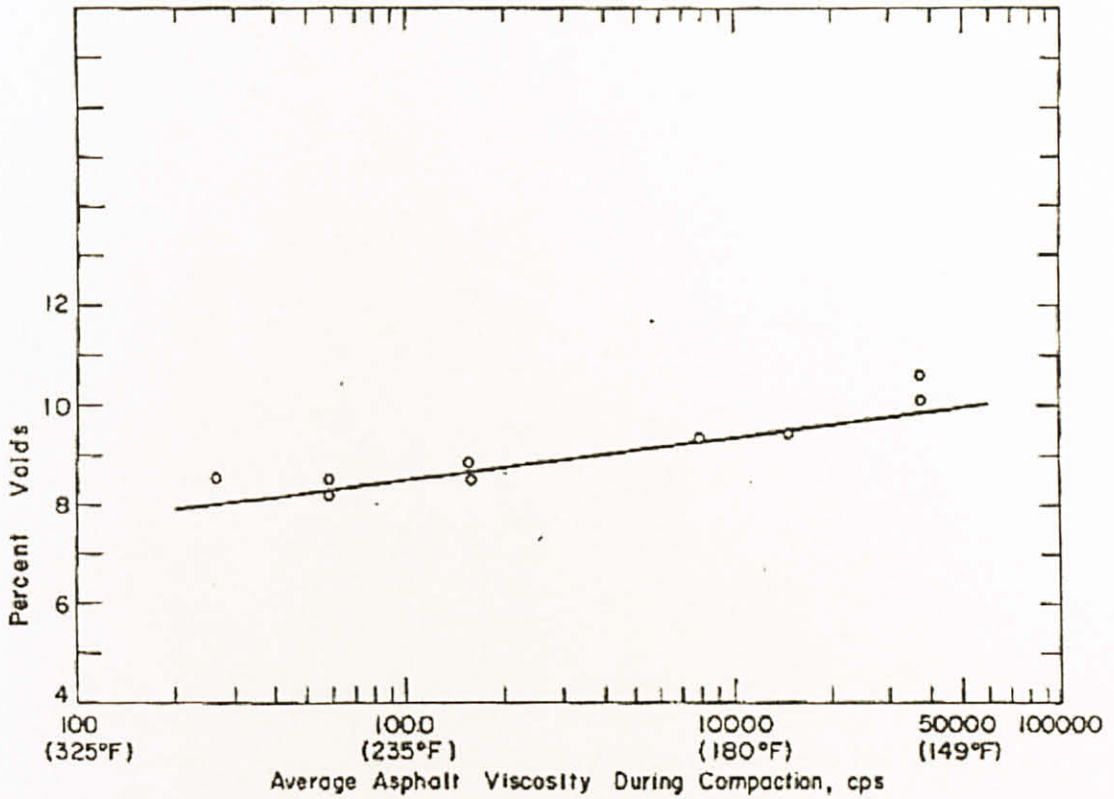


Figure 3.3 Percent Voids vs. Average Asphalt Viscosity  
(Source: Hills, 1973)

### 3.1.6 Size of Gyratory Mould

Size of gyratory mould influences the workability of specimen preparation and amount of using material. Researchers need to choose the right size of mould to produce specimens efficiently. Gyratory is capable of compacting both 150 mm (6 in.) and 100 mm (4 in.) diameter cylindrical specimens. Figure 3.4 exhibits both 150 and 100 mm stainless steel cylinder moulds that may be used with gyratory to compact HMA specimen.

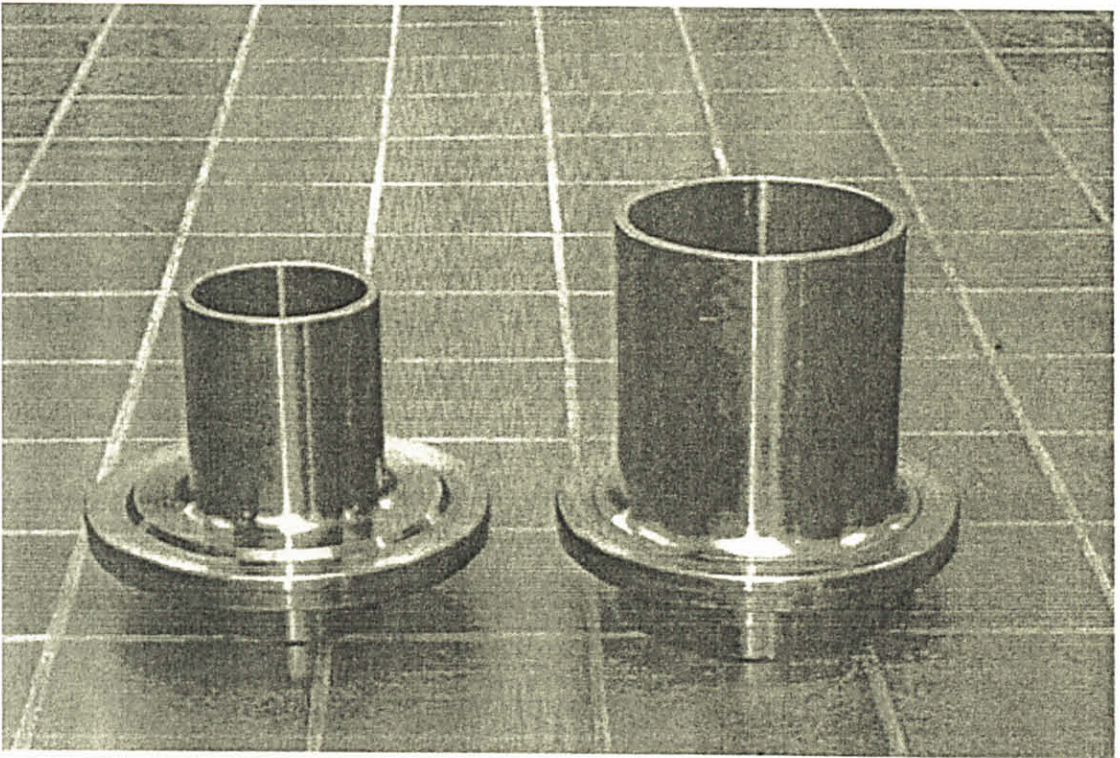


Figure 3.4 100 mm and 150 mm Diameter Cylinder Molds  
(Source: Jackson, 2003)

Previous research has been conducted to evaluate both of these moulds for testing HMA. One study evaluated large stone asphalt mix design (mixes containing aggregate larger than one inch) to determine the preferred specimen size [42]. Laboratory produced HMA specimens were compacted at 150 and 100 mm diameters using both a modified Marshall Impact Hammer and the Gyratory Testing Machine (GTM). The research recommended the use of 150-mm-diameter specimens for the design of large stone asphalt mixes.

The rate of densification of the HMA in the 100 mm mould is very similar to that recorded for the 150 mm mould [43]. This is shown in Figure 3.5. Both of these curves are parallel and nearly overlapping. Since different mould sizes do not have significant engineering, Jackson proposed the use of 100-mm-diameter specimens instead of the 150-mm-diameter specimens for verification testing of HMA. It should be noted that this recommendation is limited to mixes with a maximum aggregate size of 25.4 mm (1 in.) or less.

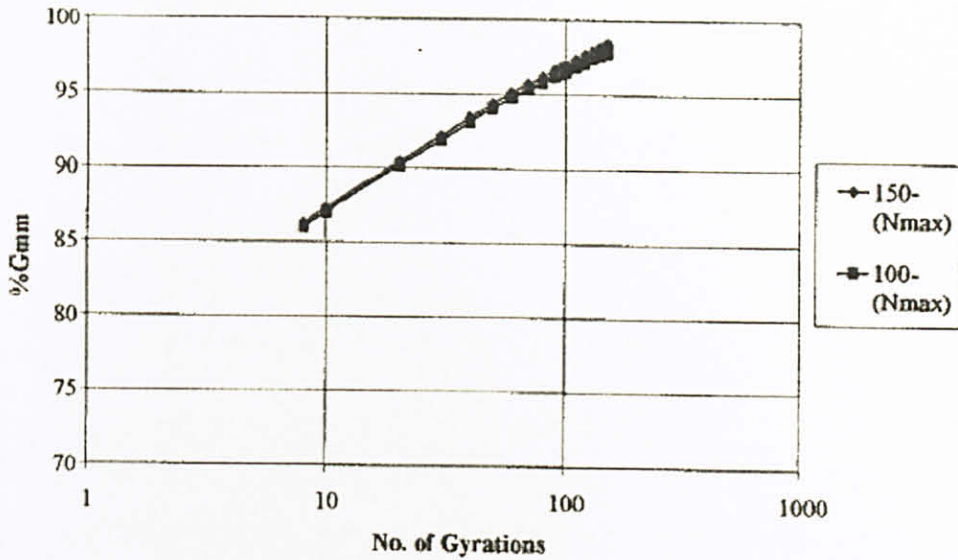


Figure 3.5 Typical %Gmm vs. Gyration Curve  
(Source: Jackson, 2003)

Another researcher categorizes the size of mould by the nominal maximum aggregate size of the mixture [2]. Nominal maximum aggregate size is defined as one sieve size larger than the first sieve that can retain more than 10 percent of aggregate. The 100 mm mould was used for nominal mixture of 19.0 mm (3/4 in.) and less, whereas the 150 mm mould was used for greater than 19.0 mm (3/4 in.) nominal mixtures.

There are three potential advantages associated with the use of the 100-mm-diameter cylinder mould [43]. First, the required sample size is reduced by 40%; thus, time of preparation, storage space and transportation of materials are similarly reduced. Second, it is possible to conduct conventional laboratory testing with the 100-mm-diameter specimen. Third, the majority of surface designs make use of 25.4 mm (1 in.) or smaller maximum aggregate size; thus, the larger 150 mm mould is often not necessary to be in compliance with ASTM and AASHTO requirements.

### 3.1.7 Number of Gyration

Typical number of gyrations used for evaluation are 30 and 60 revolutions, however the gyratory manufacturer has indicated a preference for evaluation at a point when the rate of compaction decreases to a minimum value of 16 kg/m<sup>3</sup> per 100 revolutions [32]. Strategic Highway Research Program (SHRP) compaction protocol defined gyrations at

89 and 98 percent densities as threshold limits for an acceptable mix. This specification is supported by another researcher who proved that the maximum number of gyration that ensures complete densification of the mix is 230 [2].

### 3.2 Air Void/ Porosity

Asphalt mixtures have three types of void; voids in the total mix (VTM), voids in the mineral aggregate (VMA) and voids filled with asphalt (VFA). The most important property in construction is VTM (air void). Air void is defined as the total volume of air between the coated aggregate particles of the compacted mixture. This does not include air in the aggregate pores trapped beneath the binder films. Figure 3.6 depicts a common definition of air void in mixture.

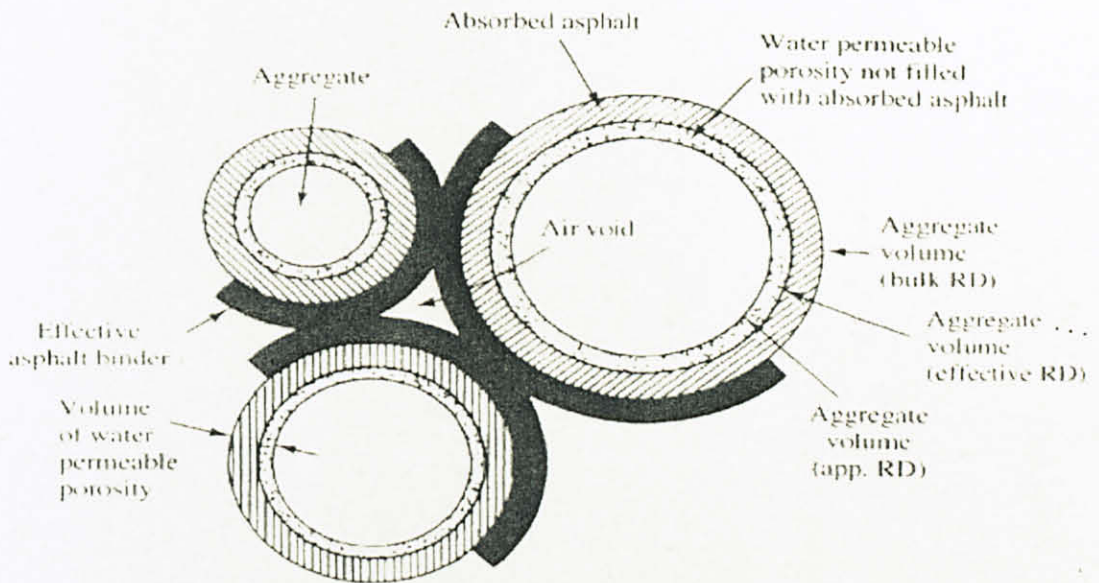


Figure 3.6 Air Void in Mixture  
(Source: Napiah, 1993)

Some researches have shown that percent compaction (or void content) is the most significant factor affecting mix performance [10, 13, 19, 20, 29, 44-47]. As shown in Table 3.2, an increase in void content is associated with a decrease in modulus, fatigue life, and resistance to permanent deformation.



Table 3.2 Effect of Compaction on Hot Mix Asphalt Pavement

Compaction Rating	Void Content (%)	Resilient Modulus (MPa)	Horizontal Strain at Bottom (micro strain)	Est. Fatigue Life (msa)	Vertical Strain at Subgrade Surface (microstrain)	Estimation Perm Deform Life (msa)
Excellent	4	3370	75	110	200	48
Good	8	2060	100	12	245	21
Poor	12	1430	120	2.6	280	12

Using the simplified Design Method developed at the University of Nottingham, Figure 3.7 demonstrates the potential increase in performance with reduction in air voids level [10]. Accordingly, control of HMA compaction during construction is essential to achieve maximum performance. This is due to in-place air void is only partly a function of design and manufacture, and more of an outcome of compaction achieved during placing [44-46]. If the pavement received insufficient compaction during construction, there would definitely be a major effect on the final void level after traffic exposure [32]. Air void should not too high or too low. If air void is too high it will increase the likelihood of asphalt stripping, accelerated oxidation, and rapid deterioration. On the other hand, if the air void is too low, it will increase the likelihood of bleeding, shear flow, and permanent deformation (i.e. rutting) in the wheel paths. In low air void mixture, the mixture will become over filled with bitumen, pushing the aggregate apart and the mixture will rut very quickly. In other words, air voids act as stress concentration points [11, 20, 46].

Voids are primarily controlled by bitumen content, compactive effort during construction and additional compaction under traffic [1, 13]. The most critical factor is the bitumen content, because a deviation from the optimum bitumen content of 0.5 percent could result in either too much or too little bitumen being used. Too much bitumen produces a mixture with low air voids that is susceptible to rutting. On the other hand, low bitumen content produces a mixture that under-compacts (has high air voids) and is likely to ravel [2]. Determination of the percentage of voids is of paramount importance, because such information may provide an indication of the behavior of a compacted surface under traffic and climate [3].

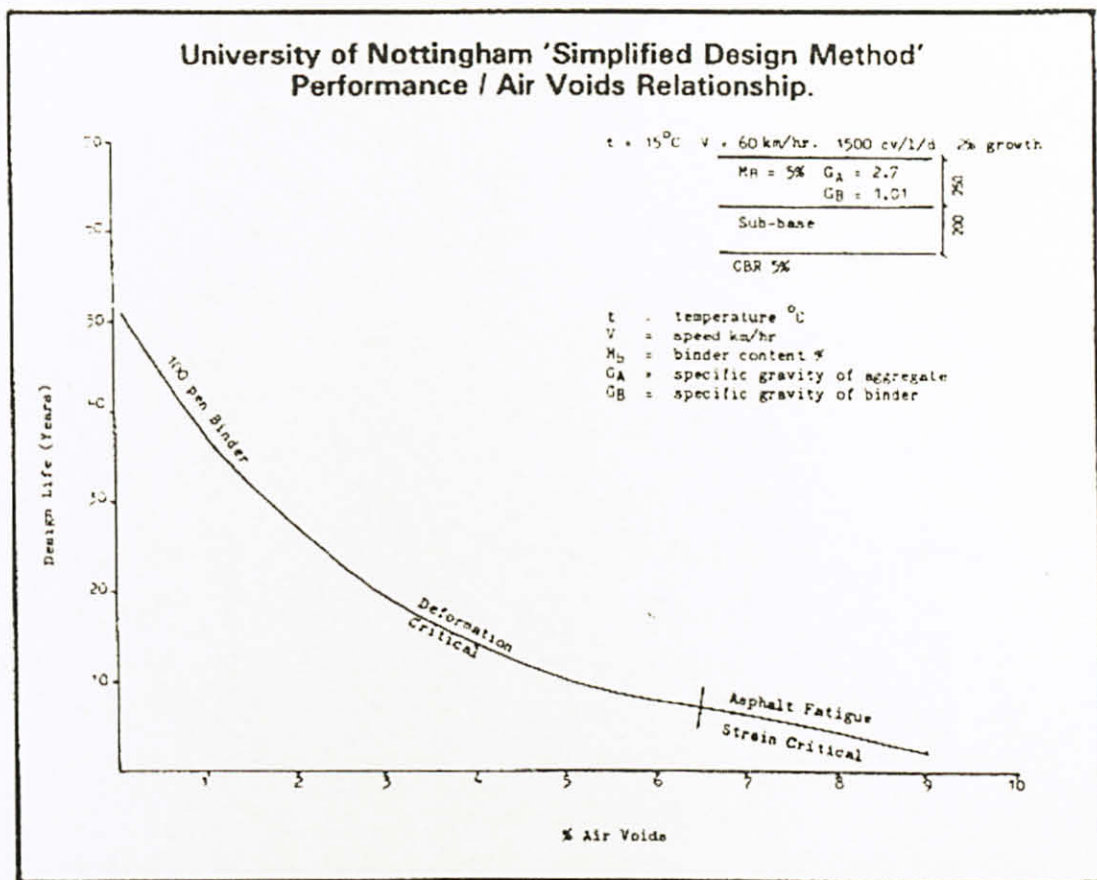


Figure 3.7 Design Life vs. % Air Void  
(Source: McNicol, 1986)

Air void content can be determined using various specific gravity of aggregate. Specific gravity is the ratio of the weight in air of a unit volume of a material to the weight of an equal volume of water at the same temperature. When air void of bituminous mixtures is calculated on the basis of the Bulk Specific Gravity (BSG) aggregate, it is assumed that no bitumen is absorbed by the aggregate. If some bitumen is absorbed, the calculated air void obviously will be lower than the true value and, in the case of highly absorbent aggregate; the calculated air void can be doubled.

When air void is calculated on the basis of the Apparent Specific Gravity aggregate (ASG), it is implied that the water permeable voids in the aggregates are filled with bitumen. While this condition sometimes could exist, and while some aggregates no doubt have a greater affinity for bitumen than for water, it is generally accepted that the water permeable voids usually are filled only partially with bitumen. The calculated air void, therefore, would be expected to be higher than the true value in most cases.

When void contents are based on Effective Specific Gravity (ESG) aggregate, the value would be lower than the aggregate's ASG and higher than its BSG. ESG is the ratio of the weight of dry aggregate to the weight of an equal volume of water, excluding the voids permeable to asphalt binder. The three types of specific gravity aggregates are depicted in Figure 3.6.

The other term that has correlation with air void is density. Density is defined as: "the quality or state of being dense; the quantity per unit volume as the weight of solids in a unit volume of material". Thus, density is simply a measure of the amount of solids in a unit volume of material. Density is equal to specific gravity of the compacted mixture (density of water is assumed as equal to one). Density is relative compaction of HMA, which is typically measured in the laboratory.

Density and compaction differ; unfortunately, this difference is often overlooked or ignored. Two aggregate materials may have the same density, but different degree of compaction. A material with one gradation of aggregate that is well compacted may have the same unit weight as another aggregate, of different gradation and poorly compacted. Good compaction generally results in good performance, whereas high density may or may not result in good performance depending on the degree of compaction achieved [26].

Although density and compaction are different, density specifications are used to judge the acceptability of compaction during construction [46]. A density specification represents a comparison between the in-place density of the pavement that is achieved after final compaction, and a reference density. The magnitude of density of HMA depends on the compaction level of the mixture. The bulk density ( $G_{mb}$ ) is typically used to represent density of compacted HMA. Bulk specific gravity is measured in the laboratory. The maximum theoretical density ( $G_{mm}$ ) has the same mass-to-volume relationship as  $G_{mb}$ ; however, it is determined using a loose sample of HMA. Thus, the volume of the air is not included. The  $G_{mm}$  is typically measured in the laboratory.

There are three primary methods of specifying field density namely percent of laboratory density, percent of Theoretical Maximum Density (TMD) and percent of control strip [13]. In the first method, the field density is expressed relative to the bulk density of a

laboratory compacted mixture as shown in Table 3.3. The field material is compacted until its density is equal to the laboratory density. Estimation of in-place air void must allow air voids in the laboratory compacted mix. Three requirements must be met to obtain satisfactory compaction. First, laboratory samples are compacted during construction to establish reference density. Second, correct laboratory compaction techniques should be used and lastly, minimum compaction requirement should be set to ensure that in-place air voids after compaction do not exceed approximately 8%. Typically, specifications will require at least 95% of laboratory density or, in some cases, 98%. Some specifications do not allow mixes to be compacted to a density greater than 100% of laboratory density. This method requires correction factor. The correction factor is the difference between field density and laboratory density.

Based on the second method, density is determined by comparing the bulk density of the in-place asphalt mixture (measured after compaction) to the TMD. In other words, density is expressed relative to the TMD. Relative density is a direct measure of air void as shown in Table 3.3. For instance, a mixture compacted to 93% of TMD will have 7% percent air voids. Generally, during construction, the asphalt mixture will be compacted to some minimum percentage of TMD. Shortcoming of this method is encouraging higher asphalt content and higher filler content. But as long as the process is properly monitored, satisfactory compaction will be obtained.

Another method of determining density is by comparing the bulk density of the in-place asphalt mixture to the bulk density of a control strip that has been constructed earlier. The control strip is compacted to some minimum percentage of the standard laboratory density or to some minimum percentage of TMD. In this method, if there are any significant changes in the mix during construction, a new test strip should be constructed and evaluated. But as long as sufficient testing is performed to ensure that the initial in-place voids and the final in-place voids are acceptable, a satisfactory compaction will be obtained. All three methods of determining density will provide acceptable results if properly used but the TMD Method has been grossly misused [13]. Field compaction can be measured in terms of TMD rather than relative to some laboratory compactive effort [20].

Table 3.3 In-place Air Voids and Density Ratio

In-place Air Voids (%)	Density Ratio (Relative Compaction)	
	Relative to Maximum density	Relative to laboratory density of 5% voids
4	96	101
5	95	100
6	94	99
10	90	95
14	86	91

Two methods of measuring bulk density of asphalt mixture are physical measurements of cores and nuclear gage. The nuclear gage is fast and non-destructive but it is not as accurate as the core method [13].

### 3.2.1 Initial and Final Air Void

The initial air void content is determined by using one of the three density specification methods. In order to achieve good compaction, Brown recommended that the initial in-place voids must be below 8%. However, there is a disagreement by Asphalt Institute, which suggested that an initial in-place void of 7% to 9% at construction is a reasonable range. The high initial voids may result in increased oxidation, causing more cracking and raveling if not subjected to significant traffic to provide further compaction. If voids are high during construction, more compactive effort, improved roller patterns, or modified mix design should be used to increase density [13].

The final in-place air voids are estimated based on the mix design and field quality control testing. The only way to estimate the final in-place voids is to compact samples in the laboratory using the specified technique and to measure the voids [13]. The final in-place air voids must be above approximately 3% [13]. A similar assumption was used by two other researchers. One designed the pavement to have final air voids of 3% to 5% [2] while other determined the pavement to have final air void of 4-7% [30].

### 3.2.2 Air Void vs. Permanent Deformation

Air void content affects resistance to permanent deformation. When air void content increases, rutting resistance decreases [48] but when air void content are less than 3%, the rutting potential of mixes increases [1, 4]. At low air voids (less than about 2%), the binder almost totally fills the void space between the aggregate particles, so that the mix acts as fluid and is less resistance to rutting when subjected to heavy traffic [44]. Poorly compacted mixes also have less resistance to rutting due to a weaker structure and secondary consolidation under traffic. Figure 3.8 gives an indication of relative rutting rate of a mix designed for 5% voids and compacted to different void levels.

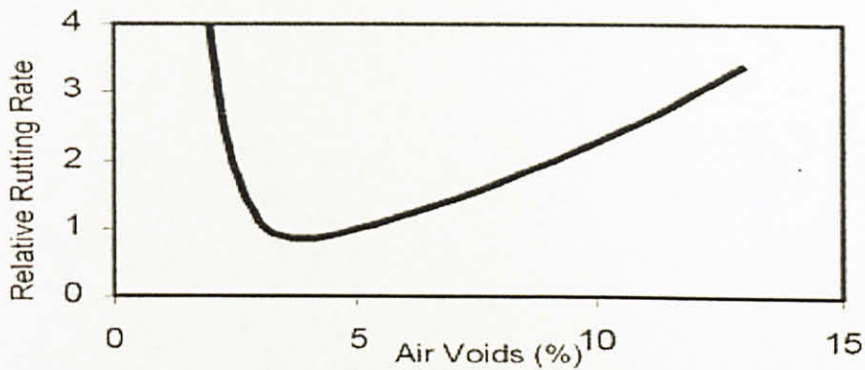


Figure 3.8 Relative Rutting vs. Air Void  
(Source: AAPA, 1999)

An air void content of 5%-6% in the field for an asphalt concrete seems like a reasonable target to realize good rutting resistance but still provides a margin of safety against the instability associated with lower void content mixes. This improved performance is caused by the ability to increase the interlock of aggregate particles in the mix [8]. The wider range of target air void has been proven by other researchers. They stated that good compaction with a target void of 4%-7% should increase the resistance of asphaltic-bound layers to deformation and improves their durability [30]. A two-fold increase in the estimated permanent deformation of a pavement appeared when the void content is reduced from 8% to 4% percent [1] (see Table 3.2).

Other researcher gives a clear evidence of the effect of air void content on resistance of mixtures to creep loads [18]. They stated that more air voids translate to weaker mixtures. The creep modulus decreases with increasing air voids. They used compressive and shear

repetitive test. The cyclic loading was characterized by a square load pulse of 0.1 sec followed by a rest period of 0.9 sec.

The extended study by other researcher determined the effect of air-void content on dynamic modulus. For the two test temperatures (20° C and 40° C) and throughout the frequency range (0.01 to 16 Hz), mixtures with higher air voids were less stiff (as indicated by smaller dynamic moduli) than those with lower air voids [18].

An analysis of results from a full scale pavement test track in Nevada, referred to as WesTrack, showed that a reduction in air void content improved the rut resistance of most asphalt pavement sections. The study illustrates the influence of air void content on rutting. The test was carried out on mixtures with various air voids. Then, the number of ESAL to produce 15 mm rut depth was recorded. Under these conditions, a 1.7-fold increase in rut resistance can be expected from a drop in air void content from 8% to 5%. [8]. The illustration is shown in Figure 3.9.

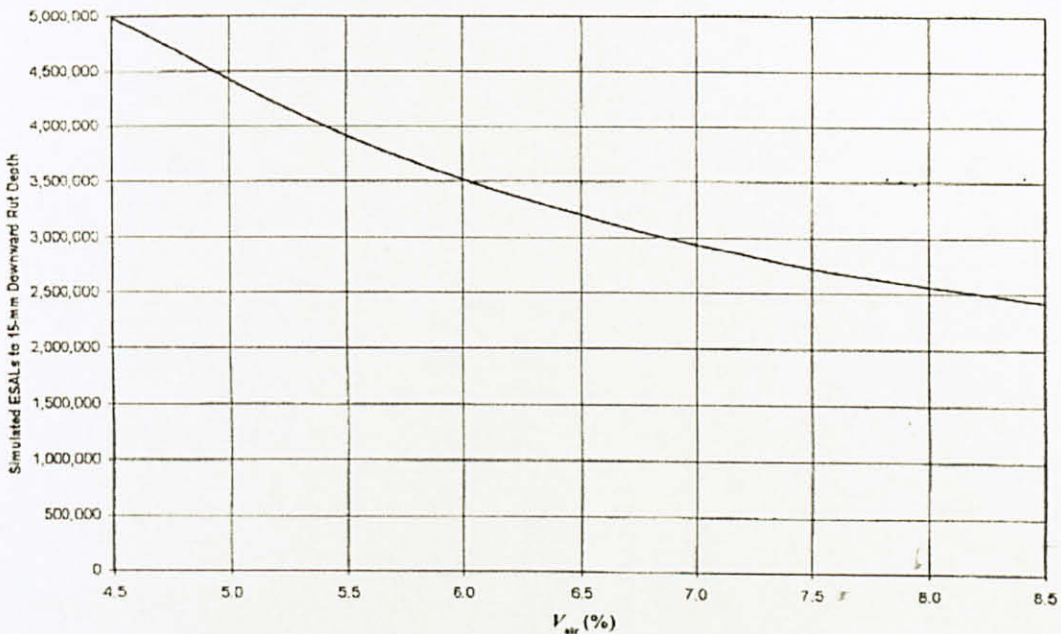


Figure 3.9 Effect of Mix Variables on Estimated ESALs to 15 mm (0.6 in) Rut depth for Various Range in Air-Void Contents  
(Source: Santucci, 2001)

A 2% increase in air void content (8% to 10%) would increase permanent shear strain by nearly 42%, with majority of the permanent shear strain occurring between 9% and 10% air void content [7]. The result, as shown in Figure 3.10, shows the relationship between

permanent shear strain and air void content. Figure 3.10 indicates that under the same loading condition, the relationship between permanent shear strain and air void content can be described by a polynomial function.

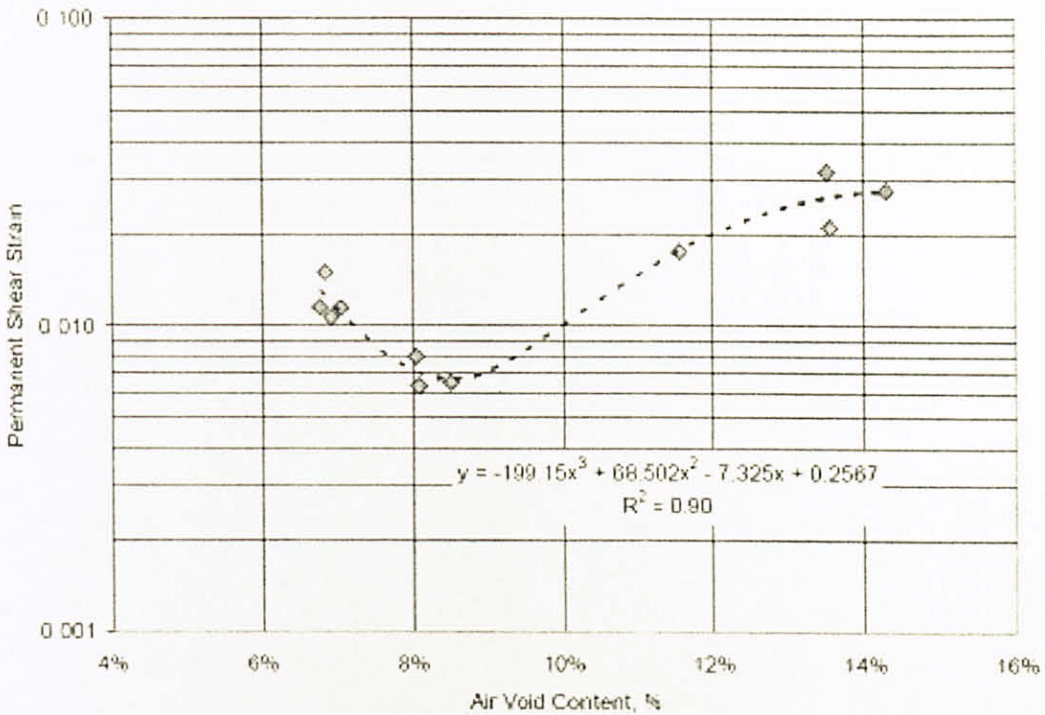


Figure 3.10 Relationship between Permanent Shear Strain and Air Void Content  
(Source: Zhou, 2006)

A 3% decrease in void content reduced deformation by about 2 mm [25]. In his study, the rut depth developed after 1000 cycles of loading decreased sharply with improved compaction.

### 3.2.3 Air Void vs. Fatigue Life

One mix characteristic that has a major effect on the fatigue resistance of asphalt concrete pavement structures, regardless of pavement thickness, is air void content. Laboratory test results from earlier study suggest that fatigue life can be improved by an order of 10 times by reducing air void content from 10% to 5% as shown in Figure 3.11 [20]. Analysis of results from a full scale pavement testing at WesTrack, shows that about a 3 fold increase in fatigue life can be expected when asphalt mix void content dropped from 8% to 5% as shown in Figure 3.12 [20].



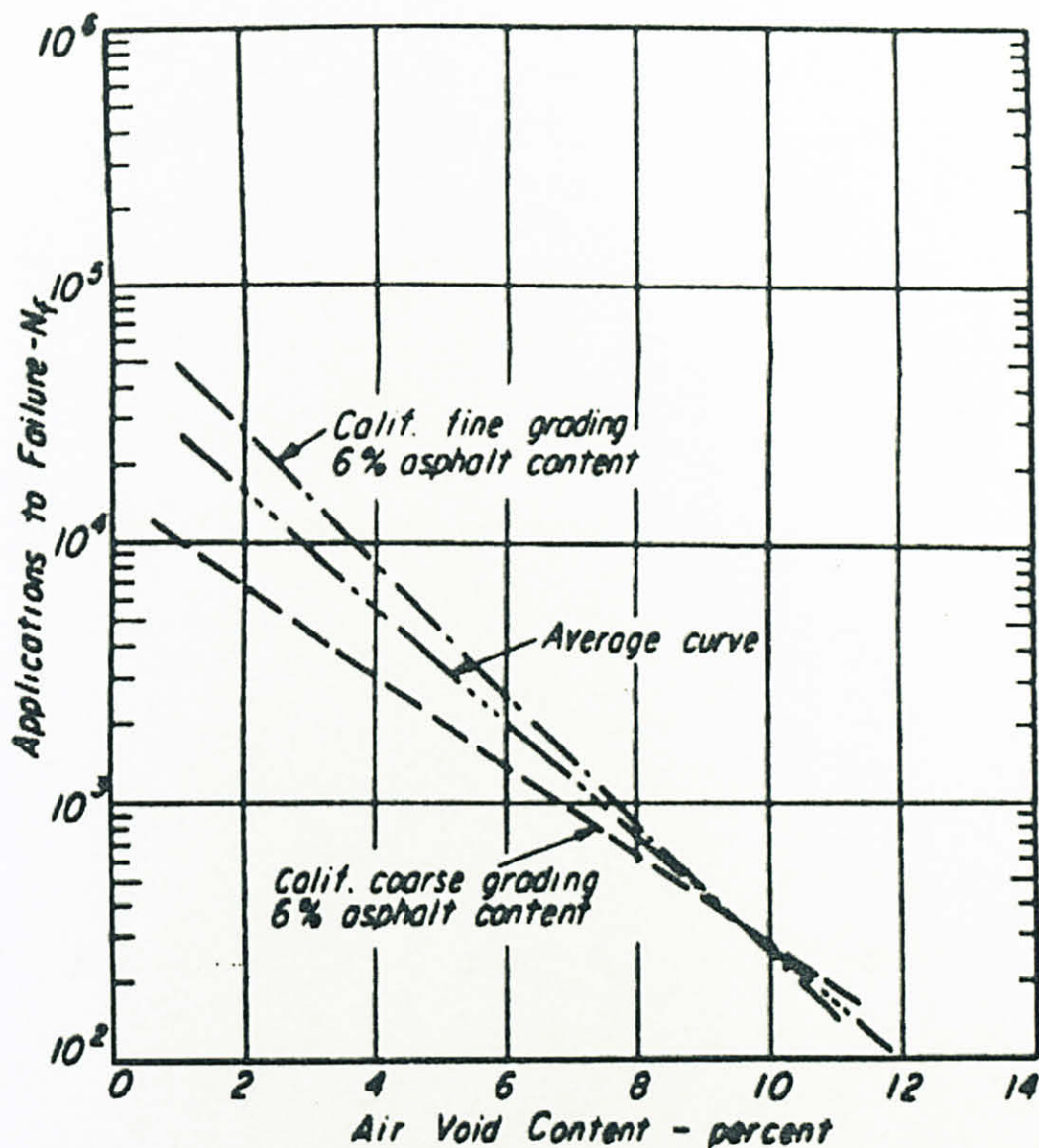


Figure 3.11 Influence of Air Void Content on Fatigue Performance  
(Source: Santucci, 1998)

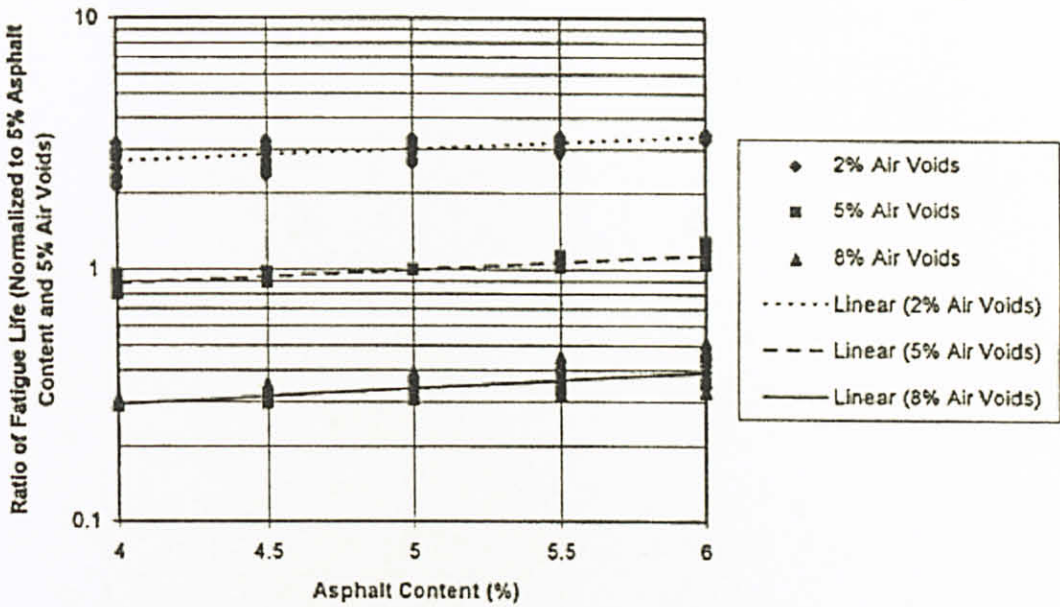


Figure 3.12 Effect of Asphalt and Air Void Contents on Simulated, Fatigue-Life Ratio for 270 Mix-Pavement Combinations  
(Source: Santucci, 1998)

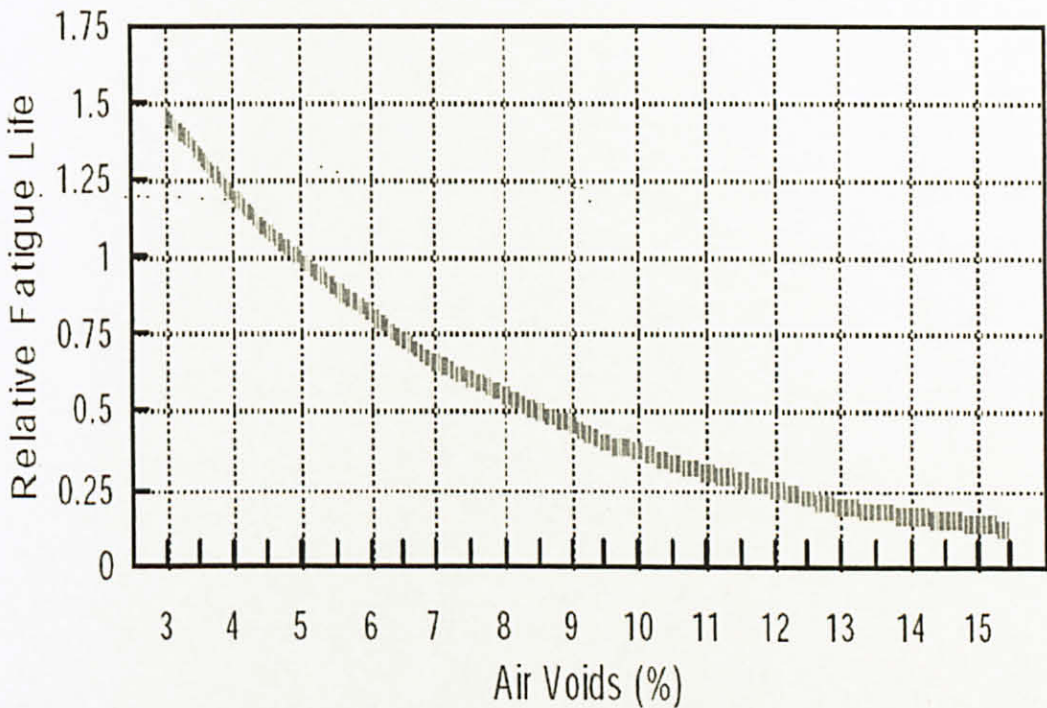


Figure 3.13 Relative Fatigue Life vs. Air Voids  
(Source: AAPA, 1999)

Similarly, another study by AAPA concluded that fatigue life, or resistance to cracking under repeated load, is directly proportional to the compaction level [44]. Figure 3.13 shows results of fatigue testing of the same mix relative to compaction at 5% voids. In

this case an increase of air voids from 5% to 8% has resulted in a 50% reduction in fatigue life.

An air void content of 5%-6% in the field for an asphalt concrete seems like a reasonable target to realize good fatigue resistance but still provides a margin of safety against the instability associated with lower void content mixes [8].

A study on how compaction, measured by air voids, influences the performance of asphalt concrete pavement surfaces [6]. The study found that a 1% increase in air void tends to produce approximately a 10% loss in pavement life. They used base-course with an air void level of 7%, and the data were collected from 48 state highway agencies in the United States. The analysis in this study was done on the basis of two performance indicators, namely fatigue cracking and aging.

A 3-fold increase in pavement fatigue life can be realized by increasing relative compaction from 95% to 98% or, in essence, reducing air void content in the asphalt concrete from approximately 8%-10% to a range of 5%-7% [8].

A 50% reduction in void content from 8% to 4% results in nearly a 10 fold increase in fatigue life [1]. It used asphalt institute equation to calculate the fatigue values shown in Table 3.2. The table clearly shows the profound effect void content has on fatigue life.

The other work also shows that a 1% increase (from 8% to 9%) in air void content would result in a decrease in fatigue life by approximately 41% [7]. The study grouped air void content range in terms of low (6.6%-7.8%), medium (8.1%-8.9%), and high (9.1%-11.1%). The number of cycle to failure for a specimen with known air void content and strain level can be estimated from Figure 3.14.

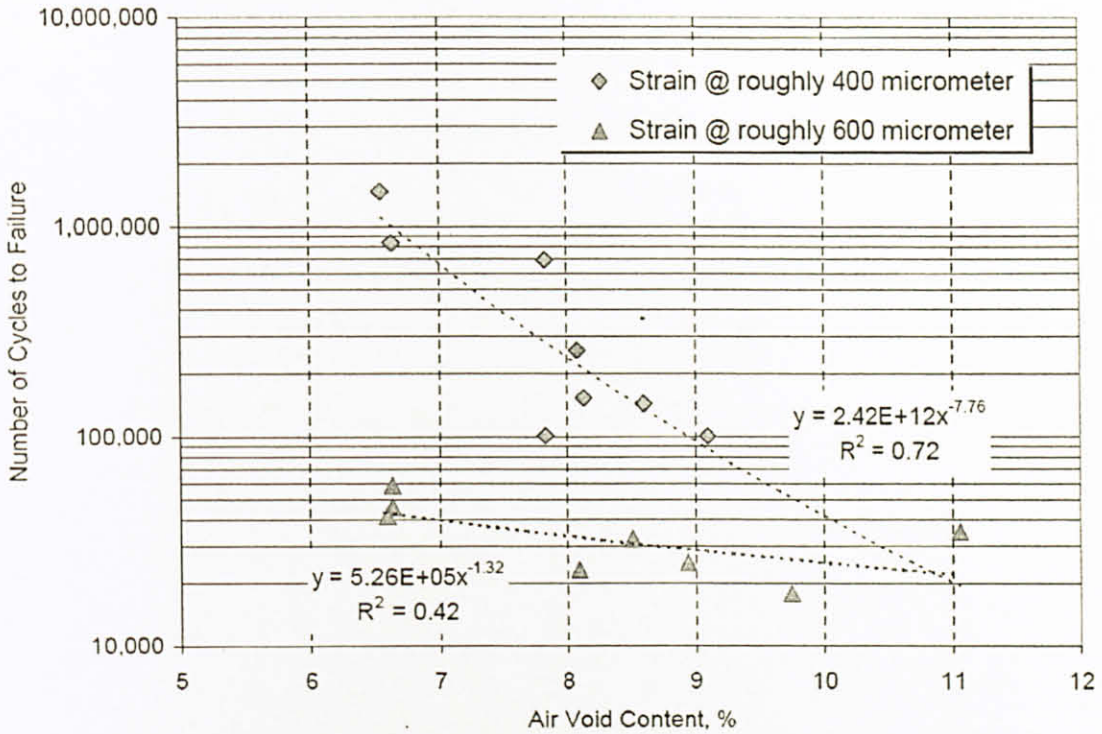


Figure 3.14 Relationship between Cycle to Failure, Air Void Content, and Strain Level (Source: Santucci, 2001)

A mathematical model is developed showing that increments in strain level and stiffness values result in a decrease in the number of cycles to failure, whereas a decrease in air void will induce a higher fatigue life [49]. Unfortunately, this study did not quantify the effect of air void on fatigue life: The mathematical model developed is as follows,

$$N_f = 2.911 \times 10^{-2} \left( \frac{1}{\epsilon_t} \right)^{4.305} \left( \frac{1}{E} \right)^{1.610} \left( \frac{V_b}{V_b + AV} \right)^{11.043} \quad \text{Equation 3-1}$$

$$V_b = 100x \frac{G_{mb} x P_{ac}}{G_b} \quad \text{Equation 3-2}$$

Where  $G_{mb}$  is bulk density of the mixture;  $P_{ac}$  is percent of asphalt by total weight of mix; and  $G_b$  is bulk specific gravity of the asphalt binder, the stiffness  $E$  is in Mega Pascals.

Another study concluded that an increase in air void content shortens the fatigue life. His study was done at two temperatures, 20°C and 0°C [34].

### 3.3 Summary

Compaction condition can be represented by air void of mixture. Compaction condition affects the performance of pavement, especially rutting and fatigue. This effect has been proven by some studies. Compaction is influenced by internal and external factors. Based on the work by previous researchers, it was found that the temperature that less effects air voids changes during compaction was 135°C (275°F), gyration was 230. The minimum pressure to manufacture the specimen was 300 bar. The efficiency of material can be achieved by using 100 mm mould for the compaction.

## CHAPTER FOUR: PERFORMANCE TEST

### 4.1 Introduction

Performance test is used to relate laboratory mix design to actual field performance. As with asphalt binder characterization, the challenge in Hot Mix Asphalt (HMA) performance testing is to develop a physical test that can satisfactorily characterize key HMA performance parameters and how these parameters change throughout the life of a pavement. These key parameters are:

i. Deformation resistance (rutting)

Rutting is a key performance parameter that can depend largely on HMA mix design. Therefore, most performance test efforts are concentrated on deformation resistance prediction.

ii. Fatigue life

Fatigue life is a key performance parameter that depends more on the structural design and subgrade support than mix design.

iii. Tensile strength.

Tensile strength can be related to HMA cracking-especially at low temperatures.

iv. Stiffness

HMA's stress-strain relationship, as characterized by elastic or resilient modulus, is an important characteristic. Although the elastic modulus of various HMA mix type is rather well defined, a test can determine how elastic and resilient modulus vary with temperature. Many deformation resistance tests can also determine elastic or resilient modulus.

### 4.2 Stiffness Modulus

There are three basic mechanical models of material namely elastic, viscous, and plastic [23]. Each model has a characteristic of the strain. The strains due to elasticity are fully recoverable and independent of time. This means that in a loading/ unloading cycle, no permanent strains are generated, and this is independent of the rate of loading and

unloading. The strains due to viscosity are irrecoverable (permanent) and time dependent. Their magnitude depends on the load duration and the rate of loading and unloading. The strains due to plasticity are permanent but time independent. No matter what the rate of loading and unloading, the same magnitude of permanent strains is obtained for the same loading history.

Asphalt concrete can show plastic deformation, which at a moderate temperature (21°C), is proportional to stress [39]. All strain components dependent upon test temperature [39].

The stiffness of a pavement is directly related to the resulting horizontal and vertical strains in the pavement resulting from vehicle loads. Pavements with higher stiffness values exhibit lower strains under the same vehicle loads. Horizontal and vertical strains are important in predicting pavement performance because they directly correlate to fatigue and permanent deformation [1].

Stiffness modulus is defined by stress over strain. This modulus, which is analogous to Young's modulus for elastic material, can be used to describe the mechanical properties of visco-elastic materials. The strain is a function of the time of loading and temperature [38]. Enough stiffness (load spreading ability) can distribute the stresses and strains developed in the entire structure over a wider area [50].

Several types of moduli have been used to represent the stiffness of asphalt concrete mixtures. Three of these are resilient, dynamic, and complex [23, 30]. Among the three, the resilient modulus is most commonly used for asphalt concrete mixture evaluation [30].

#### **4.2.1 The Resilient Modulus**

The resilient modulus is the elastic modulus for paving material. Paving materials are not elastic because they experience some permanent deformation after each load application. However, if the load is small compared to the strength of the material and is repeated for a large number of times, the deformation under each load repetition is nearly completely recoverable (proportional to the load) and can be considered elastic [23].

Figure 4.1 shows the straining of a specimen under a repeated load test. At the initial stage of load applications, there is considerable permanent deformation, as indicated by the plastic strain in the figure. As the number of repetitions increases, the plastic strain due to each load repetition decreases. After 100 to 200 repetitions, the strain is practically all recoverable, as indicated by  $\epsilon_r$  in the figure.

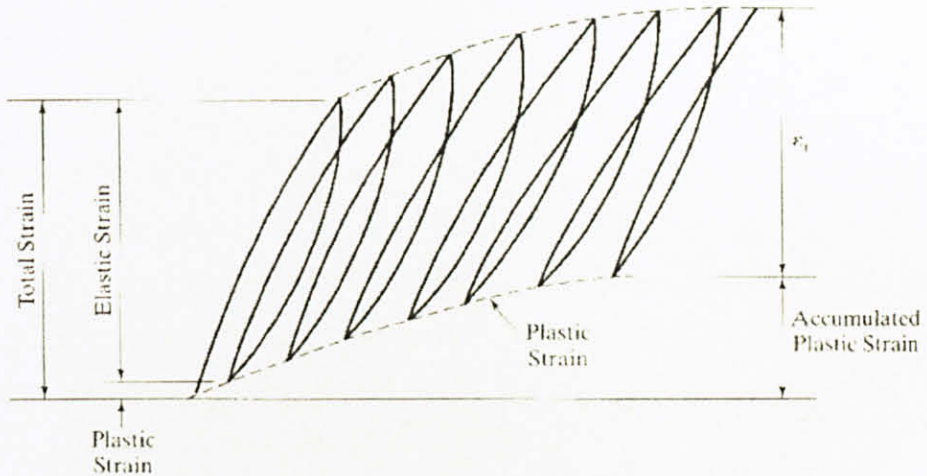


Figure 4.1 Strain Under Repeated Loads  
(Source: Huang, 2004)

The resilient modulus is determined by using a repetitive load of one cycle, after which measurement of the applied load and recoverable deformation is conducted [23, 30]. This modulus, based on the recoverable strain under repeated loads,  $M_R$ , is defined as

$$M_R = \frac{\sigma_d}{\epsilon_r} \quad \text{Equation 4-1}$$

where  $\sigma_d$  is the deviator stress, which is the axial stress in an unconfined compression test.

#### 4.2.2 The Dynamic Complex Modulus (Dynamic Modulus)

The difference between a resilient modulus test and a complex modulus test for bituminous mixtures is that the former uses loadings of any waveform with a given rest period, while the latter applies a sinusoidal or haversine loading with no rest period [23]. The complex modulus can be obtained from the stiffness modulus and phase angle. The stiffness modulus obtained from Shell nomographs is actually the dynamic modulus.



### 4.2.3 The Dynamic Stiffness Modulus

The elastic modulus based on the resilient deformation of the beam at the 200<sup>th</sup> repetition is called the dynamic stiffness modulus. The elastic model suggests that the tensile strain at the bottom of the roadbase decreases almost linearly with increasing dynamic stiffness of the bituminous material [25].

The relationship between dynamic stiffness modulus and air void can be expressed by an exponential decay function that is statistically valid as shown in Figure 4.2. The constants of the function are influenced by binder viscosity and mode of compaction [45]. Additionally, the relationship between dynamic stiffness modulus and air void can also be expressed by a linear function [10, 25]. The function difference between both studies is caused by percent variation of bitumen included in the latter study. Figure 4.3 shows dynamic stiffness measured in both 3-point bending and uniaxial loading on beams containing a wide range of binder contents. It is evident that a 3 % decrease in void content increases stiffness by 30 %, irrespective of binder content.

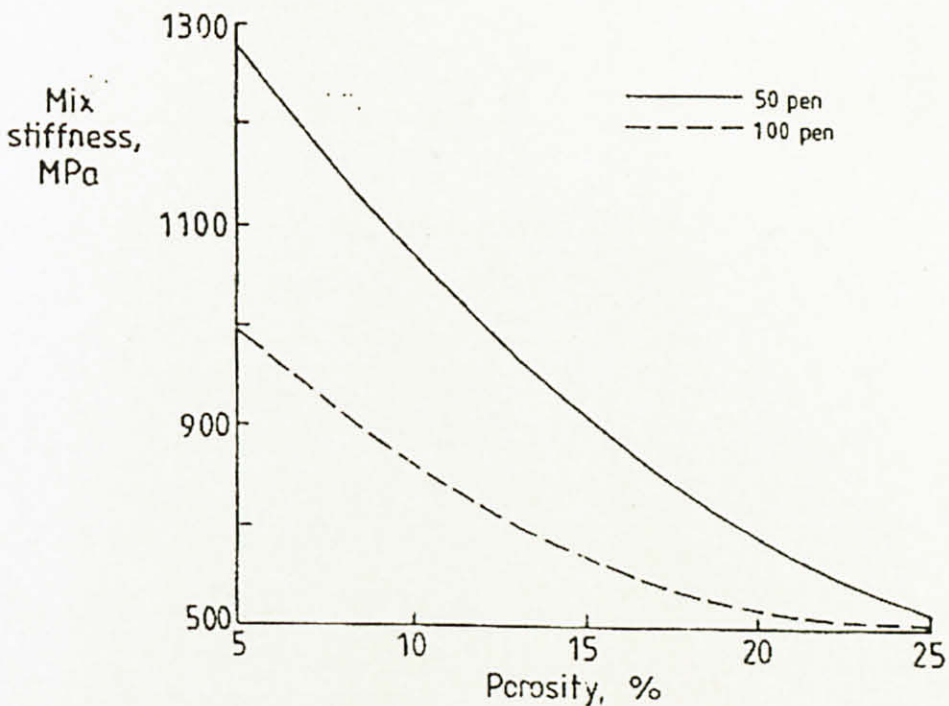


Figure 4.2 Relation between Dynamic Stiffness and Porosity  
(Source: Cabrera, 1990)

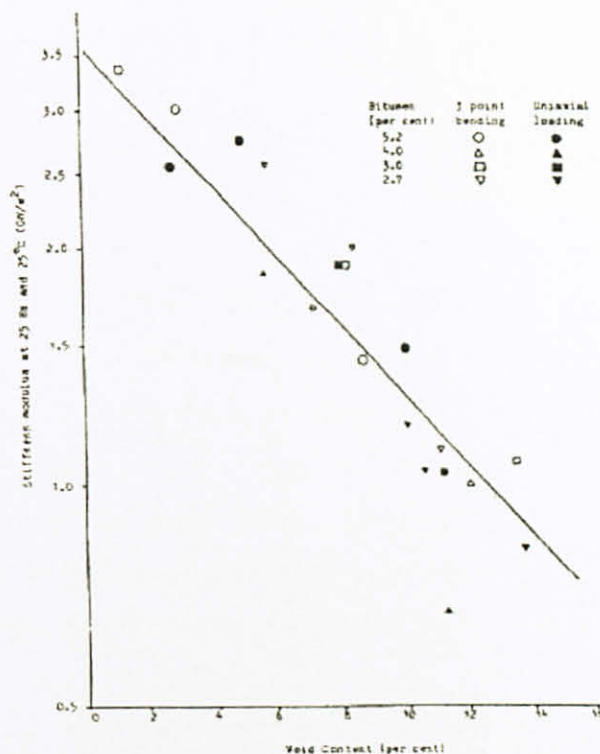


Figure 4.3 Effect of Compaction on Dynamic Stiffness  
(Source: McNicol, 1986)

### 4.3 Permanent Deformation Test

The current methods of permanent deformation can be broadly categorized as follows:

#### i. Static Creep Tests

A static load is applied to a sample and the sample recovery is measured when the load is removed. Although these tests measure a specimen's permanent deformation, test results generally do not correlate with actual in-service pavement rutting measurements.

#### ii. Repeated load tests

A repeated load at a constant frequency is applied to a test specimen for many repetitions (often in excess of 1000) and the specimen's recoverable strain and permanent deformation are measured. The test results correlate with in-service pavement rutting measurements better than static creep test results.

#### iii. Dynamic modulus tests

A repeated load at varying frequencies is applied to a test specimen over a relatively short period of time and the specimen's recoverable strain and permanent deformation are measured. Some dynamic modulus tests are also

able to measure the lag between the peak applied stress and the peak resultant strain, which provides insight into a material's viscous properties. Test results correlate reasonably well with in-service pavement rutting measurements but the test is somewhat involved and difficult to run.

iv. Empirical tests

Traditionally, there are Hveem and Marshall Mix design tests. Test results can correlate well with in-service pavement rutting measurements but these tests do not measure any fundamental material parameter.

v. Simulative tests

These involve laboratory wheel-tracking devices. Test results can correlate well with in-service pavement rutting measurements but these tests do not measure any fundamental material parameter.

#### 4.3.1 Creep Test

A test that is frequently used for evaluating time-dependent properties of asphalt concrete is the uniaxial compression creep test [51]. In this test, the specimen is subjected to a single or multiple loading/unloading cycles with the stress kept constant over the loading period.

The creep test was developed as a better means of designing and assessing asphalt mixtures for resistance to permanent deformation than using Marshall Test. Laboratory prepared specimens or cored samples are subjected to unconfined, uniaxial loading with a constant force and the resulting axial deformation is measured with time. The reversible part of the total deformation may also be determined by removing the load and measuring the deformation after recovery time, which is usually equal to the loading time [29, 51].

Two procedures have been used to limit rutting; one to limit the vertical compressive strain on top of the subgrade, and the other to limit the total accumulated permanent deformation on the surface based on the permanent deformation properties of each individual layer.

In the subgrade strain method, it is assumed that, if the subgrade compressive strain is controlled, reasonable surface rut depths will not be exceeded. Unless standard thickness and materials are used for design, the evaluation of surface rutting based on the subgrade strain does not appear to be reasonable. Under heavy traffic HMA, most of the permanent deformation occurs in the HMA rather than in the subgrade. Since rutting is caused by accumulation of permanent deformation in each layer, therefore it is reasonable to determine the permanent deformation in each layer and summing up the result.

There is a limit to the amount of deformation that such mixes will undergo however long the time of loading might be. In the creep tests, it has been found that the rate of deformation decreases until a critical strain is reached, after which the rate increases [35]. From the literature review, the limiting strain level was found to be 0.008 in/in [18].

The creep test can be used in an integrated mixture evaluation to provide data for evaluating susceptibility to deformation and for determining stiffness at longer durations of loading [51]. Some creep test parameters used by previous researchers are given in Table 4.1.

There are two types of creep loading [18], compressive creep and shear creep. Compressive creep consists of applying axial compression while shear creep consists of applying a step load in a direction parallel to the two plane faces of the specimen. In creep test, the stress field that is produced by loading process, would be uniform if the material of the specimen is homogeneous. The strain in the mix that resulted from this stress, is measured as a function of the loading time ( $t$ ) at a fixed test temperature ( $T$ ) [38].

Table 4.1 Some Parameters of Creep Test Used by Other Researchers

Test Temp.(°C)	Applied Stress(MN/m <sup>2</sup> )	Test/ Loading Time	Reference
40	N/A	N/A	Sousa[18]
40 – 60	N/A	N/A	Khan[30]
10,20,30	N/A	Uniaxial constant –load compression test/ 22 hours	Hills[35]
40	0.1 and 0.05	Static Creep test : 60 minutes followed by a 60 minutes recovery Semi-dynamic test :12 cycles of 5 minutes loading followed by 5 minutes recovery	Bolk[14]
40	0.1 (0.05-0.15)	Unconfined constant load creep compression & Unconfined uniaxial compression creep test/ 1 hour	Uge[12]
30±0.5	a pulsed stress of 100 kPa	Dynamic load creep test	Smith[52]

Creep test can be used to estimate the rut depth due to permanent deformation of bituminous layer. Van de Loo developed a method for estimating rut depth which was incorporated in the Shell Pavement Design Manual [38, 51]. The rut depth is computed from

$$RutDepth = C_m \times h \times \frac{\sigma_{AVE}}{S_{Mix}} \quad \text{Equation 4-2}$$

In which  $C_m$  is a correction factor for dynamic effect,  $h$  is the thickness of the asphalt layer,  $\sigma_{AVE}$  is the average vertical stress in the asphalt layer, and  $S_{mix}$  is the stiffness modulus of the mix. When the rut depth was calculated according to Equation 4-1, agreement between calculated and measured value was found within a factor of 1.5 [51]

Since the results from the creep test includes both the elastic and viscous components, a modification of  $S_{mix}$  based on the Van der Poel's nomograph and the viscosity of the bitumen is needed to determine the permanent deformation due to viscous component only [23].

### 4.3.2 Rutting Test

Rutting test is carried out using the reciprocating wheel tracking machine. In rutting test, the effect of the repeated loading is accounted for by a summation procedure in which it is assumed that only the viscous component of the stiffness modulus of the binder contributes to permanent deformation. This contradicts the creep test, where the stress field of rutting test is non-uniform because only part of the asphalt layer is loaded by the wheel [38].

Walsh conducted a test by subjecting a 50 mm thick slab of material to a rolling wheel load, which traversed the specimen at a constant temperature 45°C [53]. Walsh found a trend toward lower Wheel Tracking Rate (WTR) for lower voids. The six mixtures used in his study were Hot Rolled Asphalt (HRA) with air void range of 4.2% to 6.2%.

### 4.3.3 Comparison between Creep Test and Rutting Test

The results of creep test generally lead to lower predicted rutting. The lower predicted value has been assumed to be due to the 'dynamic effect'. It has been suggested that, in order to take account of the damaging effect of dynamic loading, which is more simulative of the traffic loading, an empirical correction factor should be applied. The value of such a correction factor depends on the type of mixture under test [29, 51]. Correction factor is shown in Table 4.2.

Table 4.2 Correction Factors for Dynamic Effects

Mix Type	$C_m$
Sand sheet and lean sand mixes, Lean open asphalt concrete	1.6-2.0
Lean bitumen macadam	1.5-1.8
Asphalt concrete, Gravel sand asphalt, Dense bitumen macadam	1.2-1.6
Mastic types, Hot rolled asphalt	1.0-1.3

#### 4.3.4 Correlation $S_{mix}$ and $S_{bit}$

Creep modulus refers to the stiffness modulus of mixture,  $S_{mix}$ , in dynamic creep test. The creep stiffness is taken as a measure of the deformation resistance of the test specimen. The duration of the test is 1800 load cycles [52].

Stiffness modulus of bitumen,  $S_{bit}$ , can be derived from Van der Poel's nomograph by taking into account the characteristics of the binder present in the mix (temperature  $T_{800pen}$  and Penetration Index), and the test condition (temperature, loading time) [12].

The temperature to be used is the normalized temperature, which is the difference between the testing temperature and the temperature when the penetration is 800, or  $T_{R\&B}$ . Figure 4.5 shows the nomograph for determining the stiffness modulus of bitumen [51] and .

The Penetration Index, PI is characteristic of bitumen and is defined as

$$PI = \frac{20 - 500A}{1 + 50A} \quad \text{Equation 4-3}$$

where  $A$  is the temperature susceptibility, which is the slope of the straight line plot between the logarithm of penetration ( $pen$ ) and temperature.  $A$  is also defined as

$$A = \frac{\log(pen_{atT_1}) - \log(pen_{atT_2})}{T_1 - T_2} \quad \text{Equation 4-4}$$

where  $T_1$  and  $T_2$  are two temperatures at which penetrations are measured. When the penetration of the recovered bitumen at two different temperatures is known, the penetration index can be determined by Equation 4-2.

A convenient temperature to use is the temperature at the ring and ball softening point. This is a reference temperature at which all bitumen has the same viscosity or penetration of about 800. Replacing  $T_2$  in (4-3) by  $T_{R\&B}$  and  $pen$  at  $T_2$  by 800 yields

$$A = \frac{\log(\text{pen}_{atT}) - \log 800}{T - T_{R\&B}} \quad \text{Equation 4-5}$$

By Van der Poel's nomograph, it is possible to express the results of the creep test in the form of a master curve ( $S_{\text{mix}}-S_{\text{bit}}$ ), which is characteristic of the material [14]. This master curve offers several advantages [12]:

- i. The master curve is independent of the operating parameters (temperature, loading time, stress) and may therefore be regarded as a real mix characteristic.
- ii.  $S_{\text{mix}}$  value can be derived from test result.
- iii. It is easy to compare the performance being dependent only on aggregate composition and binder content (comparisons are made for identical values of  $S_{\text{bit}}$ )
- iv. The slope of the curve indicates the sensitivity of the mix composition to changes in bitumen properties.

These statements are also supported by others researchers [14, 35, 38, 51]. Plotting the creep test results as  $S_{\text{mix}}$  against  $S_{\text{bit}}$  is a convenient and general way of expressing the creep characteristics of an asphalt mix. It can eliminate the effect of temperature, grade of the binder and the value of the applied stress.

The shape of the creep curve in an  $S_{\text{mix}}$  against  $S_{\text{bit}}$  graph depends on the voids content of a mix [35]. A linear relationship between  $\log S_{\text{mix}}$  and  $\log S_{\text{bit}}$  is observed for values of  $S_{\text{bit}}$  lower than about  $10^3 \text{ N/m}^2$  only [14].

A good relationship takes the following form [9]:

$$\begin{aligned} \text{Log } (Y) &= \text{Log } (a) + b \text{ Log } (X) \\ \text{Or } Y &= aX^b \end{aligned} \quad \text{Equation 4-6}$$

where  $a$  = the interception of the line with the Y-axis,  $b$  = the slope of the line,  $Y$  = stiffness of the mix (MPa),  $X$  = stiffness of the bitumen (MPa).



In this equation, the coefficients 'a' and 'b' represent the mixture in terms of deformation performance. Mixture stiffness is indicated by the constant 'a' and the slope 'b' indicates the sensitivity of the mixture to loading time and hence the bitumen stiffness. Therefore, a mixture with high value of 'a' and low slope 'b' will exhibit good deformation performance.

The accumulation of permanent deformation with an increasing number of loading cycles under repetitive loading follows an almost linear behavior on log-log scale, Sousa in [16]. It means that the accumulation of permanent deformation has a polynomial relationship with decreasing rate to the number of cycles on a linear scale. This behavior suggests that as the number of loading cycle increases, it is more difficult for the material to build up permanent strain. That is, the material "stiffens" and resists further accumulation of permanent deformation.

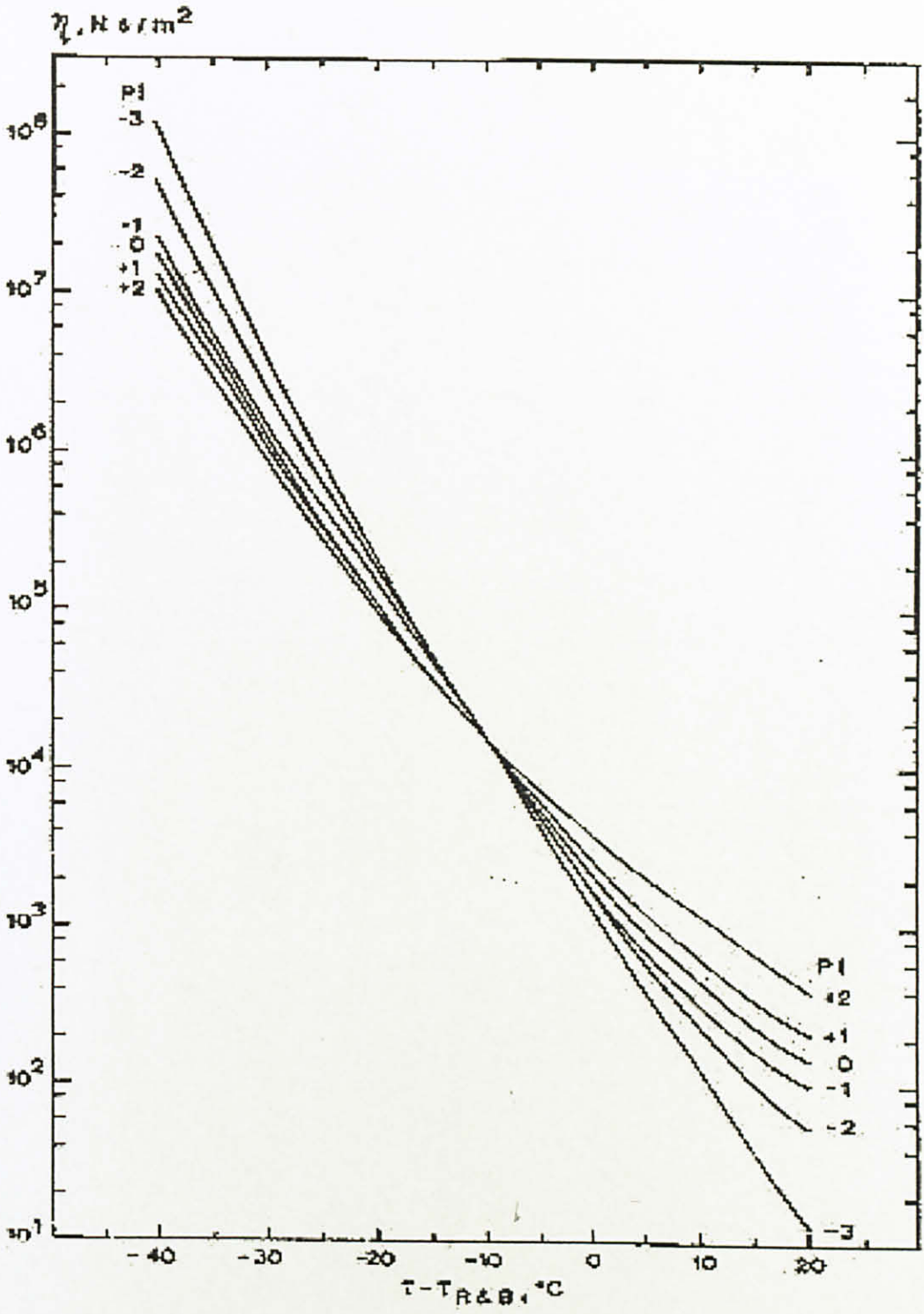


Figure 4.4 Nomograph for Viscosity of Bitumen  
(Source: Napiah, 1993)

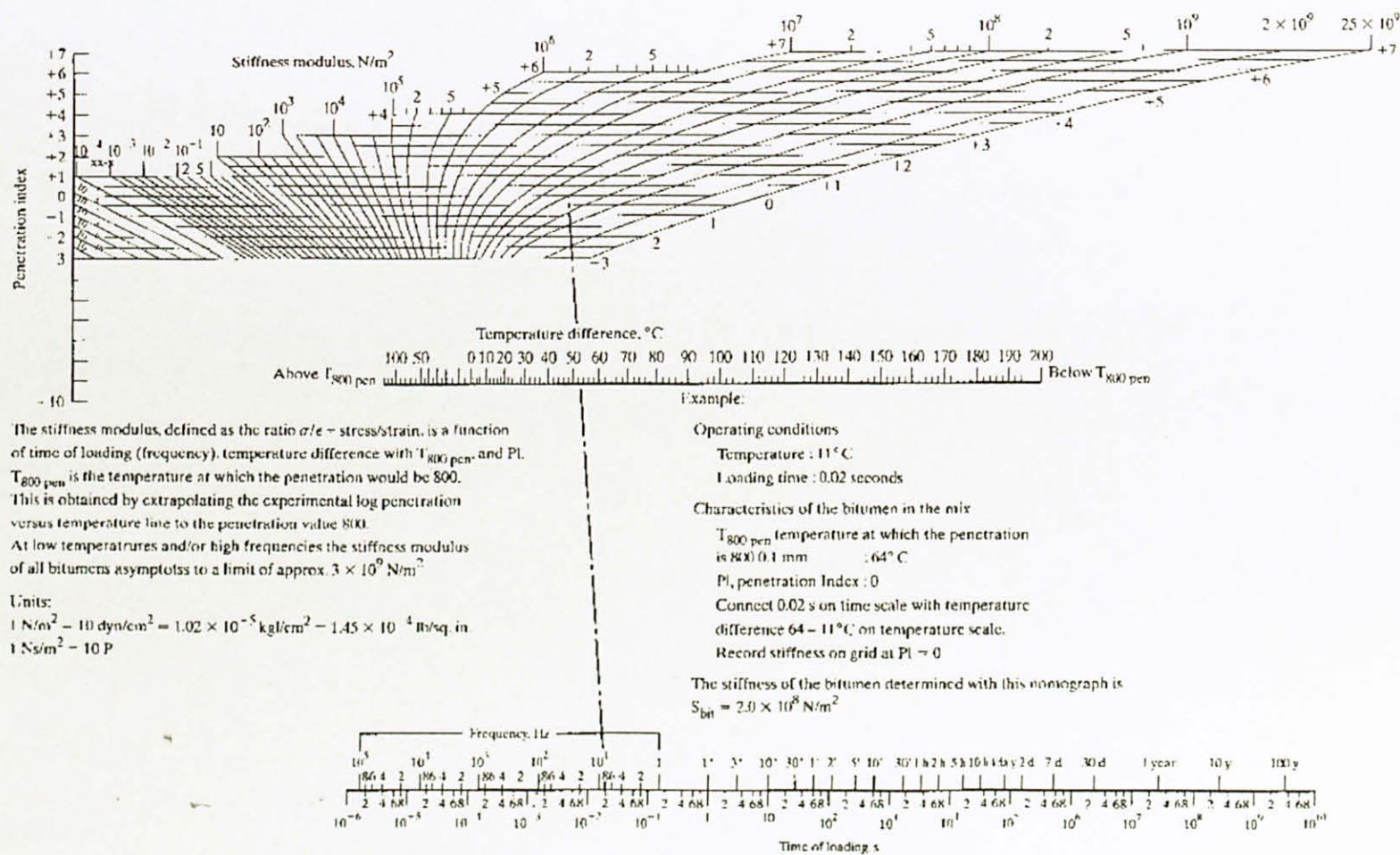


Figure 4.5 Nomograph for Stiffness Modulus of Bitumens (Source: Huang, 2004)

#### 4.4 Fatigue Test

Fatigue test on mixes is conducted to compare the computed bending tensile strains at the base of the layers of mix with the maximum strain values tolerated by a specimen of mix in the course of a laboratory fatigue test [54].

The aim of fatigue test is to simulate field behavior and is normally performed by subjecting a sample at prescribed strain (deformation) or stress (loading) amplitude [23, 55]. In other words, fatigue testing may be performed under two loading conditions, as shown in Figure 4.6, either controlled-stress or controlled-strain.

Controlled stress testing is associated with evaluation of thick asphalt layers (greater than approximately 150 mm) except when the asphalt is extremely weak or the support is exceedingly stiff. In this type, the stress is maintained constant, which increases the strain during the test so that the stiffness modulus (ratio of the stress amplitude to the strain amplitude) decreases and the energy dissipation per cycle increases.

Controlled strain testing is associated with evaluation of thin asphalt layers (less than approximately 50 mm), unless the asphalt is extremely stiff or the support is very weak. The elastic recovery properties of the pavement material have a fundamental effect on its fatigue life. In this test, the strain is kept constant by decreasing the stress during the test so that the stiffness modulus (ratio of the stress amplitude to the strain amplitude) decreases and the energy dissipation per cycle decreases.

The estimated fatigue lives will vary for the controlled stress and controlled strain tests due to the mode of loading effect. For the controlled stress test, it will be overestimated, and for the controlled strain test it will be underestimated. It is, therefore, important to account for the mode of loading condition when performing fatigue tests [21, 56].

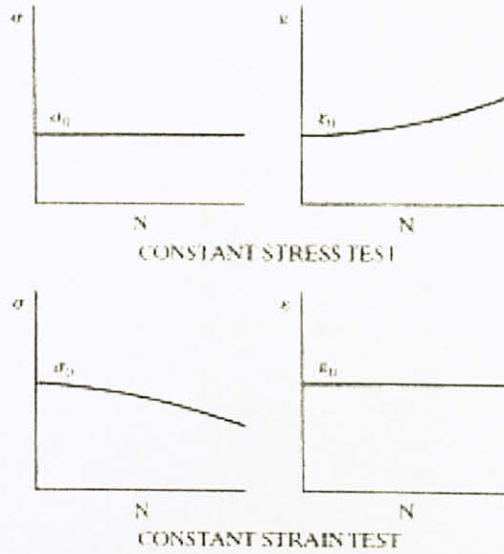


Figure 4.6 Two Types of Controlled Loading for Fatigue Testing  
(Source: Huang, 2004)

Fatigue life is commonly defined as the number of load cycles to fail the asphalt concrete specimen at a strain (stress) occurring at the bottom of the asphalt layer. Typically, fatigue life is shown by plotting the stress or strain at the bottom of the asphalt concrete layer versus number of load cycles to failure. This approach of studying fatigue is known as the phenomenological or S-N approach [56].

There are four typical deterioration paths for asphalt concrete fatigue test as shown in Figure 4.7 [55]. Each of them relates to the type of loading applied and strain field uniformity.

i. Fatigue path A

It is characterized by a decrease in stiffness followed by a stabilized stiffness (steady-state condition), which remains more or less constant with increase in number of load cycles applied. This situation occurs during controlled strain fatigue tests carried out using too low a strain amplitude (below possible threshold value), which means that no failure will occur within the time available to run the test, typically less than  $2 \times 10^6$  cycles.

ii. Fatigue path B (preferred fatigue path)

It occurs during controlled strain tests with uniform (ideal) strain field. Stiffness decreases steadily until complete failure is easy to identify, and percentage decrease in stiffness can be used as the failure criterion. The

relative decrease in stiffness at failure depends on the stiffness of the material, where high stiffness allows a smaller decrease than softer mixtures.

iii. Fatigue path C

It is characterized by an S-shaped curve. Type C is typical for controlled strain tests, which exhibit non uniform strain field. The final stage is characterized by stiffness approaching zero, but in principle, never reaching zero. For this type, the failure point is difficult to determine, as in principle, the real failure of the structure does not occur. Therefore, due to the difficulties associated with determination of failure, 50% reduction in stiffness is usually employed.

iv. Fatigue path D

It is typical for stress-controlled fatigue tests.

Lundstrom suggested that at least three properties should be accounted for at fatigue characterization: initial stiffness, deterioration path (depicted in Figure 4.7), and failure point [55]. These are important as fatigue characteristics are generally expressed as relationships between the initial stress or strain and the number of load repetitions to failure.

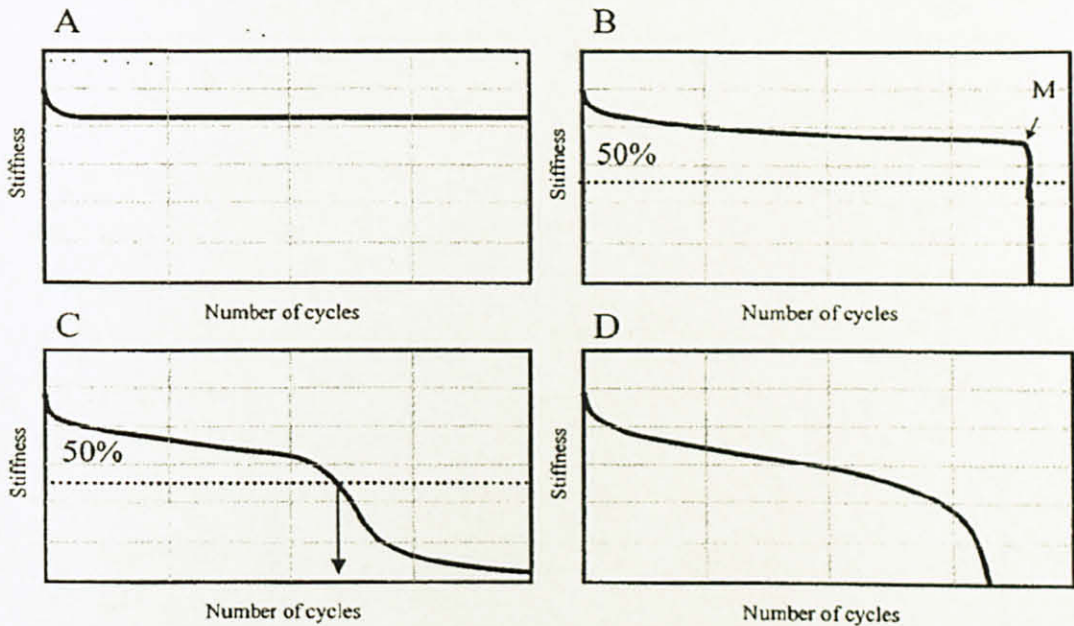


Figure 4.7 Typical Fatigue Paths for Asphalt Concrete  
(Source: Lundstrom, 2004)

#### 4.4.1 Four-Point Bending Test

Fatigue test devices are simple flexure (two, three, and four-point bending), supported flexure, uniaxial fixtures, triaxial fixtures, diametral fixtures and wheel tracking fixtures. Four-point bending is favored since failure can be initiated in an area of uniform stress between the two center loads [57].

The four-point bending test is well known method that have been widely used and readily understood. There are several advantages of the test that make it. The measured fundamental properties can be used for both mixture evaluation and pavement design. The results obtained from this test can be used directly (with appropriate shift factor) in the structural design of pavements to estimate the propensity for cracking. In addition, the results of stress controlled testing can be used for the design of thick asphalt pavements whereas the results of strain controlled testing can be used for the design of thin asphalt pavements. In this test, failure specimen is initiated in a region of relatively uniform stress which helps to reduce the coefficient of variation of the test results, therefore, requiring fewer specimens.

#### 4.4.2 Fatigue Failure

Some parameters for fatigue test obtained from the literature are tabulated in Table 4.3. The test is run until fatigue failure occurs. The fatigue life of a specimen predicted from laboratory testing is significantly influenced by the definition of failure. There is a dispute concerning the definition of failure for the controlled strain test, as it is very difficult to reach physical failure via fracture. Currently, according to AASHTO TP8-94 failure is defined as when there is a 50% reduction in the measured stiffness; initial stiffness is measured after 50 applied load cycles. Similarly Tayebali and Roche stated fatigue damage is related to a drop in stiffness [21, 54, 56]. Typically, a drop in stiffness of 50% is considered as failure of the material.

Table 4.3 Some Fatigue Test Parameters Used by Other Researchers

Test Temp. (°C)	Frequency (Hz)	Control Mode	Reference
20	0.01 to 10	A haversine load waveform, controlled strain, a loading time of 0.1 second, strain level 100, 200 and 400 micro in/in	Tayebali [21]
20	4	Sinusoidal load waveform, combined load and displacement mode	Hartman [57]
10	10	Sinusoidal load waveform, controlled strain with strain amplitude 125 and 200 micro m/m	Artamendi [58]
10	5	Sinusoidal load waveform, displacement controlled with strain amplitude 80, 200, 600, and 1000 micro m/m	Medani [59]
20	10	A Haversine load waveform, control strain	Ghuzlan [56]

#### 4.4.3 Output of Fatigue Test/ Fatigue Characteristics

The results are generally approximated by straight line in logarithmic diagrams and relate input (initial strain or stress amplitude) versus number of repetitions (cycles) to failure [21, 23, 55, 57, 60], as expressed by

$$N_f = c_2 (\varepsilon_t)^{-f_2} \quad \text{Equation 4-7}$$

where  $N_f$  is the number of repetitions to failure (number of load application to initiate a fatigue crack (failure)),  $\varepsilon_t$  = maximum value of applied tensile strain.  $c_2$  is a fatigue constant that is the value of  $N_f$  when  $\varepsilon_t = 1$  and  $f_2$  is the inverse slope of the straight line.  $c_2$  and  $f_2$  are factoring depending on the composition and properties of the mix [60, 61].

Under the same initial strain, laboratory test show that the number of repetitions to failure decreases with the increase in stiffness modulus, so Equation (4-5) can also be written as

$$N_f = c_2 (\varepsilon_t)^{-f_2} (E_s)^{-f_3} \quad \text{Equation 4-8}$$

where  $E_s$  is HMA stiffness modulus and  $f_3$  is the inverse slope of the  $E_s$  straight line.



Equation (4-6) is based on laboratory test. Using Equation (4-6) several models have been proposed to predict fatigue lives of pavements [21]. To develop these models, laboratory results have been “calibrated” by applying shift factors based on field observations to provide reasonable estimates of pavement lives (repetitions). The major difference in the various design methods is models that relate the HMA tensile strains to the allowable number of load repetitions. In The Asphalt Institute and Shell design methods, the allowable number of load repetitions  $N_f$  to cause fatigue cracking is related to the tensile strain  $\epsilon_t$  at the bottom of the HMA and to the HMA modulus  $E_s$  by Equation (4-6).

The Asphalt Institute found that changes in stiffness and void content affect fatigue life according to the following expression;

$$N_f = 18.4(C) \times (4.32 \times 10^{-3} \epsilon_t^{-3.29} E^{-0.854}) \quad \text{Equation 4-9}$$

where  $N_f$  is number of load applications to failure,  $C$  is a factor dependent on the asphalt and void contents,  $\epsilon_t$  is tensile strain,  $E$  is modulus of asphalt mixture, 18.4 is a factor to account for differences between laboratory and field conditions. This Equation (4-7) applies to a standard mix with an asphalt volume of 11% and air void volume of 5% and for 20% of cracked area.

Some agencies (Illinois Department of Transportation, Transport and Road Research Laboratory, and Belgian Road Research Center) use Equation (4-5) because  $f_2$  is much greater than  $f_3$ ; the effect of  $\epsilon_t$  on  $N_f$  is much greater than that of  $E_1$ . Therefore, the  $E_1$  term may be neglected. From these agencies, it can be found that the exponent  $f_2$  of the fatigue equations varies from 3.0 to 5.671, but the coefficient  $c_2$  varies over several orders of magnitude [23, 56]. The exponent  $f_2$  and  $f_3$  are usually determined from fatigue tests on laboratory specimens, but  $c_2$  must shift from laboratory to field value by calibration. The difference in materials, test methods, field conditions, and structural models imply that a large variety of models is expected. No matter what models are used, it is important to calibrate the function carefully by applying an appropriate shift factor, so that the predicted distress can match field observations [23].

#### 4.5 Summary

Performance test for permanent deformation can be carried out by creep test and rutting test. Meanwhile for fatigue testing, four point bending test can be used. The result of permanent deformation is depicted by the relationship of  $S_{mix}$  and  $S_{bit}$ . Fatigue test have two loading conditions and four typical deterioration paths. The determination for permanent deformation and fatigue failure is correlated by stiffness of mixture.

## CHAPTER FIVE: EXPERIMENTAL WORK

### 5.1 Materials

Material preparation was the onset of experimental work. All the materials have been provided in the highway laboratory of University Teknologi PETRONAS (UTP). The 20 mm nominal size of granite, readily available, was used as coarse aggregate. It was angular in shape and rough in texture. Forty two percent of the total aggregate consists of this type of aggregate. Fifty two percent of sand and 6% cement of total aggregate were used as fine aggregate and mineral filler respectively. These percentages were determined by try and error according the calculation in Table 6.2. These percentages can make design gradation which fulfills JKR specification. Since the main objective of this research was to study the effect of compaction degree of asphalt mixture on asphalt concrete, the same aggregate type and gradation were used throughout the research. Sample was compacted to simulate the range of field air voids. This was achieved by varying the compactive effort. Various pressures were applied to the Servopac Gyrotory compactor to attain compaction energy variation. Besides using gyrotory compactor, a hand compactor was also used to get the desired range of air void in the specimen. Figure 5.1 presents the flowchart of this research methodology.

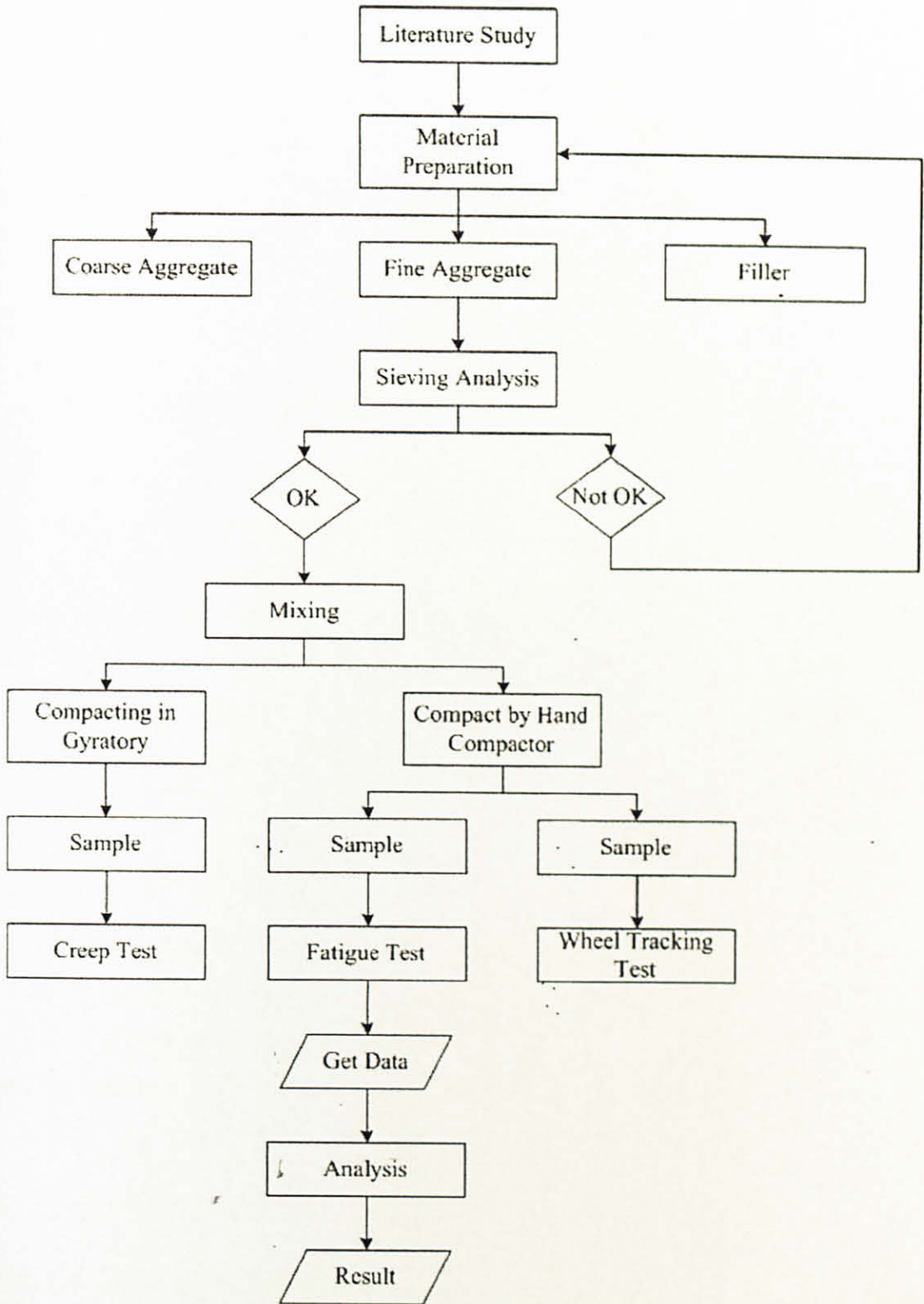


Figure 5.1 Flowchart of Research

## 5.2 Test on Aggregate

A major proportion of the mixture was aggregate, consist a mixture of coarse and fine aggregate. Due to this, aggregate properties have strong influence on performance of pavement. Before mixing process, some information of particle size, gradation and specific gravity are required to assess the influence of the mixture on life performance. The shape and texture of aggregate are examined by visual.

### 5.2.1 Particle Size Analysis

The particle size distribution of the aggregate was determined by passing the material through a series of sieves stacked with progressively smaller openings, and weighing the material retained on each sieve. The sieve sizes used were 20 mm to 5 mm for coarse aggregate and 5 mm to 0.075 mm for fine aggregate. For the filler, all of the cement that was used was passed through a 0.075 mm sieve. Sieve analysis was conducted to meet the gradation. Sieve analysis was performed as described in BS812: Part 103:1985 [62]. Three series of tests were performed for each aggregate fraction.

### 5.2.2 Specific Gravity

Specific gravity is a ratio between the weights of a unit volume of the material and the weight of the same volume of water at 20 to 25°C. The specific gravity measurement was conducted according to BS 812-103.1: 1985 [62]. In this investigation, specific gravity of coarse aggregate is 2.69, fine aggregate is 2.65 and cement as mineral filler is 3.15.

## 5.3 Bitumen Tests

Bitumen (known as 'asphalt cement' in the United States) is a thermoplastic material that gradually softens, and eventually liquefies when heated. Bitumen is characterized by its consistency at certain temperatures. The consistency is measured by a penetration test and a softening point test [63].

Penetration is determined using an empirical test method. A sample of the bitumen in a small container is stabilized in a water bath at standard temperature (normally 25°C). A

prescribed needle, weighing 100 g, was allowed to bear on the surface of the bitumen for 5 second. The penetration is defined as the distance, in units of 0.1 mm, which the needle penetrates into the bitumen. The experimental set-up of the penetration test is illustrated in Figure 5.2.

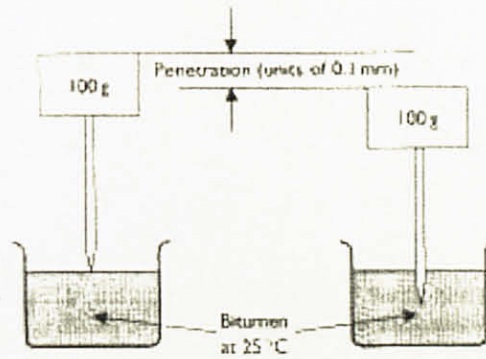


Figure 5.2 Penetration Test [63]

Determination of the softening point is also an empirical test. A hot sample of bitumen was poured into a brass ring and allowed to cool. The top was then leveled with a hot spatula, and the ring placed in a holder and lowered into water at 5°C. It was then loaded with a steel ball of specified weight and diameter. The water was then heated at a rate of 5°C per minute. As the water was heated, the disc has sagged over a distance of 25.4 mm; the temperature of the water at that instance was recorded as the 'softening point' of the bitumen.

In this study, the penetration of bitumen was 80 and softening point was 44°C.

#### 5.4 Mix Design

This study focuses on the 20 mm asphalt concrete mixture, which is used for the construction of wearing course in Malaysia, and as specified by JKR (accordingly Marshall mix design). The mechanical properties of the mixture arise largely from the internal friction within the mixture due to the interlocking of the aggregate particles and to a lesser extent from the binder cohesion.

The outline of mix design is:

- i. Selection of materials (aggregate and binders)

- ii. Selection of aggregate grading
- iii. Proportioning of aggregates
- iv. Preparation of compacted specimens at a bitumen content
- v. Determination of density of compacted specimens
- vi. Calculation of total porosity (air voids) in compacted specimens
- vii. Testing for permanent deformation/ fatigue properties of specimens (For permanent deformation properties, dynamic creep test and wheel tracking test were employed, and for fatigue properties, fatigue test was used)

#### **5.4.1 Preparation**

The aggregate proportions for bituminous mixes was 42% of total aggregate in the mix was coarse aggregate, 52% consist of fine aggregate and 6% filler. As the objective of this study was to investigate the correlation between compaction degree and life performance of asphalt concrete, the same aggregate type and gradation was used. The one value of bitumen content was used in this study, which is 5% bitumen content. This bitumen content is in the range of optimum bitumen content from JKR specification. JKR determined bitumen content based on Marshall Method.

The bituminous binder used in this study was asphalt cement having penetration 80. The coarse aggregate was angular in shape and rough in texture meanwhile fine aggregate was river sand and filler was Portland cement.

#### **5.4.2 Mixing**

Mix type in this study is wearing course and mix designation is ACW20. Before mixing, each aggregate should be sieved. The coarse aggregate was sieved 2,000 g for 20 minutes and the fine aggregate was sieved 750 g for 15 minutes. The composition of mixture is coarse aggregate 42%, fine aggregate 52% and filler 6%. Four sizes in coarse aggregate which is 1% total (20 mm), 16% total (14 mm), 16% total (10 mm) and 9% total (5 mm). The temperature of mix and mould was set at 135°C.

For creep test, the total material for one sample is 1200 g . The percentage of filler is 6% (72 g) and bitumen content is 5% (63 g), based on JKR for ACW20. Heated aggregate and binder at 135°C were thoroughly mixed and placed in the 100 mm diameter mould previously heated. Compaction was applied for 230 gyrations with gyratory compactor. After the specimen was sufficiently cooled the initial density was determined by weighing it in air and water.

For fatigue test, the total material for one sample is 2400 g. The beams that were produced measure 380 mm in length. The percentage of filler is 6% (144 g) and bitumen content is 5% (126 g).

For wheel tracking test, the total material for one sample is 10,000 g. The percentage of filler is 6% (600 g) and bitumen content is 5% (526 g).

#### 5.4.3 Compaction

The compactors used were gyratory compactor and hand compactor as shown in Figure 5.3. and Figure 5.4. Gyratory compactor was utilized for compact creep specimens; meanwhile hand compactor was utilized for beam and wheel tracking specimens.

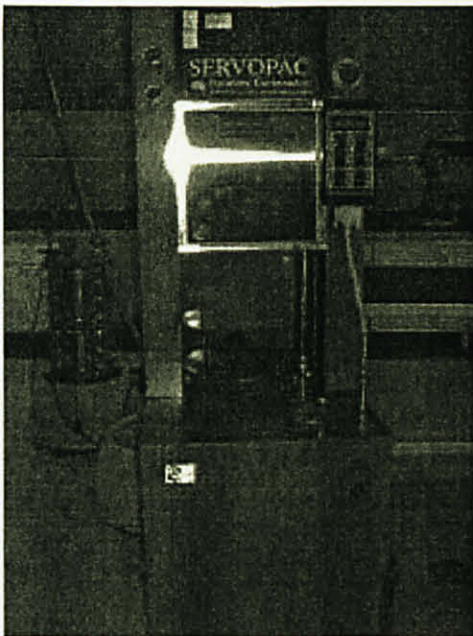


Figure 5.3 Gyratory Compactor

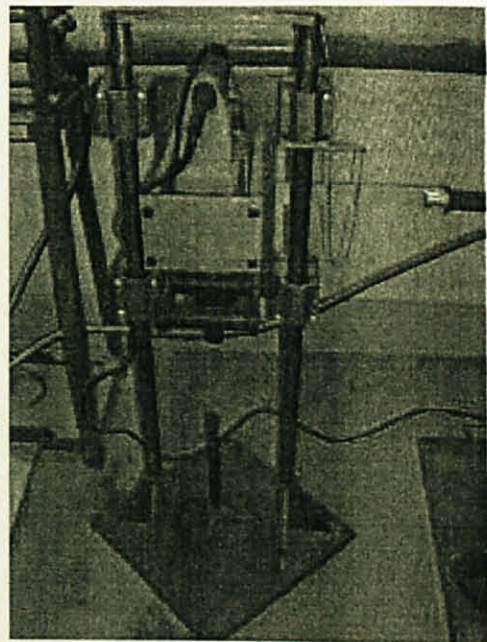


Figure 5.4 Hand Compactor



#### 5.4.3.1 Compaction of Creep Specimens

The mixture for creep specimen was loaded into preheated mould for compaction. The size of mould used was 100 mm in diameter. This size was chosen based on the nominal maximum size of aggregate. In this study, the nominal maximum aggregate is 20 mm. In other words, the first size sieve that retains more than 10% is 14 mm. After that, the mould was placed into the gyratory for compacting. The Gyratory compactor used in this study is Servopac Gyratory Compactor, IPC global model no 2500. The design specifications are as follows:

- i. Angle of Gyration, 1.00 degree
- ii. Vertical Pressure, variation between 300 kPa-700 kPa
- iii. Gyration, 230

Size of creep specimen was 100 mm in diameter and 65 mm in height.

#### 5.4.3.2 Compaction of Beam and Wheel Tracking Specimens

All beam specimens were compacted in the laboratory using a Kango vibrating hammer compactor. A kneading type action acquired by a tamping foot was matted to give a specimen having an aggregate orientation similar to that developed by the gyratory in the laboratory and in the field under the action of a roller compactor.

The Kango that was used to compact the specimens is shown Figure 5.4 together with the tamping foot constructed specially to compact the specimens. The 60x60 mm tamping foot was made from stainless steel. Prior to compaction, the inner surface of the mould and tamping foot were treated with a thin layer of grease to prevent the mixture from sticking to the mould and to ensure easy demoulding of the compacted beam.

The mixture for beam specimen was loaded into the beam mould for compaction. The beam mould was fabricated from a 754 x 154 x 150 mm mould. From this mould, two 380 x 64 x 50 mm specimens can be fabricated. Two of these beams were separated by wood.

In order to get variation of porosity, there are three types mixture, namely a, b, and c. The mixture was compacted in one layer for type a, two layers of compacting for type b and three layers of compacting for type c.

The tamping foot attached to the vibrating hammer was then moved forward approximately 50 to 60 mm and 3 second tamping duration was applied. These movements ensured that at the end of the travel, the layer would have been compacted by 7 tamping blows. Similarly, when the tamping foot was being moved backwards, another 7 tamping blows were applied to the mixture layer. The Kango compactor moved 10 times backward and forward for each mixture layer. The same procedure was repeated for second and third layers.

The other specimen that used hand compactor was wheel tracking specimen. The mixture for wheel tracking specimen was loaded into the wheel tracking mould for compaction. The size of the specimen used was 305 mm square and 50 mm thick. The same procedure with beam specimen was applied.

#### 5.4.4 Density Determination

The purpose of density determination is to finally calculate the air void content in the sample. After being compacted, the specimen was extracted from the mould and allowed to cool overnight. Afterwards, BSG and MSG of each compacted specimen were then measured. Bulk density test was performed on all compacted HMA samples in accordance with BS 598-104: 2005 was used for analysis purposes in this study.

Bulk Specific Gravity of Compacted Bituminous Mixtures based on BS 598-104: 2005

$$\text{BulkSpec.Gravity} = \frac{A}{A - B} \quad \text{Equation 5-1}$$

Where A is mass (g) of sample in air and B is mass (g) of sample in water

Specific gravity of aggregate was calculated by Equation 5-2, then this result was used to obtain maximum specific gravity of mixture by Equation 5-3.

$$SG_{Aggregate} = \frac{100}{\frac{\%FineAgg}{SG_{FineAgg}} + \frac{\%CoarseAgg}{SG_{CoarseAgg}} + \frac{\%Filler}{SG_{Filler}}} \quad \text{Equation 5-2}$$

$$SG_{Mixture} = \frac{100}{\frac{100\% - \%Bitumen}{SG_{Aggregate}} + \frac{\%Bitumen}{SG_{Bitumen}}} \quad \text{Equation 5-3}$$

From the density determination, the percent relative compaction (Equation 5-4) and air void (Equation 5-5) in the sample were calculated.

$$\text{Percent relative compaction} = \frac{BulkSp.Gravity}{Max.Sp.Gravity} \times 100\% \quad \text{Equation 5-4}$$

$$\text{Air void (Porosity)} = 100\% - \text{Percent relative compaction} \quad \text{Equation 5-5}$$

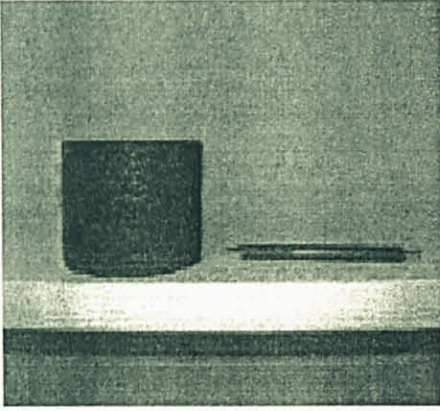
For each porosity determination, averages of at least three measurements were performed.

## 5.5 Dynamic Creep Test

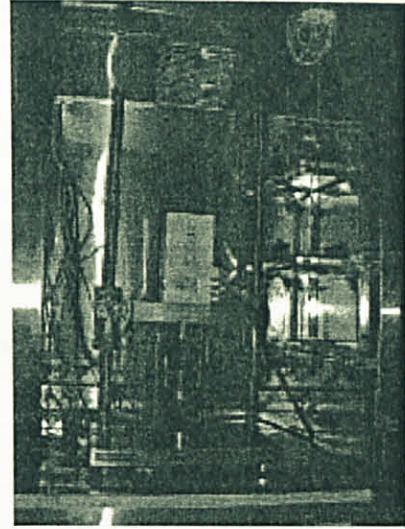
In this investigation, Universal Testing Machine 4-19 was used to perform dynamic creep test in order to measure creep properties. The dynamic creep test was a test that applies a repeated pulsed uniaxial stress/ a load to a specimen and measures the resulting deformations in the same axis using Linear Variable Displacement Transducers (LVDTs).

The testing parameters were based on British DD 226

- i. Preload Option; Stress (kPa) = 12 and Hold Time (s) = 120
- ii. Confining Option = Not Used
- iii. Loading Options; Waveshape = square pulse, Pulse width (ms) = 1,000, Rest Period (ms) = 1,000, Contact Stress (kPa) = 2, and Deviator Stress (kPa) = 100
- iv. Termination Option; Axial micro-strain = 30,000 or = 0 if strain displayed as a percentage (%), Radial micro-strain = Not Used and Loading cycle = 1,800



(a) Creep Test Specimen



(b) Apparatus for Creep Test

Figure 5.5 Universal Testing Machine 4-19

The specimens were kept in a chamber at  $40^{\circ}\text{C}$  for a minimum of one hour before testing. The same temperature was applied to specimen during testing. For controlled temperature testing, the specimen's skin and core temperatures were estimated by transducers inserted in dummy specimen and placed near the specimen undergoing testing.

A constant load was applied to the test specimen to provide an axial stress of 2 kPa and deviator stress of 100 kPa for loading time of 1 hour with the test temperature maintained at  $40^{\circ}\text{C}$ . The testing conditions of temperature and loading were considered to be similar to those experienced by the material on the road. After setting up the specimen (Figure 5.5a), in the apparatus (Figure 5.5b), the specimen was preloaded at the test temperature for 2 minutes with a conditioning load 12 kPa, to provide a stress equivalent to 10% of the normal applied stress of 102 kPa, and any axial deformation was recorded [29].

The load was then quickly increased to the test load and the axial deformation was measured with time; from displacement readings on a dial gauge or from the output of electrical displacement transducers. The time intervals for readings were predetermined. Those are 20, 40, 60, 120, 360, 840, 1200, 2400 and 3600 seconds after the load started to increase. Data collection was accomplished using Universal Testing Machine (UTM) 4-19 software.

Care was required in the preparation of specimens for test. The end faces are planar, smooth and perpendicular to the axis of the specimen. Friction forces between the load platens and the end faces should be as small as possible, in order to ensure that the stress distribution in the loaded specimen was correct [29].

## 5.6 Fatigue Test

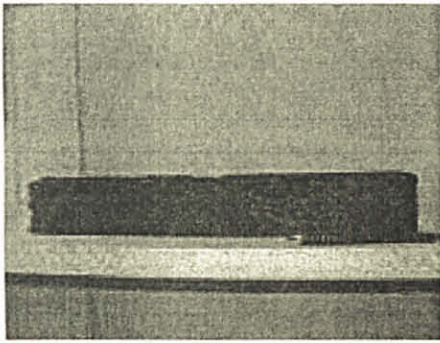
In this investigation, Universal Testing Machine 4-21 was used to perform fatigue test. The fatigue test is a test that applies a repeated flexural bending to a specimen at a specific applied force. The resulting beam deflection was measured using on-specimen Linear Variable Displacement Transducer (LVDTs)

A four point bending test was conducted with a loading frequency of 5 cycles per second (5 hz). The tests were carry out at 20<sup>0</sup>C in a controlled strain condition with the parameter listed below. In strain controlled cyclic loading test, the strain amplitude was held constant during cycling. The parameters used for testing were;

- i. Default Poisson Ratio = 0.4
- ii. Loading Condition =Control Mode = Haversine strain , Pulse width (ms) = 200 peak to peak micro strain = 100 , Conditioning cycles = 50
- iii. Termination conditions =Termination stiffness (MPa) is 50% initial stiffness or stop test after cycle = 1,000,000

Twenty degree Celsius was chosen as the test temperature based on the study by Kim which suggested that the effect of air void content on fatigue life at 68<sup>0</sup>F (20<sup>0</sup>C) is more pronounced than at lower temperatures [34].

Figure 5.6 (b) shows the apparatus for four point loading fatigue testing. The load was applied to the beam specimen, 380 mm long with a width and depth not exceeding 65 mm, as shown in Figure 5.6 (a). A testing machine applied repeated loads in the form of haversine wave for 0.2 s duration. The dynamic deflection of the beam at the midspan was measured with LVDT.



(a) Beam Specimen



(b) Apparatus for Fatigue Test

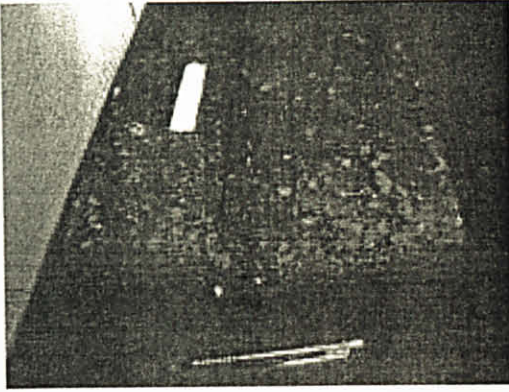
Figure 5.6 Universal Testing Machine 4-21

Due to bituminous material's viscoelastic nature, which causes a beam specimen to sag under its own weight, four point loading fatigue for testing asphalt beam specimens have generally been design with clamping mechanisms. The MATTA fatigue tester relied on precision torque motors to automatically readjust the clamping of the specimen during testing. The clamping was applied throughout the duration of the test and automatically adjusted itself when the specimen experienced deformation [57].

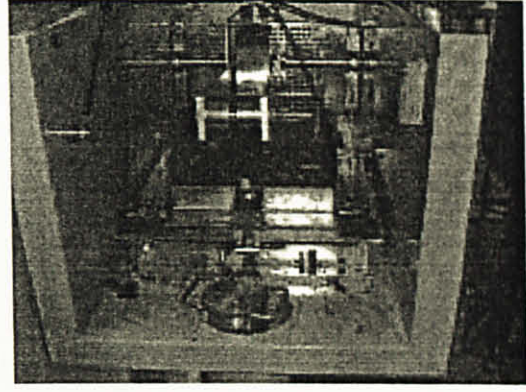
The tests were monitored continuously. The magnitude and time history of the load and deformation were recorded at a specified number of load repetitions until a stiffness reduction of about 50 percent was obtained in controlled strain test. The load and deformation were then converted to the tensile stress and strain in the specimen [21]. Data collection was accomplished using Universal Testing Machine (UTM) 4-21 software.

### 5.7 Wheel Tracking Test, Simulative Test

Wheel Tracking Test determines plastic deformation of asphalt-based road surface wearing course under temperature and pressure similar to those experienced under road use. The use of Wheel Tracking Tests will prevent road surfaces being laid, which rut in hot weather.



(a) Wheel Tracking Specimen



(b) Apparatus for Wheel Tracking Test

Figure 5.7 Wheel Tracking

The Wessex Wheel Tracker is a machine designed to carry out tests on asphalt samples in accordance with BS 598-110: 1998 and provides a fully automated test with automatic calculation of tracking rates.

The wheel tracking test was done by running a standard wheel backwards and forwards across a compacted sample of an asphalt. The rate was set at 21 or 24 cycles per minute. The temperature for this test was 40° C. The slab of 305 mm square and 50 mm asphalt concrete was mounted on a rigid base. The rut depth developed after 45 minutes of testing was measured and recorded.

## CHAPTER SIX: RESULTS AND DISCUSSION

### 6.1 Introduction

In this study, only certain porosity ranges were examined. The limitation of porosity range is due to the type of aggregate and gradation. Only one type of aggregate and one gradation were used.

The primary analysis tool is a simple correlation/regression analysis. A correlation/regression analysis was conducted on the data in order to determine the best fit line and the coefficient of determination ( $R^2$ ). Selection of the best correlation was based upon the highest  $R^2$  value obtained from the regression analyses.

### 6.2 Particle Size of Aggregate

The results of the analysis are tabulated in Table 6.1. The percentage passing of the material plotted against respective sieve size is shown in Figure 6.1.

Table 6.1 Particle Size Distribution of the Aggregates used in the Investigation

Sieve Size (mm)	Test 1	Test 2	Test 3	Average
28	100.00	100.00	100.00	100.00
20	98.16	99.63	99.10	98.97
14	61.90	71.44	66.49	66.61
10	25.84	32.63	27.27	28.58
5	2.50	1.60	1.37	1.83

(a) Coarse Aggregate: Percentage Passing

Sieve Size (mm)	Test 1	Test 2	Test 3	Average
5	98.65	97.87	97.33	97.95
3.35	94.59	93.62	92.00	93.40
1.18	67.57	65.96	57.33	63.62
0.425	22.97	23.40	17.33	21.24
0.15	1.35	0.00	1.33	0.89
0.075	0.00	0.00	0.00	0.00

(b) Fine Aggregate: Percentage Passing



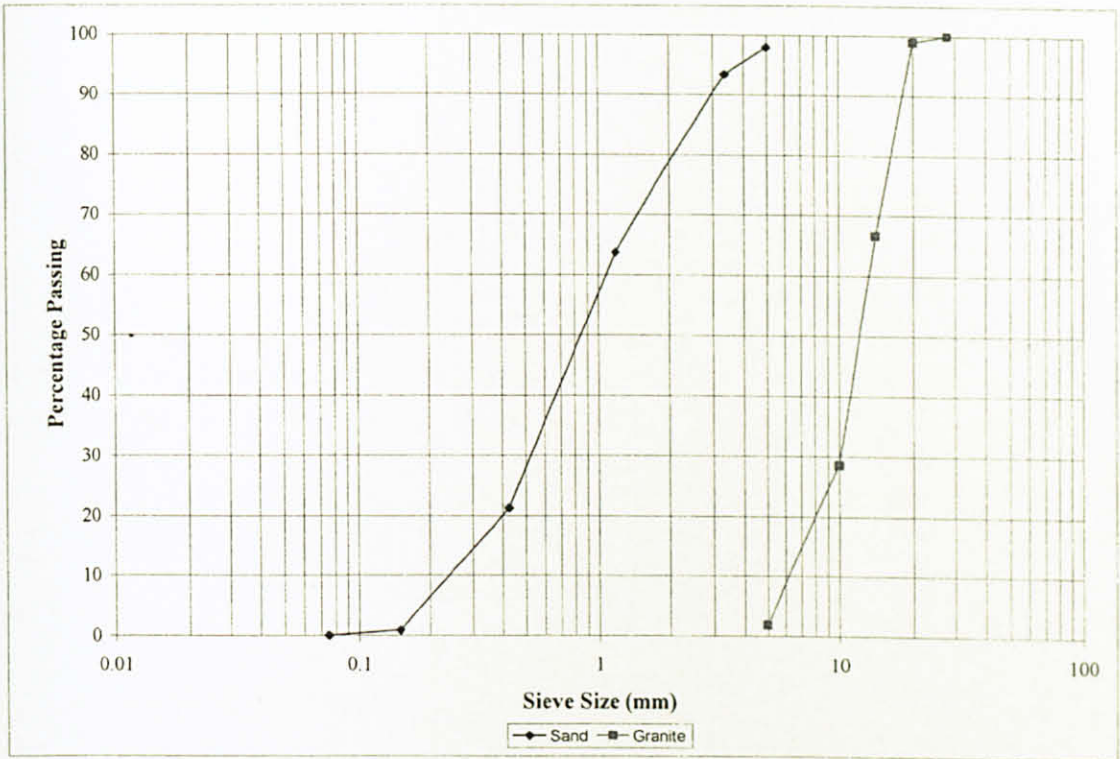


Figure 6.1 Particle Size Distribution of the Aggregates

Table 6.2 Result of Sieve Analysis

Sieve Size (mm)	JKR Specification	Total Sample that Passing			Mix Gradation
		Coarse Aggregate (42%)	Fine Aggregate (52%)	Filler (6%)	
28	100 - 100	100	100	100	100.00
20	76 - 100	98.97	100	100	99.57
14	64 - 89	66.61	100	100	85.98
10	56 - 81	28.58	100	100	70.00
5	46 - 71	1.83	97.95	100	57.70
3.35	32 - 58		93.40	100	54.57
1.18	20 - 42		63.62	100	39.08
0.425	12 - 28		21.24	100	17.04
0.15	6 - 16		0.89	100	6.47
0.075	4 - 8			100	6.00

The envelope covering the grading of the aggregate for ACW20 as listed in Table 6.2, has been plotted in Figure 6.2 together with the Malaysian Public Works Department's (JKR) grading envelope. This figure illustrates that the grading in this study conforms to JKR grading specification.

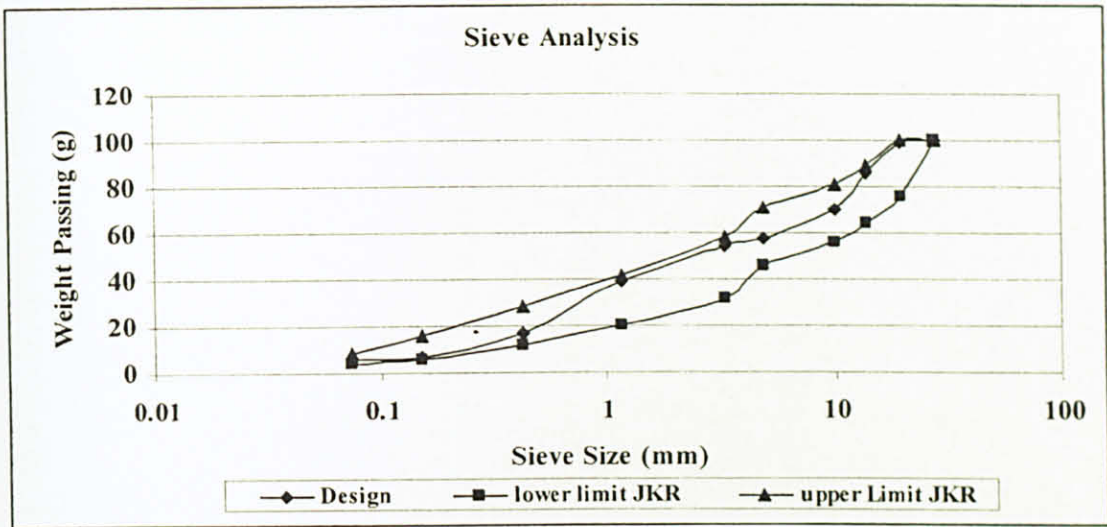


Figure 6.2 Sieve Analysis

### 6.3 Creep Test Results

The results of creep test in this study were the average values determined from some specimens. A total of 102 specimens were prepared for the creep test. In this investigation, only one variable namely porosity was investigated to study its effect on the creep properties of the asphalt concrete.

In order to obtain wider porosity range, the specimens were made in five variations of weight, namely 1,200 g, 1,300 g, 1,400 g, 1,500 g and 1,600 g. From Figure 6.3, in the weight range 1,200 g to 1,600 g, only slight differences in the porosity results were observed. At the pressure of 999 kPa, the 1,200 g, 1,400 g and 1,500 g specimen give same porosity value of 6%.

A similar trend is also observed at other pressures, where same porosity value is obtained for the entire test specimen. This seems to indicate that porosity is not affected by the weight of specimen but rather by the applied pressure during testing.

Another graph of porosity against pressure was plotted as shown in Figure 6.4. Different porosity values are obtained for specimen of the same weight when subjected to different pressures. From Figure 6.4, it can be seen that pressure has significant effect on porosity. Therefore, based on this test, it was decided that all the specimens were 1200 g. weight

and the variable parameter was pressure. The range of pressure was 100 kPa (minimum pressure in gyratory compactor) to 999 kPa (maximum pressure in gyratory compactor).

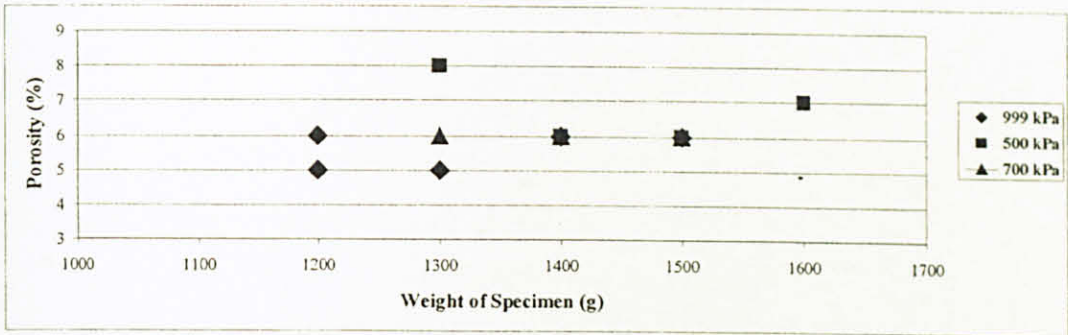


Figure 6.3 Porosity vs. Weight of Specimens

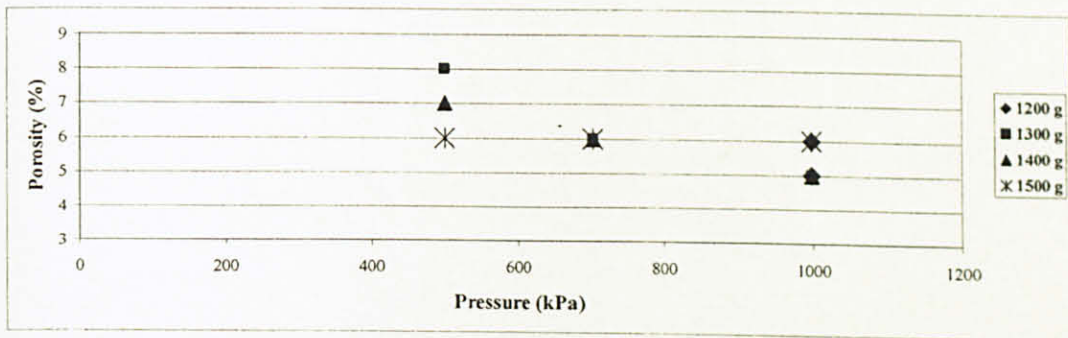


Figure 6.4 Porosity vs. Pressure

### 6.3.1 Correlation between Bitumen Stiffness vs. Mixture Stiffness

The results of creep test are depicted in the graph in Figure 6.5, which shows the relationship between the stiffness modulus of the mix ( $S_{mix}$ ) and stiffness modulus of bitumen ( $S_{bit}$ ).  $S_{mix}$  is derived from dynamic creep test. Creep modulus from creep test as mixture stiffness are taken at cycle number 10, 20, 30, 60, 180, 420, 600, 1200 and 1800 (20s, 40s, 60s, 120s, 360s, 840s, 1200s, 2400s and 3600s).  $S_{bit}$  is derived from Van der Poel's nomograph (Figure 4.5). This graph eliminates the effect of temperature,  $T$ , binder grade, and value of the applied stress,  $\sigma$  [12].  $S_{bit}$  is determined based on bitumen properties, test temperature and time of loading. For bitumen properties, softening point is 44°C and penetration 80 leading to get Penetration Index (PI) is -1. Test temperature is 40°C is typically use. Time loading of  $S_{bit}$  is similar with time loading of  $S_{mix}$ .

$$A = \frac{\log 80 - \log 800}{25 - 44} = 0.05$$

$$PI = \frac{20 - 500(0.05)}{1 + 50(0.05)} = -1$$

From Figure 6.5, the stiffness of sample of different porosities can not be compared because the graphs have different slopes. The only information that can be deduces from this graph is the mix susceptibility to time of loading. Smaller slope indicates less susceptibility. From Table 6.3, it is observed mixtures with smaller porosity are less susceptible to time of loading than the mixtures with greater porosity. This agrees with the study by Sousa that state the creep modulus decreases with increase porosity [18]. A good correlation for  $S_{mix}$  and  $S_{bit}$  is a power type,  $Y = a X^b$ . It is chosen as good correlation because of R-square values. All of R-square values are more than 90%. This correlation is in agreement with Bolk's study [14], which concluded that a linear relationship exist between  $\log S_{mix}$  and  $\log S_{bit}$  for values of  $S_{bit}$  lower that about  $10^3$  N/m<sup>2</sup>. The values of a and b for each porosity are tabulated in Table 6.3.

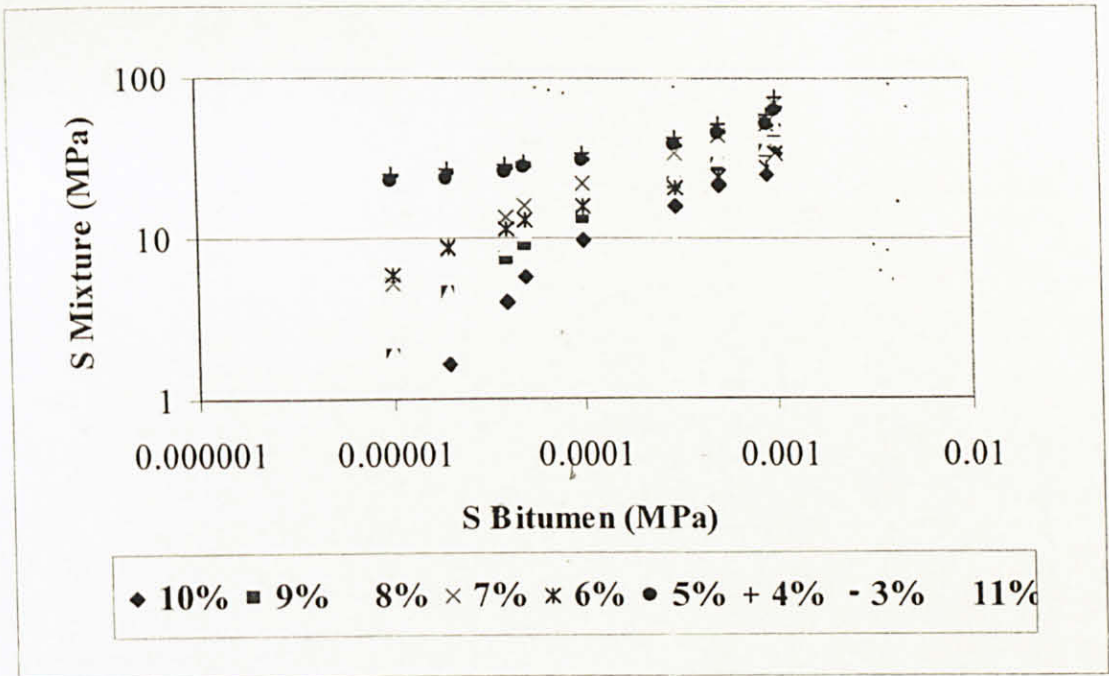


Figure 6.5  $S_{Mix}$  vs.  $S_{Bit}$

Table 6.3 Creep Test Results

No.	Porosity (%)	Total no. of Specimens	Mixture Stiffness (a)	Sensitivity of Mixture (b)	R-square
1	11%	4	18703	0.9491	0.9775
2	10%	4	3620.9	0.6754	0.9510
3	9%	7	3069.2	0.6091	0.9650
4	8%	29	3383.6	0.6094	0.9488
5	7%	23	2209.4	0.5121	0.9838
6	6%	20	327.2	0.3369	0.9774
7	5%	6	232.17	0.212	0.9450
8	4%	4	289.14	0.2232	0.9131
9	3%	5	200.16	0.1934	0.9113
Total		102			

### 6.3.2 Calculation of Viscous Bitumen Stiffness ( $S_{bit\ viscous}$ ) and Mixture Stiffness

The component of stiffness modulus of bitumen is both reversible and irreversible deformation. Not both of them affects permanent deformation, only irreversible one is responsible for it. So, recalculate  $S_{mix}$  by using  $(S_{bit})_v$  is needed. Hills suggested Equation 6-1 to determine the stiffness modulus of bitumen corresponding to its viscous part [38].

$$(s_{bit})_v = \frac{3\eta}{NT_w} \quad \text{Equation 6-1}$$

where:

$(S_{bit})_v$  = the viscous or irrecoverable component of the stiffness modulus of the bitumen, which is responsible for permanent deformation.

$\eta$  = the viscosity of the bitumen as a function of Penetration Index and Ring Ball Temperature

$N$  = the number of wheel passes in standard axles

$T_w$  = the time of loading for one wheel pass

In this study,  $\eta = 5000 \text{ Ns/m}^2$  (Viscosity of bitumen which is function of  $T-T_{R\&B}$  and PI),  $N = 10^6, 2 \times 10^6, 4 \times 10^6, 8 \times 10^6, 9 \times 10^6, \dots, 10^7, \dots, 10^8$  standard axles,  $T_w = 0.02$  second. For specimen with porosity 3 %,  $S_{mix} = 200.16 \times S_{bit}^{0.1934}$ . The  $S_{bit(v)}$  and  $S_{mix}$  value for each  $N$  are tabulated in Table 6.4.

Table 6.4 Creep Test Results Presented as  $S_{mix}$  vs.  $S_{bit(v)}$ 

3 %, $S_{mix} = 200.16 \times S_{bit}^{0.1934}$		
$N \times 10^6$	$S_{bit(v)}$ ( $10^{-9}$ Mpa)	$S_{mix}$ (Mpa)
1	750	13.1
2	375	11.4
4	188	1.00
8	93.8	8.75
9	83.3	8.56
10	75	8.38
20	37.5	7.33
40	18.8	6.41
80	9.38	5.61
90	8.33	5.48
100	7.50	5.37

### 6.3.3 Calculation of Rut Depth

The rut depth of asphalt concrete was calculated using the following equation.

$$RutDepth = C_m \times h \times \frac{\sigma_{AVE}}{S_{Mix}} \quad \text{Equation 6-2}$$

where,  $C_m$  = Correlation factor for dynamic effect

$h$  = Pavement layer thickness

$\sigma_{AVE}$  = Average stress in the pavement, related to wheel loading and stress distribution.

The permanent deformation was determined based on Table 6.4 in which the  $S_{mix}$  value (in fact  $S_{mix,visc}$ ) was derived from  $S_{mix} - S_{bit}$  creep characteristic at a value of  $S_{bit}$  equal to  $S_{bit,visc}$ .

In this study,  $C_m = 1.5$ ,  $h = 70$  mm,  $\sigma_{AVE} = 0.25$  MPa. For specimen with porosity 3%, The Rut depth values for each  $N$  are tabulated in Table 6.5

Table 6.5 Rut Depth for Specimen with 3% Porosity

3 %, $S_{mix} = 200.16 \times S_{bit}^{0.1934}$		
$N \times 10^6$	$S_{mix}$ (Mpa)	Rd (mm)
1	13.10	2.01
2	11.40	2.29
4	1.00	2.62
8	8.75	3.00
9	8.56	3.07
10	8.38	3.13
20	7.33	3.58
40	6.41	4.09
80	5.61	4.68
90	5.48	4.79
100	5.37	4.89
2.5	1.10	2.39

In this analysis, the porosity was divided into three categories namely 3% to 5% porosity as low porosity, 6% to 8% as moderate porosity and 9% to 11% as high porosity. Each category was examined based on the severity level of permanent deformation. The severity level classified by Jabatan Kerja Raya Malaysia was used in this work. All data are presented in the following sub chapters.

#### 6.3.4 Rut Depth vs. Number of Wheel Passes

Refer to Figure 6.6 until Figure 6.8, the vertical line, N, is equal to 2.5 million standard axle (msa). Meanwhile, the horizontal continuous line is 12 mm, the maximum tolerable rut depth. A rut depth lower than 12 mm is considered as low severity, 12 mm to 25 mm as moderate severity and more than 25 mm as high severity. The 25 mm boundary is marked by a horizontal dash line.

From Figure 6.6 until Figure 6.8 show that rut depth exhibited an increase trend with an increase in number of wheel passes as expected. This trend is in agreement with theory, which said rutting in pavements accumulates as the number of traffic loads on the pavements increases [17].

Figure 6.6 shows that all high porosity specimens had undergone high severity of rutting after 1 msa. Otherwise, from a Figure 6.8 show that all low porosity specimens were able to tolerate permanent deformation throughout the entire load range.

From a Figure 6.7, it is observed that only specimen with 6% porosity were able to tolerate permanent deformation at 1 msa. Other specimen having 7% and 8% porosity experienced permanent deformation throughout the entire load range. Specimens with 8% porosity have experienced high severity of rutting beyond 1 msa load. Meanwhile, specimen with 7% porosity experienced high severity of rutting after 2.5 msa load and specimen with 6% porosity experienced high severity of rutting after 20 msa.

The accumulation of rut depth, with increasing number of wheel passes, shows a linear behavior on a log – log scale. The linear pattern on a log-log scale means that the accumulation of rut depth has a decreasing exponential relation to the number of wheel passes on a linear scale. This shows that as the number of wheel passes increases, it is more difficult for the material to build up permanent strain. In other words, the material “stiffens” and resists further accumulation of rut depth (permanent deformation).

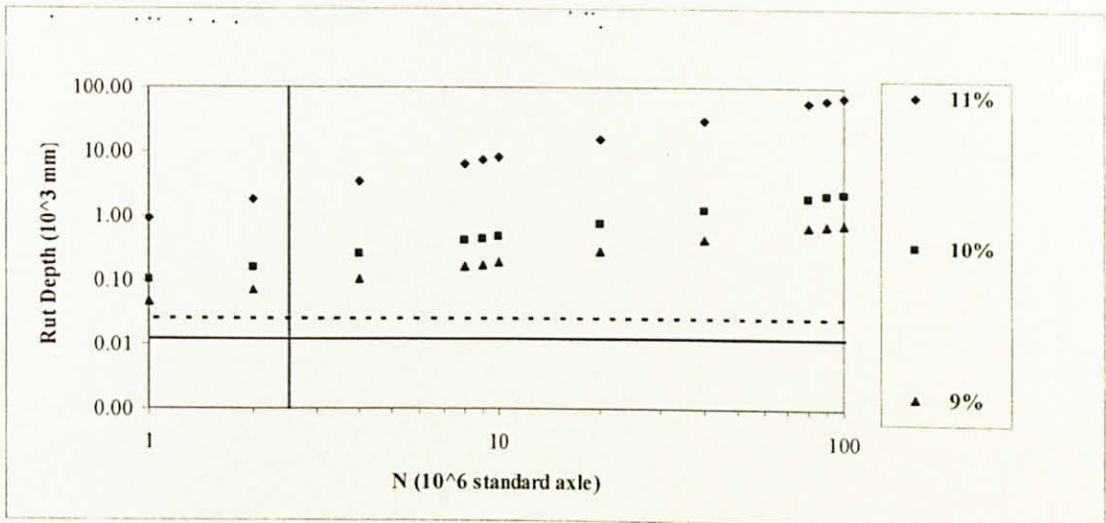


Figure 6.6 Rut Depth vs. N for High Porosity



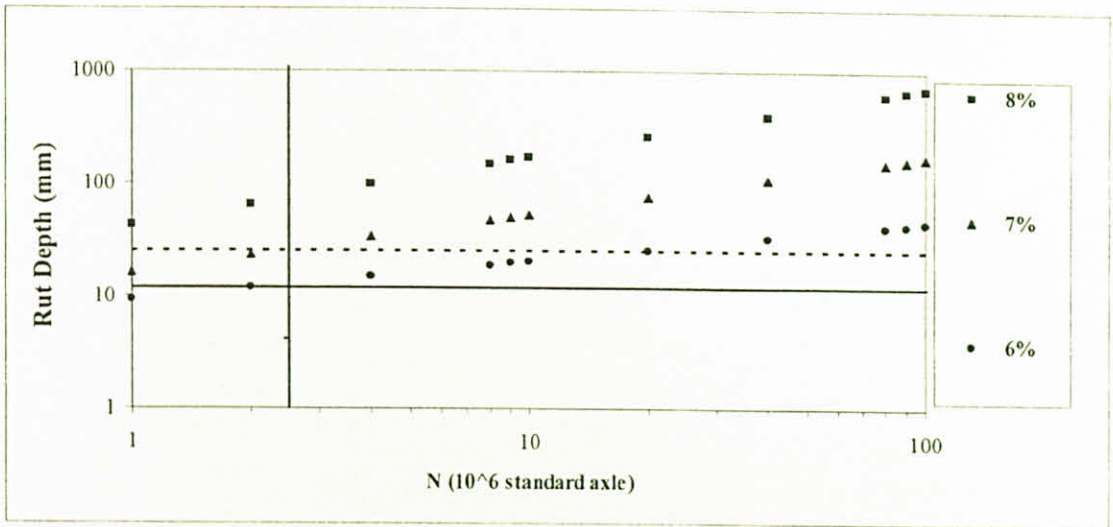


Figure 6.7 Rut Depth vs. N for Moderate Porosity

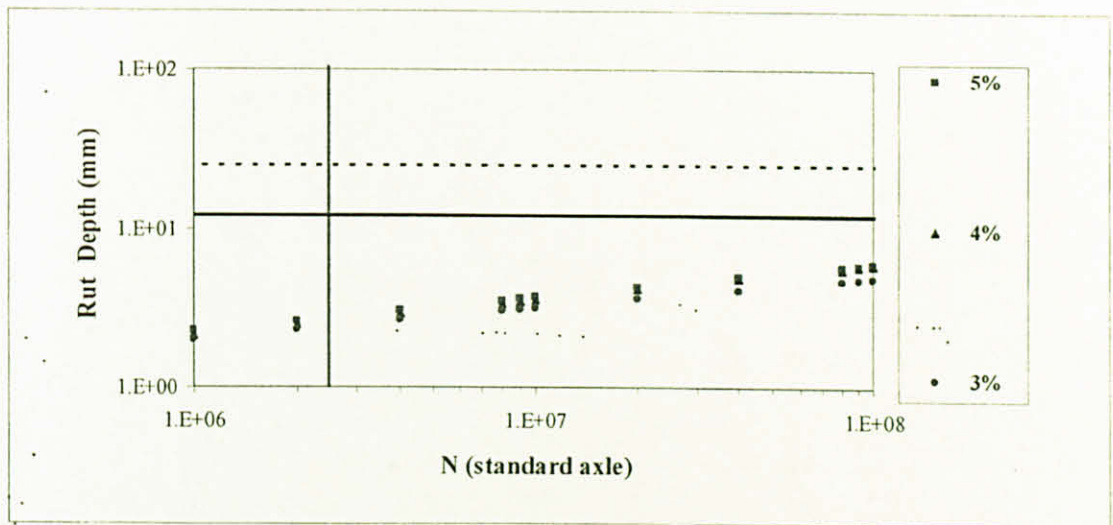


Figure 6.8 Rut Depth vs. N for Low Porosity

### 6.3.5 Rut Depth vs. Porosity

Mixes containing low porosity perform better in term of resistance to deformation. This observation is illustrated in Figure 6.9 and Figure 6.10. Two levels of loading, one million and ten million standard axles were studied. At load 1msa (Figure 6.9), specimen with porosity 10% and 11% are considered fail because the rut depth is more than 70mm. Seventy millimeters is the thick of pavement. Increasing ten fold loading (Figure 6.10) result all specimen high porosity and one third specimen moderate porosity are considered fail.

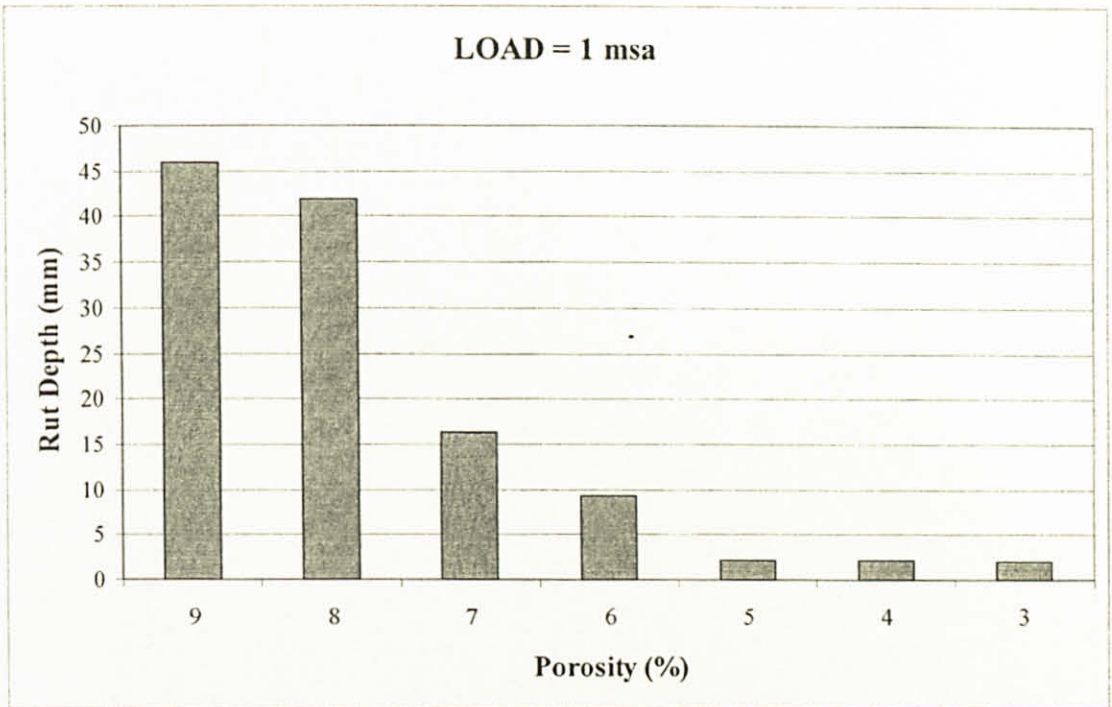


Figure 6.9 Rut Depth vs. Porosity

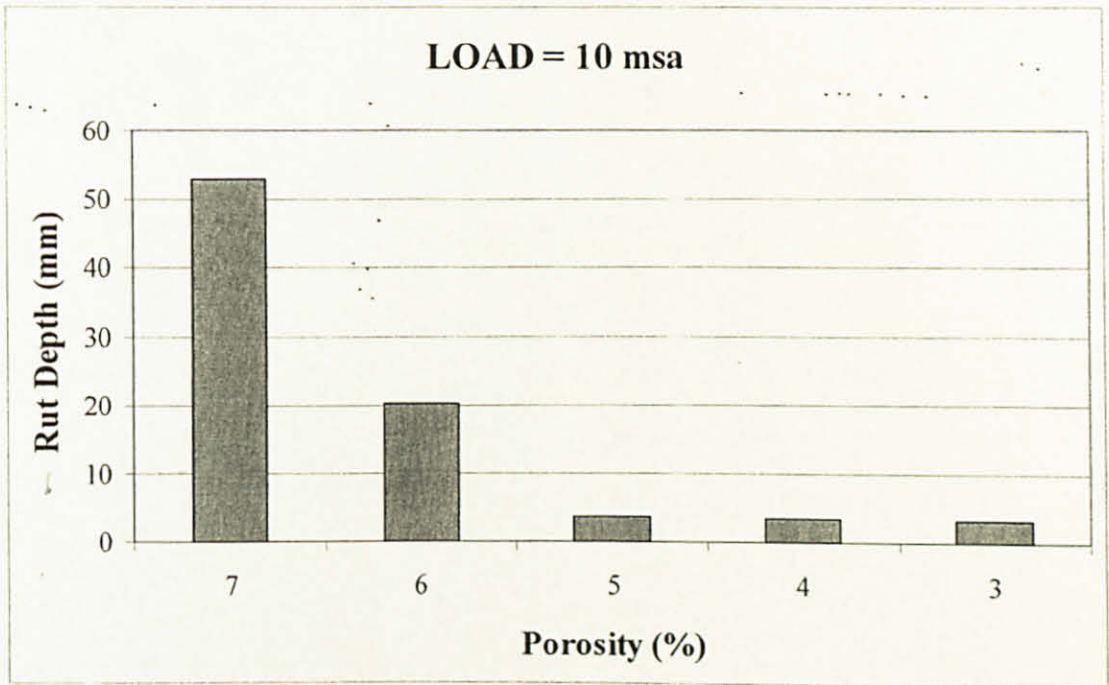


Figure 6.10 Rut Depth vs. Porosity

Results as shown in Table 6.6 indicate that the rates at which rut depth increase with respect to the increase in loading is smaller with the low porosity specimen compared to

the high porosity specimen. When ten fold loading increase, the porosity (%) is in the range of 3-5 % have a slight rate in the increment of rut depth. It is observed, approximately 1.6 fold increasing. Conversely, for porosity values larger than 5%, the rate increase 4 fold for specimen of high porosity and 9 fold for specimen of moderate porosity. In this range, the effect of porosity on rut depth is considerable. This suggests that asphalt mixtures characterized by high values of porosity are more susceptible to deformation. The low porosity specimen will perform satisfactorily under wider range of loading compared to high porosity specimen.

Table 6.6 Rate of Rut Depth

For N = 1 msa					
Porosity	(Bitumen Stiffness) $\nu$ ( $10^7$ MPa)	Mixture Stiffness (MPa)	Rut depth (mm)	Rate	
11	7.50	0.03	913	814	290.31
10	7.50	0.26	99	53	
9	7.50	0.57	46	4	
8	7.50	0.63	42	26	13.22
7	7.50	1.61	16	7	
6	7.50	2.83	9	7	
5	7.50	11.68	2	0	0.75
4	7.50	12.42	2	0	
3	7.50	13.09	2	2	

For N = 10 msa					
Porosity	(Bitumen Stiffness) $\nu$ ( $10^8$ MPa)	Mixture Stiffness (MPa)	Rut depth (mm)	Rate	
11	7.50	0.003	8119	7648	2649.47
10	7.50	0.06	470	283	
9	7.50	0.14	187	17	
8	7.50	0.15	170	118	55.61
7	7.50	0.50	53	33	
6	7.50	1.30	20	17	
5	7.50	7.17	4	0	1.22
4	7.50	7.43	4	0	
3	7.50	8.38	3	3	

### 6.3.6 Number of Wheel Passes vs. Porosity

Figure 6.11 shows the limitation for permanent deformation. A rutting below 12 mm is considered as low severity and above 25 mm is considered high severity. The range of moderate severity of rutting decreases when the porosity of specimen increases.

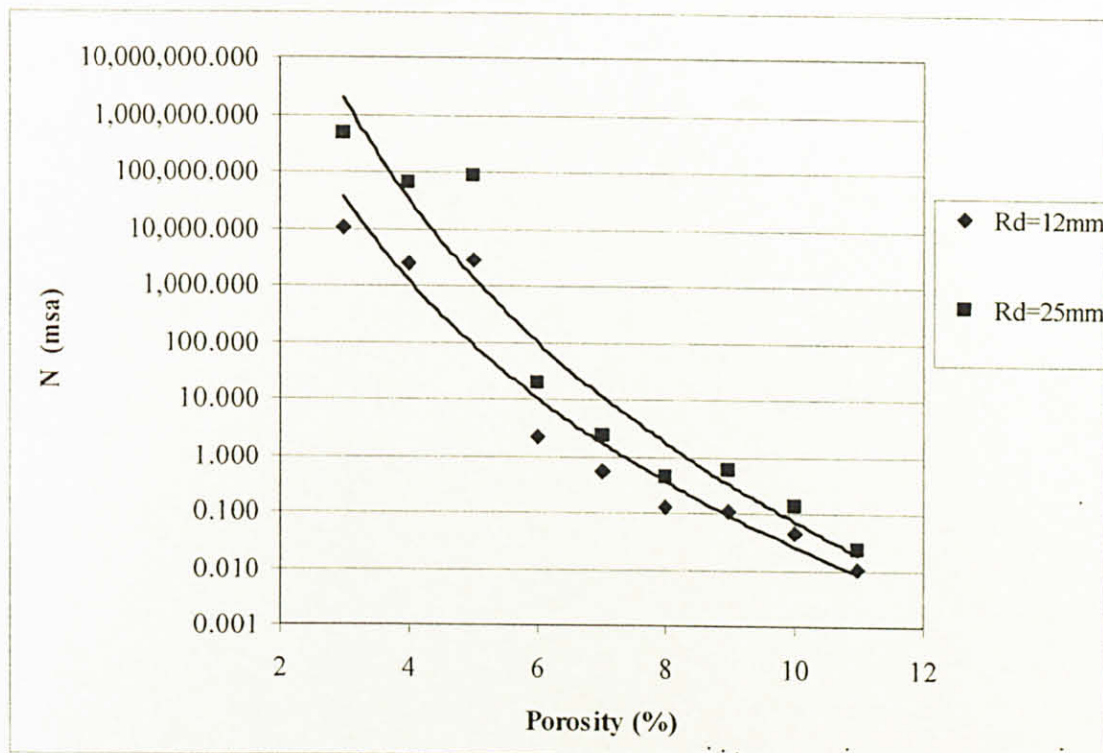


Figure 6.11 Number of Wheel Passes vs. Porosity in Limit of Severity Level

### 6.3.7 Compaction Degree vs. Number of Wheel Passes (N)

Shown in Table 6.7 and Figure 6.12 is the relationship between compaction degree and number of wheel passes, derived using test data from laboratory specimens. This relationship can be expressed by the equation in Figure 6.12. An increment in compaction degree will cause an increment in the number of wheel passes. The performance life, in terms of permanent deformation, of mixture with high compaction degree is longer than that of mixture with lower compaction degree.

Results as shown in Table 6.7 and Figure 6.12 indicate that low porosity specimen is less susceptibility to rut depth than the high porosity specimen. It is proved with slope of

trendline for each group porosity value. Trendline of high porosity specimen is steeper than trendline of low porosity specimen.

Table 6.7 Compaction Degree vs. N (standard axle)

Porosity	Density	Comp. Degree	a	Rd (mm)=	b	N (msa)
				12		
11	2.22	89	760.04		1.0536	0.01
10	2.24	90	1104.3		1.4806	0.04
9	2.26	91	1862.4		1.6418	0.11
8	2.29	92	2177.2		1.641	0.13
7	2.31	93	4309		1.9527	0.55
6	2.34	94	1340.6		2.9682	2.14
5	2.37	95	21904		4.717	2,697.87
4	2.38	96	34948		4.4803	2,390.44
3	2.41	97	27343		5.1706	10,395.87

Porosity	Density	Comp. Degree	a	Rd (mm)=	b	N (msa)
				25		
11	2.22	89	760.04		1.0536	0.02
10	2.24	90	1104.3		1.4806	0.13
9	2.26	91	1832.7		1.7784	0.56
8	2.29	92	2177.2		1.641	0.43
7	2.31	93	4309		1.9527	2.31
6	2.34	94	1340.6		2.9682	18.91
5	2.37	95	21904		4.717	86,021.39
4	2.38	96	34948		4.4803	64,063.84
3	2.41	97	27343		5.1706	462,418.04

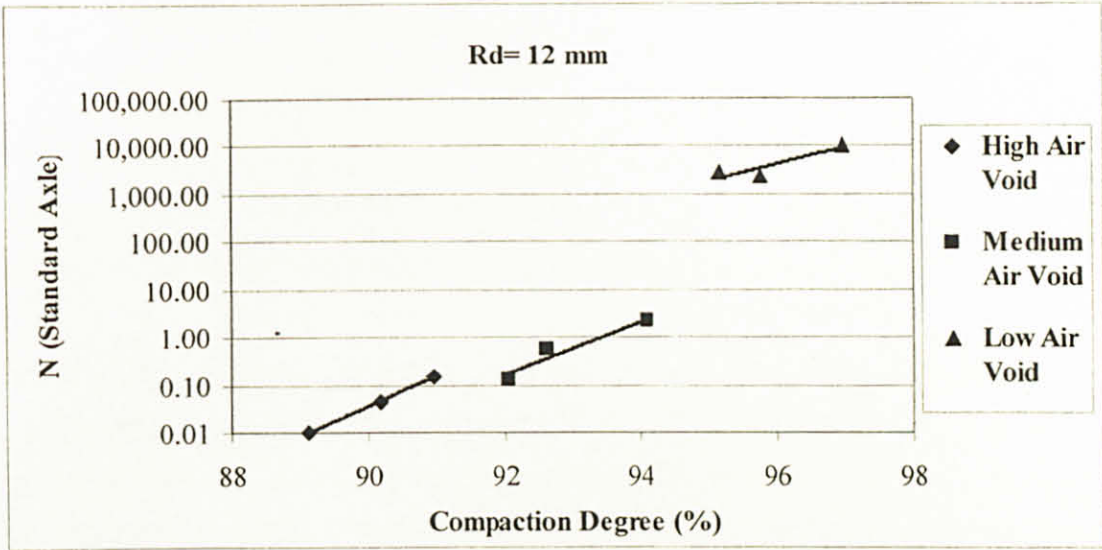


Figure 6.12 Compaction Degree vs. N

#### 6.4 Wheel Tracking Test Results

The total number of specimens for wheel tracking test was 19 specimens. Wheel tracking result (Figure 6.13) shows that the rate of wheel tracking increases while the porosity increase. The rate of WT progressively increases in the porosity range 11%- 12%. This suggests that permanent deformation tends to occur more in high porosity mixture than in mixtures having low porosity.

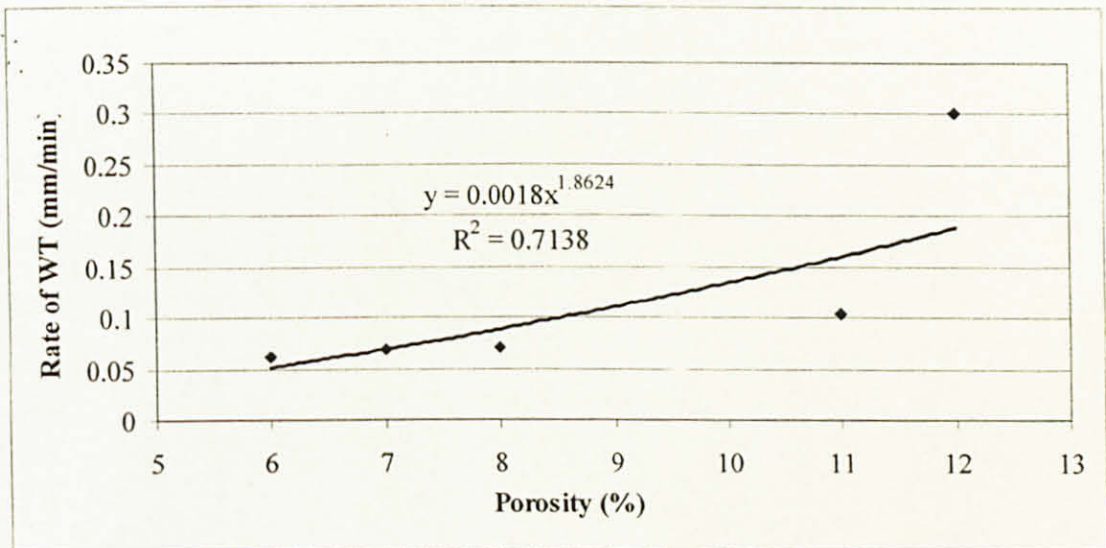


Figure 6.13 Wheel Tracking Test Results

## 6.5 Fatigue Test Results

A total of 73 specimens were used for Fatigue test. In this analysis, the porosity values were classified into three categories, 11%-16% classified as high porosity, 8%- 10% as medium porosity, and 5%-7% as low porosity. Of the specimens used in this test, 20% fall in the low porosity, 45% in medium porosity and 35% in high porosity.

In this study, the deterioration path for the asphalt concrete during fatigue test is fatigue path C as indicated by the S-shape curve which cut at termination cycle (Figure 6.14). The final stage is characterized by stiffness approaching zero, even though in principle, it never reaches zero. The failure point is difficult to determine as, in principle, the real failure of the structure does not occur. Therefore, due to the difficulties associated with the determination of failure, a 50% reduction in stiffness is employed. After conditioning cycle, the initial stiffness can be determined. Then the termination stiffness is calculated from 50% of initial stiffness.

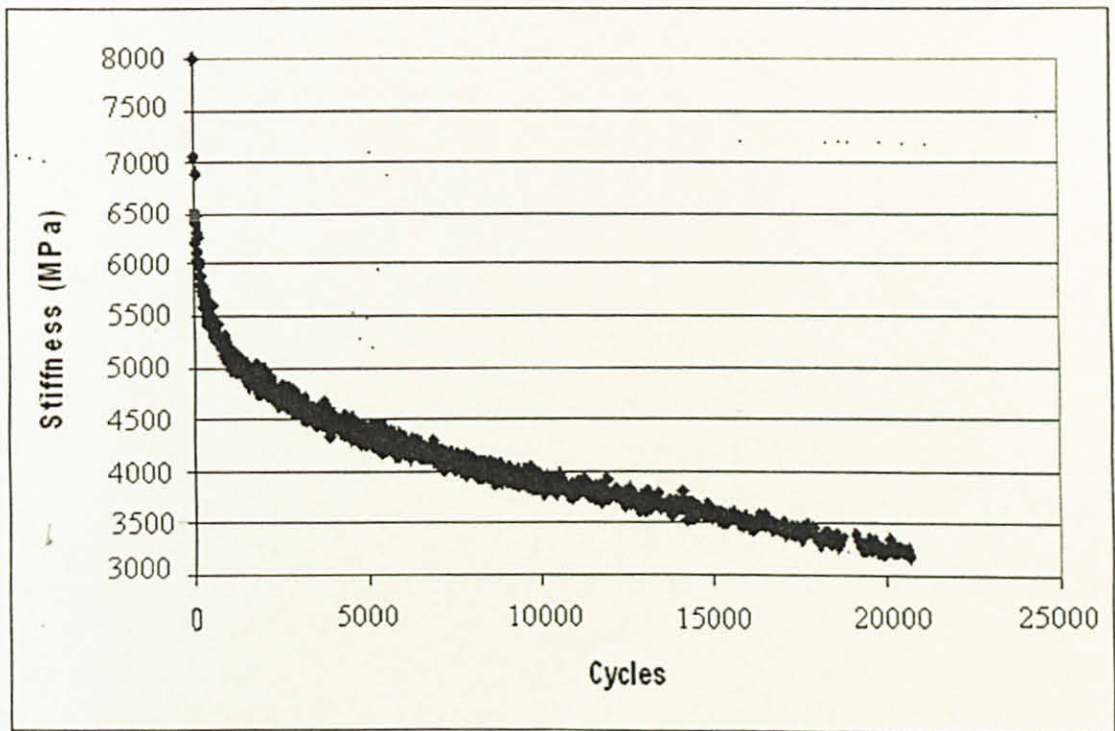


Figure 6.14 Deterioration Path of Fatigue Test Result

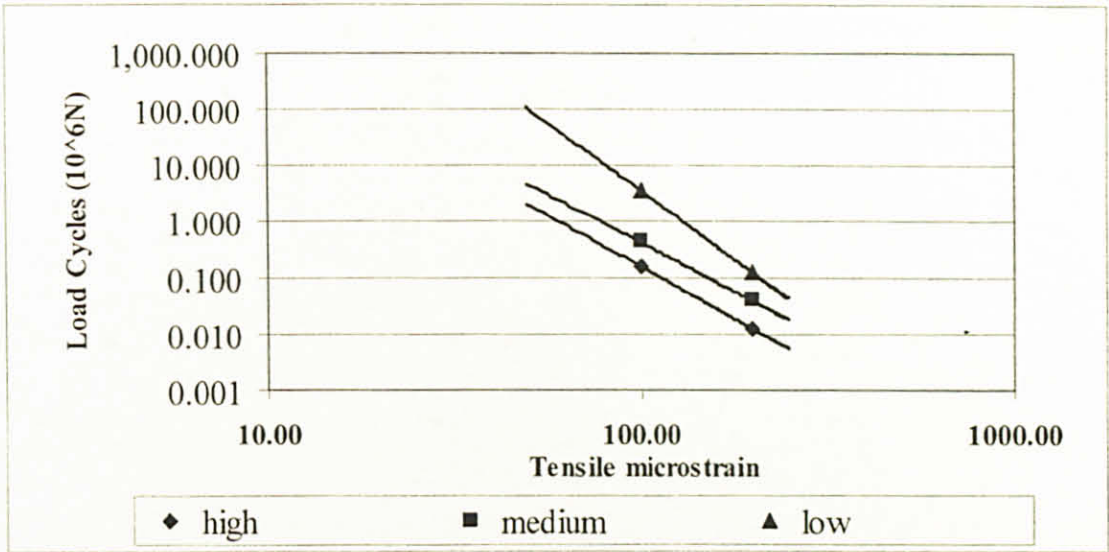


Figure 6.15 Load Cycles vs. Test Tensile microstrain at 20°C

Figure 6.15 is a plot of the  $N$  versus applied tensile strain on log-log scale. It shows that for the same test strain level, the high porosity fails in the cycle that is lower than the cycle failure of low porosity. This seems to suggest that the low porosity is more resistant to fatigue than the high porosity. This is because the low porosity mixture is stiffer than the high porosity mixture. High stiffness mixtures can resist the load longer than low stiffness mixture. Therefore, they have high fatigue life.  $N$  generally exhibited a decreasing trend with an increase in test tensile micro strain as expected.

The fatigue characteristic of asphalt mixtures is expressed in the relationship between the applied tensile strain and the number of load repetition to failure as shown in Figure 6.15. It was determined using repeated flexure at several strain levels (100, 150 and 200 micro strain). As indicated from the graph, beam containing low porosity possess a superior fatigue properties compared to the beam with high porosity. The fatigue characteristic relationship is described as  $N_f = K (1/\epsilon)^n$

Table 6.8 Fatigue Curve Regression Parameter

Porosity	Intercept, K	Slope, n
Low	$2 \times 10^{16}$	4.8466
Medium	$3 \times 10^{12}$	3.4261
High	$3 \times 10^{12}$	3.6512



The intercept and slope of each graph in Figure 6.15 are tabulated on Table 6.8, showing the statistical difference among the three categories of porosity. The slope of the fatigue equations agrees reasonably well with the theory that specifies a variation of 3.0 to 5.671 [23, 61].

From Figure 6.16, it can be concluded that fatigue life or resistance to cracking under repeated load, is directly proportional to the compaction level.

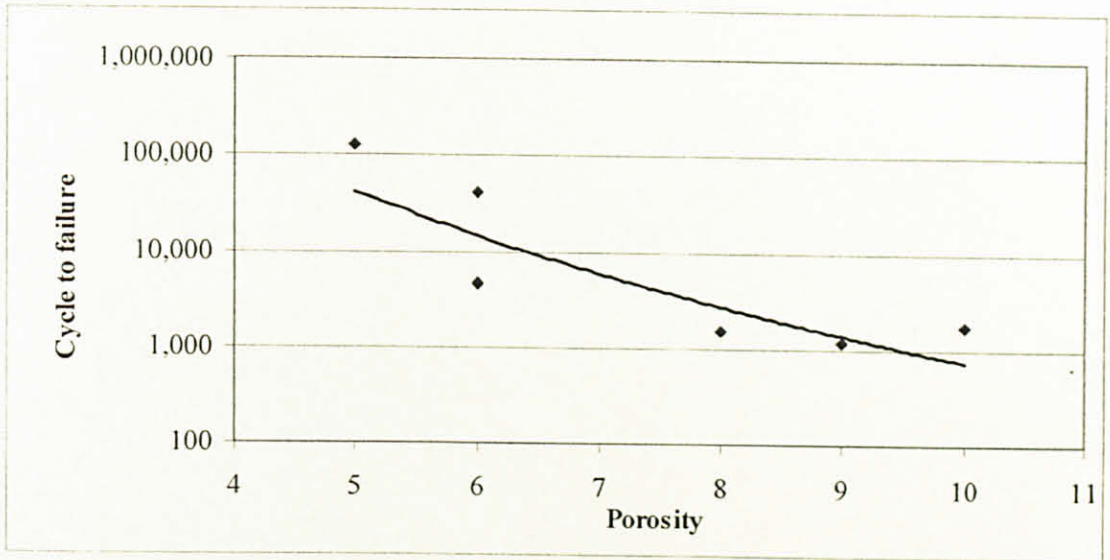


Figure 6.16 Cycle to Failure vs. Porosity

## 6.6 The Practical Implication of the Study

From this finding, the contractor can see the effect of porosity in performance of pavement. This correlation can be used as decision making in pavement construction because it gives limitation of porosity for better performance. During the pavement construction, some of the cores from the field are checked for their porosity. If the porosity of the core is considered high, the contractor can make a comparison between taking out the pavement or paying a punishment bill to the owner based on the reduction of pavement life (N).

## CHAPTER SEVEN: CONCLUSIONS AND RECOMMENDATION

### 7.1 Conclusion

Asphalt concrete (AC) wearing course specimens of various porosities have been evaluated with respect to their resistances to fatigue cracking and rutting. The experimental work, dynamic creep test, wheel tracking test and flexural fatigue tests on AC beams, has resulted in the following conclusions:

- (1) The results from creep test, conducted on samples of three different porosity categories, show a linear relation between  $\log (S_{mix})$  and  $\log (S_{bit})$ . A smaller slope of the linear log-log relation was obtained for samples with lower porosity. This indicates that stiffness of the higher porosity specimen is less sensitive to loading time and temperature. In this study, the slope of the equation relating  $\log (S_{mix})$  and  $\log (S_{bit})$  in the form of  $S_{mix} = a (S_{bit})^b$  is reduced from 0.9491 for 11% porosity AC specimen to 0.1934 for 3% porosity AC specimen. The good correlation between  $\log (S_{mix})$  and  $\log (S_{bit})$  obtained from this investigation ( $r^2 > 0.90$ ) also indicates the validity of the dynamic creep test being employed as means of predicting the rutting of specimen.
- (2) The rates at which rut depth increase with respect to the increase in loading is smaller with the low porosity specimen compared to the high porosity specimen. When ten fold loading increase, the porosity (%) is in the range of 3-5 % have a slight rate in the increment of rut depth. It is observed, approximately 1.6 fold increasing. Conversely, for porosity values larger than 5%, the rate increase 4 fold for specimen of high porosity and 9 fold for specimen of moderate porosity.
- (3) The correlation between compaction degree and rutting life  $Y = (4 \times 10^{-145}) X^{77.67}$  (low porosity),  $Y = 10^{-232} X^{120.70}$  (medium porosity) and  $Y = (3 \times 10^{-256}) X^{133.08}$  (high porosity) where Y as rutting life in msa and X as compaction degree in percentage. Low porosity specimen is less susceptibility to rut depth than the high porosity specimen.
- (4) The trendline of rate of wheel tracking is  $y = 0.0018x^{1.8624}$  and  $R^2 = 0.7138$ . This result is in agreement with the creep test to measure permanent deformation of asphalt concrete.

- (5) The fatigue performance of AC wearing course of the materials tested in this study can be predicted using the relationship between the applied tensile strain and the number of the cycles to failure using the following equation:

$$N_f = K (1/\epsilon)^n$$

The value of 'K' and 'n' obtained from this study varies from  $3 \times 10^{12}$  to  $2 \times 10^{16}$  and 3.42 to 4.84, respectively, for strain ranging from 100 to 200 micro strain. The equation proposed in this investigation is valid for  $N_f$  value ranging from  $10^4$  to  $10^5$  load cycles.

## 7.2 Recommendation

This study used laboratory specimen (JKR) to assess the effect of porosity on the rutting and fatigue performance of asphalt concrete material. This limited test data indicated that variation in porosity could have a significant effect on potential pavement performance. Additional studies using field-mixed and field-compacted and/or field-mixed and laboratory-compacted should be performed to substantiate the finding presented in this study.

## REFERENCES

1. Clyne, T.R., A. Drescher, and D.E. Newcomb, Superpave Level One Mix Design at the Local Government Level. July 2001, Department of Civil Engineering, University of Minnesota: Minnesota.
2. Blankenship, P.B., K.C. Mahboub, and G.A. Huber, Rational Method for Laboratory Compaction of Hot-Mix Asphalt. *Journal of Transportation Research Record* 1454, TRB, 1994: p. 144-153.
3. Larsen, O., Development and Use of High Pressure Apparatus for Determining Voids in Compacted Bituminous Concrete Mixtures. *Journal of AAPT*, Vol 26, 1957: p. 403-435.
4. Harun, M.H. and G. Morosiuk, A Study of the Performance of Various Bituminous Surfacing for Use on Climbing Lanes. *Proceeding of the Eighth REAAA Conference*, Taipei, April 1995.
5. McClaran and Robert, Talk on Road Compaction. 2005, Master Builders Association Malaysia: Malaysia.
6. Linden, R.N., J.P. Mahoney, and N.C. Jackson, Effect of Compaction on Asphalt Concrete Performance. *Journal of Transportation Research Record* 1217, TRB, 1992: p. 20-28.
7. Zhou, H., M.C. Cook, and T. Bressette, Case Study on Air Void Effect on Laboratory Performance of Rubberized Asphalt Concrete Mix. *The Eighty-fifth Annual Meeting of the Transportation Research Board*, Washington, DC, January 2006.
8. Santucci, L., Rut Resistant asphalt pavements. 2001, Technology Transfer Program, Institute of Transportation Studies, University of California Berkeley.: Berkeley.
9. Napiah, M., Fatigue and Long Term Deformation Behaviour of Polymer Modified Hot Rolled Asphalt. Phd. Thesis, 1993, University of Leeds: Leeds.
10. McNicol, A. and G. Bell, Air Voids Versus PRD. *Journal of the Institution of Highways and Transportation*, February 1986: p. 3-8.
11. Gibb, J.M., Evaluation of Resistance to Permanent Deformation in the Design of Bituminous Paving Mixtures. Phd. Thesis, 1996, University of Nottingham Nottingham.
12. Uge, P. and P. VanDeLoo, Permanent Deformation of Asphalt Mixes. *Proceeding of the Nineteenth Annual Conference Canadian Technical Asphalt Association*, Regina Saskatchewan, Canada, November 1974: p. 307-341.
13. Brown, E.R., Density of Asphalt Concrete-How Much Is Needed? *The Sixty-ninth Annual Meeting of the Transportation Research Board*, Washington, DC, January 1990.
14. Bolk, H.J.N.A., Prediction of Rutting in Asphalt Pavements on the Basis of the Creep Test. *Proceeding of the Fifth International Conference on Structural Design of Asphalt Pavement*, Vol.1, Delft, the Netherlands 1982.
15. Turner-Fairbank Highway Research Center, Distress Identification Manual for the Long-Term Pavement Performance Program (Fourth Revised Edition). <http://www.tfhr.gov/pavement/ltp/tp/reports/03031/01.htm>, October 9th, 2005.
16. Bahuguna, S., V.P. Panoskaltisis, and K.D. Papoulia, Identification and Modeling of Permanent Deformations of Asphalt Concrete. *Journal of Engineering Mechanics*, ASCE, March 2006: p. 231-239.

17. Panoskaltsis, V.P., S. Bahuguna, and K.D. Papoulia, A Model Explaining And Predicting the Permanent Deformations of Asphalt Pavements. The Sixteenth ASCE Engineering Mechanics Conference, July 2003.
18. Sousa, J.B., J.A. Deacon, and C.L. Monismith, Effect of Laboratory Compaction Method on Permanent Deformation Characteristics of Asphalt Aggregate Mixtures. *Journal of AAPT*, Vol 60, 1991: p. 553-585.
19. Abdullah, W.S., M.T. Obaidat, and N.M. Abu-Sa'da, Influence of Aggregate Type and Gradation on Voids of Asphalt Concrete Pavements. *Journal of Materials in Civil Engineering*, ASCE, May 1998: p. 76-85.
20. Santucci, L., The Role of Compaction in the Fatigue Resistance of Asphalt Pavement. 1998, Technology Transfer Program, Institute of Transportation Studies, University of California Berkeley: Berkeley.
21. Tayebali, A.A., G.M. Rowe, and J. B.Sousa, Fatigue Response of Asphalt Aggregate Mixtures. *Journal of AAPT*, Vol 61, 1992: p. 333-360.
22. Hye, K.T., M.S. Mustafa, and M.S. Hasim, A Guide To Visual Assessment Of Flexible Pavement Surface Conditions. JKR 20709-2060-92. December 1992: Institut Kerja Raya Malaysia (IKRAM).
23. Huang, Y.H., *Pavement Analysis and Design*. second ed. 2004, USA: Pearson Prentice Hall.
24. Li, Y. and J.B. Metcalf, Crack Initiation Model from Asphalt Slab Tests. *Journal of Materials in Civil Engineering*, ASCE, August 2002: p. 303-310.
25. Powell, W.D., N.W. Lister, and D. Leech, Improved Compaction of Dense Graded Bituminous Macadams. *Journal of AAPT*, Vol.50, 1981: p. 394-416.
26. Marek, C.R., Compaction of Graded Aggregate Bases and Subbases. *Journal of Transportation Engineering*, ASCE, January 1977: p. 103-112.
27. Keyser, J.H. and L.S. Horng, A Study of the Variations of Compatibility of Bituminous Mixtures within the Specifications Limits. *Proceeding of the Nineteenth Annual Conference Canadian Technical Asphalt Association*, Regina Saskatchewan, Canada, November 1974: p. 451-469.
28. Fordyce, D. and H.K.A. Nageim, Profiles of Material Resistance to Compaction. *Journal of the Institution of Highways and Transportation*, March 1988: p. 13-20.
29. Hunter, R.N., *Asphalt in Road Construction*. 1 ed. 2000, London: Thomas Telford.
30. Khan, Z.A., H.I.A.-A. Wahab, and I. Asi, Comparative Study of Asphalt Concrete Laboratory Compaction Methods to Simulate Field Compaction. *Journal of Construction and Building Materials* 12, Elsevier Science, March 1998: p. 373-384.
31. Bissada, A.F., Compactibility of Asphalt Paving Mixtures and Relation to Permanent Deformation. *Journal of Transportation Research Record* 911, TRB, 1983: p. 1-10.
32. Maupin, G.W., Determination of Compactive Effort to Duplicate Pavement Voids for Corps of Engineers Gyrotory Testing Machine. *Journal of Transportation Research Record* 1492, TRB, 1995: p. 12-17.
33. Swanson, R.C. and J. Joseph Nemecek, Effect of Asphalt Viscosity on Compaction of Bituminous Concrete. *Highway Research Record*, Vol.117, thrc, 1996: p. 23-53.
34. Kim, Y.R., N.P. Khosla, and N. Kim, Effect of Temperature and Mixture Variable on Fatigue Life Predicted By Diametral Fatigue Testing. *Journal of Transportation Research Record* 1317, TRB, 1991: p. 128-138.

35. Hills, J.F., The Creep of Asphalt Mixes. *Journal of the Institute of Petroleum*, November 1973: p. 248-262.
36. Button, J.W., D.N. Little, and V. Jagadam, Correlation of Selected Laboratory Compaction Methods with Field Compaction. *Journal of Transportation Research Record* 1454, TRB, 1994: p. 193-201.
37. Peterson, R.L., K.C. Mahboub, and R.M. Anderson, Comparing Superpave Gyrotory Compactor Data to Field Cores. *Journal of Materials in Civil Engineering*, ASCE, February 2004: p. 78-83.
38. Hills, J.F., D. Brien, and P.J. VanDeLoo, The Correlation of Rutting and Creep Tests on Asphalt Mixes. *Journal of the Institute of Petroleum*, January 1974: p. 1-19.
39. Drescher, A., J.R. Kim, and D.E. Newcomb, Permanent Deformation in Asphalt Concrete. *Journal of Materials in Civil Engineering*, ASCE, February 1993: p. 112-128.
40. Azari, H., R.H. McCuen, and K.D. Stuart, Optimum Compaction Temperature for Modified Binders. *Journal of Transportation Engineering*, ASCE, September 2003: p. 531-537.
41. Lee, S.-J., S.N. Amirkhani, and C. Thodesen, Effect of Compaction Temperature on Rubberized Asphalt Mixes. *Proceeding of Asphalt Rubber International Conference*, Palm Springs, Calif, Oktober 2006.
42. Kandhal, P.S. and E.R. Brown, Comparative Evaluation of 4-inch and 6-inch Diameter Specimens for Testing Large stone Asphalt Mixes. 1990, National Center for Asphalt Technology: Auburn, Alabama.
43. Jackson, N.M. and L.J. Czor, 100-mm-Diameter Mold Used with Superpave Gyrotory Compactor. *Journal of Materials in Civil Engineering*, ASCE, February 2003: p. 60-66.
44. Australian Asphalt Pavement Association, Air Void in Asphalt, *Pavement Work Tips*. June 1999, Austroads: Victoria.
45. Cabrera, J.G., A. Ridley, and E. Fekpe, Lab Design and Field Compaction of Bitumen Macadam. *Journal of the Institution of Highways and Transportation*, July 1990: p. 27-34.
46. Asphalt Institute, Density Specifications for Hot-Mix Asphalt, *Technical Bulletin No.9*. 1992, Asphalt Magazine: Lexington.
47. Gibb, J.M. and S.F. Brown, A Repeated Load Compression Test for Assessing the Resistance of Bituminous Mixes to Permanent Deformation, in *Performance and Durability of Bituminous Materials*, J.G. Cabrera and J.R. Dixon, Editors. March 1994, E&FN SPON: UK. p. 199-209.
48. Meyer, F.R.P., R.C.G. Haas, and E.T. Hignell, The Prediction of Rut Depths in Asphalt Pavements. *Proceeding of the Nineteenth Annual Conference Canadian Technical Asphalt Association*, Regina Saskatchewan, Canada, November 1974: p. 343-375.
49. Haggi, E.Y., P.E. Sebaaly, and D. Weitzel, Fatigue Characteristics of Superpave and Hveem Mixtures. *Journal of Transportation in Civil Engineering*, ASCE, April 2005: p. 302-310.
50. Read, J.M., *Fatigue Cracking of Bituminous Paving Mixtures*. Phd. Thesis, May 1996, University of Nottingham: Nottingham.
51. VanDeLoo, P.J., The Creep Test: A Key Tool in Asphalt Mix Design and in the Prediction of Pavement Rutting. *Journal of AAPT*, Vol. 47, 1978: p. 522-557.

52. Smith, T.M., A Comparison of Different Methods of Analysing Dynamic Creep Test Results. 1996, Transport Research Laboratory Report 159: Crowthorne, Berkshire.
53. Walsh, I.D., The Use of The Wheel Tracking Test for Wearing Course Design and Performance Evaluation, in Performance and Durability of Bituminous Materials, J.G. Cabrera and J.R. Dixon, Editors. March 1994, E & FN SPON: UK. p. 210-225.
54. Roche, C.d., J. Charrier, and P. Marsac, An Assessment of Fatigue Damage in Bituminous Mixes Contribution of Infrared Thermography. Bulletin Des Laboratoires Des Ponts Et Chaussees 232, May 2001: p. 21-30.
55. Lundstrom, R., H.D. Benedetto, and U. Isacson, Influence of Asphalt Mixture Stiffness on Fatigue Failure. Journal of Materials in Civil Engineering, ASCE, December 2004: p. 516-525.
56. Ghuzlan, K.A., Traditional Fatigue Analysis of Asphalt Concrete Mixtures. The Annual Meeting of the Transportation Research Board, Washington, DC, Januari 2003.
57. Hartman, A.M. and M.D. Gilchrist, Evaluating Four-Point Bend Fatigue of Asphalt Mix Using Image Analysis. Journal of Materials in Civil Engineering, ASCE, February 2004: p. 60-68.
58. Artamendi, I. and H. Khalid, Different Approaches to Depict Fatigue of Bituminous Materials. The fifteenth European Conference of Fracture. Advance Fracture Mechanics for Life and Safety Assessments, August 2004.
59. Medani, T.O., M. Hurman, and A.A.A. Molenaar, A Proposed Fatigue Based Design Methodology for Asphaltic Mixes Applied on Orthotropic Steel Briges. Proceeding of the fifth RILEM International Conference, May 2004.
60. Whiteok, D., The Shell Bitumen Handbook. 1990, Surrey, UK: Shell Bitumen
61. Walubita, L.F., Comparison of Fatigue Analysis Approaches for Predicting Fatigue Lives of Hot-Mix Asphalt Concrete (HMAC) Mixture. Phd. Thesis, May 2006, Texas A&M University: Texas.
62. BritishStandardsInstitution, BS 812-103.1:1985 "Testing Aggregates, Methods for Determination of Particle Size Distribution, Sieve Size". 1985, BSI: London.
63. Robinson, R. and B. Thagesen, Road Engineering for Development. Second ed. 2004, London: Spon Press.

## APPENDIX A JKR STANDARD SPECIFICATION

### Gradation Limits for Asphalt Concrete

Mix Type	Wearing Course
Mix Designation	ACW20
B.S. Sieve	% Passing by Weight
37.5 mm	
28.0 mm	100
20.0 mm	76-100
14.0 mm	64-89
10.0 mm	56-81
5.0 mm	46-71
3.35 mm	32-58
1.18 mm	20-42
425 $\mu$ m	12-28
150 $\mu$ m	6-16
75 $\mu$ m	4-8

### Design Bitumen Contents

ACW20 Wearing Course	4.5 - 6.5 %
----------------------	-------------

### Parameter for Asphalt Concrete

Air Void in Mix	3%-5%
-----------------	-------



## APPENDIX B CALCULATION OF POROSITY

1	<b>Percentage (%)</b>			
	Aggregate		Filler	Bitumen
	Coarse	Fine		
	42	52	6	5
2	<b>Specific Gravity (SG)</b>			
	Aggregate		Filler	Bitumen
	Coarse	Fine		
	2.69	2.65	3.15	1.02
3	<b>SG of Aggregate</b>		<b>SG of Bitumen</b>	
	2.69		1.02	
4	<b>SG of Mixture (Max SG)</b>			
	2.49			
5	<b>Bulk SG of Mixture</b>			
	Weight in air		Weight in water	
	1245.5		731.2	
	2.42			
6	<b>Percent Relative Compaction (%) = 97</b>			
	<b>Air Void (Porosity) (%) = 3</b>			